

Chapter 4

GAMMA-RAY STRENGTH FUNCTIONS

G. A. Bartholomew, E. D. Earle,
A. J. Ferguson, J. W. Knowles,
and M. A. Lone

*Atomic Energy of Canada Limited
Chalk River Nuclear Laboratories
Chalk River, Canada*

1. INTRODUCTION

The study of the energy dependence of multipole transition probabilities is a broad subject in which certain subfields have progressed much more rapidly than others. Thus for gamma rays $\lesssim 2$ MeV, $E1$, $M1$, and $E2$ transition probabilities have been well studied (Per 66, SHR 66, SG 65), and at higher energies, $\gtrsim 10$ MeV, the absorption cross section and other properties of the $E1$ giant resonance are well known (Fir 70), but between these energies there are large gaps in our knowledge. In the present review we are concerned with the distribution of reduced radiation width, particularly for $E1$ and $M1$ radiation, in the less well-known “tail region” well below the peak of the $E1$ giant resonance. We will concentrate on elements with mass number $A \gtrsim 90$, where a statistical description of radiative processes is appropriate, and on γ -ray energies above ~ 2 MeV.

The gamma-ray strength function as used herein is the distribution, as a function of γ -ray energy, of the average reduced width for transitions of a particular multipole type. Specifically, for transitions of energy E_γ and multipole type XL (X is either E (electric) or M (magnetic) and L

is the multipolarity), between states of energies E_i and E_λ ($E_i < E_\lambda$), the strength function is

$$f_{i\lambda XL}^J(E_\gamma) = \frac{\bar{\Gamma}_{\gamma i\lambda XL}^J}{E_\gamma^{2L+1}} \varrho_J(E_\lambda) \quad (1.1)$$

where $\bar{\Gamma}_{\gamma i\lambda XL}^J$ is the γ -ray partial width averaged over states λ of a given spin and parity (denoted together by J) in the neighborhood of E_λ , $\varrho_J(E_\lambda)$ is the average level density for such states and E_γ^{2L+1} is the energy dependence for multipolarity L . The factor E_γ^{2L+1} is analogous to the penetration factor which is removed from nucleon widths to obtain nucleon reduced widths or strength functions.

The γ -ray strength function is thus an average quantity like the nuclear-level density. Regions where it is appropriate to discuss level densities instead of single levels are also regions where it is useful to think in terms of γ -ray strength functions instead of individual radiation widths. In some experiments in thermal neutron capture and γ -ray resonance scattering, radiation widths of a few individual γ -rays from a particular excitation region are all that can be extracted from any one nucleus. This type of data have been surveyed by Bartholomew (Bar 61, Bar 62) Demidov and Shadiev (DS 68), and Bollinger (Bol 68) for (n, γ) reactions and by Ben David, Moreh, and others (Ben+ 66, MSW 70) for (γ, γ) reactions. Because of Porter-Thomas fluctuations (PT 56), these individual transition widths have limited usefulness as indicators of average strength and, apart from a brief historical treatment in this section, we will have only occasional recourse to such data in this review. Average data may be obtained more directly from photoabsorption or inelastic scattering cross-section measurements with a photon beam with energy spread large compared to the spacing $D_J(E_\lambda)$ or by neutron capture or other reactions in which many resonances near the energy E_λ are excited and resonance-averaged radiation is detected.

The surveys of individual γ -rays from thermal neutron capture (Bar 61, Bar 62, DS 68) shed light on the relative strength of various multipoles, the level-spacing dependence, and also on the A -dependence of γ -ray reduced widths. All such studies were limited to a narrow range of E_γ near the neutron separation energy because it was only in this range that multipolarities could be established from the known spins and parities of the initial and final states. For each γ -ray, a “strength”

$$k_{E1} = \frac{\Gamma_{\gamma E1}}{E_\gamma^3 D_J A^{2/3}} \quad (1.2)$$

or

$$k_{M1} = \frac{\Gamma_{\gamma M1}}{E_\gamma^3 D_J} \quad (1.3)$$

was evaluated and average values \bar{k}_{E1} and \bar{k}_{M1} , averaged over both E_γ and A , were obtained. Here the $E1$ strength contained an $A^{2/3}$ dependence as suggested by the single-particle formula (BW 52). These strengths were found, on the average, to compare reasonably well in absolute magnitude with the single-particle estimates (BW 52) when certain plausible values were assumed for a level-spacing parameter appearing in the theory. Because of the small energy range covered, these data provided no definitive test of the energy dependence of $E1$ or $M1$ radiation widths predicted by the single-particle formula. That the single-particle estimates, which imply constant strength functions, were inadequate in this regard was evident from the failure to obtain realistic estimates of total radiation width of neutron resonances (Cam 59) with the same \bar{k}_{E1} as found for the high-energy transitions (Bar 61). However, the true significance of that discrepancy was somewhat obscured because the energy dependence of level densities also entering the calculations was poorly known experimentally and had to be taken from semiempirical formulas (New 56, Cam 59).

It was pointed out by Brink (Bri 55) and emphasized by Axel (Axe 62, Axe 63) that a more realistic energy dependence of the $E1$ transition probability is provided by the energy dependence of the $E1$ photoabsorption cross section. As shown in Sec. 2.2 the strength function for $E1$ photoexcitation from the ground state may then be written

$$\vec{f}_{0\lambda E1} = K \frac{\Gamma_G E_\gamma}{(E_\gamma^2 - E_G^2)^2 + \Gamma_G^2 E_\gamma^2} \quad (1.4)$$

where the arrow is used to distinguish photoexcitation strength functions from strength functions determined in decay processes, K is constant for any particular nucleus, and the quotient, involving the width Γ_G and energy E_G of the electric giant dipole resonance, is derived from the classical Lorentz line. The application of this strength function to γ -ray transitions from highly excited states to the ground state is straightforward, but its application generally to describe γ -decay to states other than the ground state requires an additional assumption. This assumption, usually referred to as the Brink hypothesis, states that an excited state has built on it a giant resonance similar to that for the ground state but shifted upward in energy by the energy of the excited state. With the strength function thus determined by the photoabsorption cross section, both the energy-dependence and A

dependence of the transition probability for $E1$ radiation vary more rapidly than in the Weisskopf estimate. Axel (Axe 62) showed from Eq. (1.4) that radiative widths should vary approximately as E_γ^5 and $A^{8/3}$ in the region of 7 MeV. Support for this A -dependence was first obtained by Carpenter (Car 62) who analyzed data from photonuclear reactions and thermal and resonance-averaged neutron-capture data. Support for the E_γ^5 dependence has been found by Bollinger and co-workers (Bol 68, BT 70) in several elements but examples where high powers of E_γ fit the observations better have been reported in other examples (e.g., Bol 70, Smi+ 72).

Evidence that subthreshold strength functions may have local irregularities or fine structure was early noted by Axel and co-workers (Axe+ 63). Of course the demonstrable fact that such irregularities are present in the giant resonance itself in light elements and at closed shells in heavy elements (FH 62b, Bow+ 70) makes it scarcely surprising that irregularities are present to some degree in the giant resonance tail in nuclei where the statistical model is more secure. The important questions are really: in what nuclei does this substructure occur, how important is it relative to the smooth statistical background, i.e., how does it modify or modulate the general Lorentz-like dependence, and to what nuclear structure is it related?

An important manifestation of irregular behavior of the strength function is the so-called 5.5-MeV “anomalous” bump appearing in various γ -ray spectra, particularly those following neutron-transfer reactions near closed shells. It was first noticed by Kinsey and co-workers (JK 51, K in 55) that the spectral distribution of high-energy γ -rays in elements near closed shells contained too much radiation to be easily accounted for by an E_γ^3 energy dependence for the transition probability and an exponential level-density energy dependence. The same effect was emphasized by Groshev and co-workers (Gro+ 58) and a quantitative demonstration of the effect in terms of the fraction of the total available energy (separation energy) radiated in γ -rays in the top half of the spectrum was given by Groshev (Gro 55). It was early pointed out by Bartholomew and co-workers (Bar+ 57), (Bar 62) that while this radiation near the top of the spectrum indeed had an anomalous *intensity* it did not appear to result from anomalously large *radiation widths*; i.e., strengths for the γ -rays concerned when compared to γ -rays from neighboring nuclei that did not exhibit the effect. Alternative explanations involving level-density effects were considered (Bar 62) but the crucial experiments identifying the effect not with irregularities in level density but in strength function were carried out by Bergqvist, Lundberg, and Starfelt (BS 62, LS 65) in fast-neutron capture. They showed that since

the 5.5-MeV γ -ray bump remained at ~ 5.5 MeV regardless of neutron bombarding energy from thermal energies to ~ 4 MeV it could not be accounted for by level-density effects. They also showed that neither a simple E_γ^3 law, nor the more rapid energy dependence derived from the Lorentz line, was sufficient to account for the observed spectral distribution and postulated instead that the true strength function be represented by a smooth giant resonance tail with a "pigmy resonance" superimposed on it at 5.5 MeV.* This work was shortly followed by evidence that the γ -rays in the bump were predominantly $E1$ (BGE 67). A similar γ -ray bump was found for excitation below the neutron threshold in studies of the $(d, p\gamma)$ reaction (Bar+ 70) and while strength functions extracted in that work in Au and neighboring nuclei showed departures from a smoothly varying energy dependence, it was again noted that the absolute strengths of γ -rays at 5.5 MeV were nevertheless little greater than those in Ta where no γ -ray bump was found. It became apparent that the 5.5-MeV radiation might, at least in some nuclei, be caused as much, or more, by a deficit of strength below 5.5 MeV than by a "resonance" at 5.5 MeV (Bar 69). Recent demonstrations by Loper and coworkers (LBT 72) that the strengths of γ -rays in the 5.5-MeV region in Au were not greater than those of γ -rays of the same energy in Ta further confirm this view. Recently, careful fitting of available capture γ -ray spectra with trial strength functions and recalculation of the strength functions extracted from $(d, p\gamma)$ reactions, both carried out with more realistic level densities (LBE 72, Lon+ 73) has led to a consolidation of previously conflicting data.

Evidence for the 5.5-MeV bump radiation has been found also in (γ, γ') (MW 69) and (p, γ) (Brz+ 71) reactions. However, it was early reported (Ber+ 66a) that no such radiation appears in the $(n, n'\gamma)$ reaction in elements where it is seen strongly in the (n, γ) reaction. Subsequent experiments showed that it was also absent in (μ^-, xny) reactions (EB 71) and in $(p, p'\gamma)$ reactions (Lon+ 72). An exception is $^{207}\text{Pb}(p, p'\gamma)^{207}\text{Pb}$ where a γ -ray spectrum very similar to that from $^{206}\text{Pb}(d, p\gamma)^{207}\text{Pb}$ was found (Bar 69).

* It is important not to confuse the bump in the γ -ray spectrum with the pigmy resonance in the strength function. The γ -ray bump is an experimental fact. The pigmy resonance, as originally presented, was primarily an analytical device introduced by analogy with the giant resonance in order to explain the bump. As we shall show, the bump can be generated with little or no pigmy resonance in the strength function. The adjective "anomalous" has also caused confusion. It applied only to the bump, not to features of the strength function, and reflected the difficulty of accounting for the bump with the aid of a smoothly varying strength function.

Recent information on individual $M1$ γ -ray strengths has been tabulated by Bollinger (Bol 68). It was found that, for γ -rays near 7 MeV in elements with $A > 90$, the average γ -ray width for $M1$ radiation is closer to that for $E1$ radiation than was deduced earlier from more limited data (Bar 61). Furthermore, exceptionally strong $M1$ transitions have been reported near closed shells in (n, γ) reactions (HSM 65, UVL 66) and local concentrations of strength have been observed in photonuclear (Bow+ 70, TJ 72, Wol+ 72) and electron scattering (PW 71) reactions. The energy dependence of $M1$ strength in the region between 5 and 8 MeV approximately has been studied in a few elements (Bol 68, BT 70, LEB 70). Although the above information taken together is fragmentary, support for the neutron spin flip mechanism (Mot 60, Bri 63) and for predicted peaks in the $M1$ strength function below 9 MeV approximately (SE 69) appears to be accumulating.

Recent reviews stressing the determination of radiation strengths for individual γ -rays, mostly by the resonance-average technique, have been given by Bollinger (Bol 68, BT 70). A review of experimental and theoretical work concerning the reaction mechanism of neutron capture has been published by Bergqvist and Starfelt (BS 70a). A general review of radiative properties following resonant neutron capture has been provided by Chrien (Chr 72). Axel (Axe 68) has discussed the significance of the γ -ray strength function in relation to intermediate structure and the spreading of single-particle strength. Lane (Lan 71, Lan 72) has reviewed the theoretical implications of the 5.5-MeV anomalous radiation in the broader context of partial width correlations and common doorway states. In the present paper we study the functional form and other properties of the gamma-ray strength function as determined experimentally in photoexcitation, neutron transfer, and other reactions in heavy elements. This review supersedes an earlier survey (Bar 69) that covered some of this material. The subject of beta strength functions is reviewed in the companion paper by Hansen (Han 73).

In Sec. 2, a brief review is given of the theoretical concepts and expressions needed for subsequent discussion. In Sec. 3 we review critically the several methods for measuring and extracting strength function information. In Sec. 4 we compare the strength functions from these various methods, discuss their accuracy and reliability, and review the evidence for gross substructure. In Sec. 5 we summarize the present experimental picture in photon strength functions and attempt to relate this to theoretical notions in current use.

2. THEORETICAL BACKGROUND

The theory of radiative process in nuclei has been discussed by many authors (see for example BW 52, LL 60, dST 63, Lyn 68, BM 69). Since this review is concerned mainly with determinations from experiment of the energy dependence of strengths of various multipoles in a restricted energy range in heavy elements, no attempt is made to provide a comprehensive summary of the theory. In this section we merely establish nomenclature and outline concepts based on statistical models needed for the ensuing presentation and discussion of results.

2.1. Nomenclature

In discussing radiative processes we shall use the convention illustrated in Fig. 1. In order to identify the γ -ray transitions between states, two indices will be used. The index λ for the upper state or group of states (hereafter, for the sake of clarity, referred to as *levels*) and the index i for the lower state or group of states ($E_i < E_\lambda$) involved in the transitions of interest. Both λ and i are running indices. For brevity we use J as short for J_λ^π to indicate a specific spin and parity of the upper level or group of levels, λ . Symbols are defined in Table I.

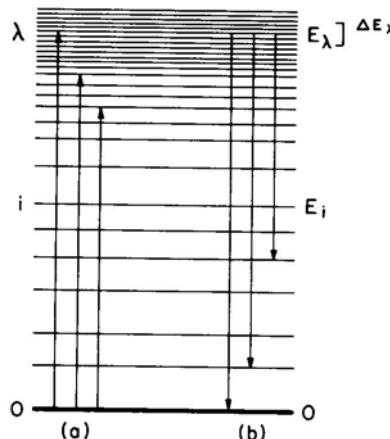


Fig. 1. Nomenclature. The index λ denotes the upper level or group of levels of the same J_λ^π and the index i the lower state or group of states. Radiation width distributions (a) for photoabsorption to a range of levels, λ , and (b) for γ -decay from a localized interval of levels, λ , to a range of lower states, i , are illustrated.

TABLE I
Nomenclature

Symbol	Abbreviation	Definition
B_{XL}		Reduced transition rate for multipole XL
C_{XL}		Energy weighted sum of the reduced matrix elements for multipole XL
$D_J(E)$	D_J	Spacing of levels of spin J at excitation E
E_B		Neutron separation energy
E_G		Giant resonance peak energy
E_γ		Gamma-ray energy
E_n		Neutron bombarding energy
E_t		Energy below which discrete levels are adopted for spectra calculations
$\hat{f}_{i\lambda XL}^J$	\hat{f}	Strength function for photoexcitation, from the initial state at excitation E_i , of levels of single spin J within unit energy interval at $E_\lambda = E_\gamma + E_i$ by radiation of type X and multipolarity L . Normally the initial state is the ground state ($i = 0$). The arrow implies that the target state i is fixed and the excited level λ is variable.
$\hat{f}_{i\lambda XL}^J$	\hat{f}	Strength function for decay of levels of single spin J within unit energy interval at E_λ to a state at energy E_i by emission of radiation of multiple XL . The arrow indicates that the initial level λ is fixed and the final state i is variable.
g_J	g	Statistical factor $(2J + 1)/(2J_0 + 1)$
$\Gamma_{\gamma i \lambda XL}^J$	$\Gamma_{\gamma i \lambda}$	Partial radiative width for the transition between level λ of spin J and state i . ($E_\lambda > E_i$)
$\Gamma_{\gamma T \lambda}^J$	$\Gamma_{\gamma T \lambda}$	Total radiative width of a spin- J level at excitation energy E_λ .
$\Gamma_{T \lambda}^J$	$\Gamma_{T \lambda}$	Total width of the spin- J level at excitation energy E_λ .
I_G		Width of the giant resonance
I_γ		Individual γ -ray intensity
J, J_0		J and J_0 represent spin of the compound and target state respectively.
k_{E1}		Individual electric dipole γ -ray strength $\Gamma_{\gamma i \lambda E1}/[E_\gamma {}^3D_J(E_\lambda)A^{2/3}]$
k_{M1}		Individual magnetic dipole γ -ray strength $\Gamma_{\gamma i \lambda M1}/[E_\gamma {}^3D_J(E_\lambda)]$
$\nu_{i\lambda XL}^J$	$\nu_{i\lambda}$	Average γ -ray spectral distribution per unit γ -ray energy interval of primary γ -radiation of multiple XL from a level at an excitation E_λ with unit population to states at excitation E_i .

TABLE I (*continued*)

Symbol	Abbreviation	Definition
$\nu_{t\lambda XL}$	$\nu_{t\lambda}, \nu$	Average γ -ray spectral distribution per unit γ -ray energy interval of primary plus secondary and subsequent γ -radiations of multipole XL per γ -ray energy interval from a level at excitation E_λ with unit population.
P_λ		Population of level λ
$P(E_\gamma)$		Pulse-height distribution
$\varrho_J(E)$	ϱ_J, ϱ	Level density of spin- J states at excitation E
S		Statistical fluctuation factor $\bar{\Gamma}_i \bar{\Gamma}_j / \bar{\Gamma}_i \bar{\Gamma}_j$
σ_{OG}		Peak giant dipole resonance cross section
σ		Spin-cutoff parameter
$\bar{\sigma}_{\gamma a XL}^J(E_\gamma)$	$\bar{\sigma}_{\gamma a}$	Average photoabsorption cross section for γ -rays of type X and multipolarity L and excitation of compound level of spin J at energy E_γ . The symbols $\bar{\sigma}_{\gamma\gamma}$, $\bar{\sigma}_{\gamma\gamma'}$, $\bar{\sigma}_{\gamma n}$, $\bar{\sigma}_{\gamma f}$, and $\bar{\sigma}_{\gamma p}$ are used for (γ, γ) , (γ, γ') , (γ, n) , (γ, f) , and (γ, p) reactions respectively. The total cross section $\sum_{\gamma'} \bar{\sigma}_{\gamma\gamma'}$ is indicated by $\bar{\sigma}_{\gamma T}$.
XL		X represents the multipole type, electric (E) or magnetic (M), and L the multipolarity.

2.2. Strength Functions

Experimentally one encounters two types of radiation width distribution with respect to γ -ray energy; the distribution for photoabsorption from a low energy state, usually the ground state, to a range of excited levels and the distribution for γ -decay from a localized interval of excited levels to a range of lower states. These are illustrated by the arrows in Fig. 1. We use \vec{f} and \bar{f} to differentiate between the corresponding photoexcitation and γ -decay strength functions.

The strength function for photoexcitation from the ground state of levels of spin J within unit energy interval at E_λ by radiation of type X and multipolarity L is

$$\vec{f}_{0\lambda XL}^J(E_\gamma) = \frac{\bar{\Gamma}_{\gamma 0\lambda XL}^J \varrho_J(E_\lambda)}{E_\gamma^{2L+1}} \quad (2.1)$$

where $E_\gamma = E_\lambda$ and other symbols are defined in Table I. The strength function is proportional to the amount of reduced matrix element squared, $(2J + 1) B_{XL}$ (BM 69, p. 382) per unit excitation energy interval.

The strength function for decay of levels of spin J within unit energy interval at E_λ to a state at energy E_i by emission of radiation of multipole XL is

$$\tilde{f}_{i\lambda XL}^J(E_\gamma) = \frac{\bar{\Gamma}_{\gamma i\lambda XL}^J \varrho_J(E_\lambda)}{E_\gamma^{2L+1}} \quad (2.2)$$

where $E_\gamma = E_\lambda - E_i$. In this process E_λ is fixed and E_i is a variable. It is understood that the averages in Eqs. (2.1) and (2.2) are over large numbers of levels of the same spin and parity, at E_λ .

At high excitation energies the wavefunctions of the physical states contain a large number of configurations. These give rise to a broad distribution of the individual reduced widths. There is now much evidence (Bol 70) that, for γ -rays, this distribution is a χ^2 distribution with one degree of freedom or the Porter–Thomas (PT 56) distribution

$$P\left(\frac{\Gamma_\gamma}{\bar{\Gamma}_\gamma}\right) = \left(\frac{2\pi\Gamma_\gamma}{\bar{\Gamma}_\gamma}\right)^{-1/2} e^{-\Gamma_\gamma/2\bar{\Gamma}_\gamma} \quad (2.3)$$

With this distribution the uncertainty in the strength function for a sample of m states is

$$\Delta f = f \sqrt{2/m} \quad (2.4)$$

Predictions of the energy dependence of the gamma-ray strength function vary with the model used. On the extreme statistical assumption, that the single-particle strength is distributed equally among the physical states of the nucleus, Blatt and Weisskopf (BW 52) predicted that the strength function for any multipole is independent of energy. In this model there is no distinction between \vec{f} and \tilde{f} . The absolute magnitudes of the strength function depend on the values of the nuclear radius and the spacing between single-particle shells. These estimates have been discussed by several authors (e.g., Bar 61, Bol 70). As discussed in Sec. 1 these single-particle estimates are too crude to explain the observed energy dependence of the $E1$ strength function or to give accurately the relative strengths of various multipoles (see Sec. 4).

A more refined estimate of the strength function \vec{f} is obtained from the photoabsorption cross section (Axe 68):

$$\vec{f}_{0\lambda XL}^J(E_\gamma) = 26 \cdot 10^{-8} \frac{\bar{\sigma}_{\gamma a XL}^J(E_\gamma)}{g_J E_\gamma^{2L-1}} (\text{MeV})^{-(2L+1)} \quad (2.5)$$

where g_J is the statistical factor $(2J + 1)/(2J_0 + 1)$, $\bar{\sigma}_{\gamma a XL}^J$ (mb) is the average absorption cross section of a nucleus in the ground state of spin J_0 for excitation of levels of spin J at energy $E_\lambda = E_\gamma$ (MeV).

On a classical damped simple harmonic oscillator model, the energy dependence of the average absorption cross section summed over all allowed J 's is given by the Lorentz line shape (Bri 55, Bri 63, DG 65)

$$\begin{aligned}\bar{\sigma}_{\gamma aXL}(E_\gamma) &= \sum_J \bar{\sigma}_{\gamma aXL}^J(E_\gamma) \\ &= C_{XL} \frac{\Gamma_G E_\gamma^2}{(E_\gamma^2 - E_G^2)^2 + \Gamma_G^2 E_\gamma^2}\end{aligned}\quad (2.6)$$

where the quantity C_{XL} depends on the multipolarity and can in principle be obtained from sum rules (Jac 67). For electric dipole radiation the sum rule is independent of nuclear models; however, there is an uncertainty of up to a factor of two due to the lack of precise knowledge of the magnitude of exchange terms in nuclear forces (LB 50). For other multipoles (electric or magnetic) the sum rule depends on specific nuclear models and details of two-body forces.

From the electric dipole sum rule we obtain (Hay 65)

$$\bar{\sigma}_{\gamma aE1}(E_\gamma) = 38 \frac{NZ}{A} (1 + 0.8x) \frac{\Gamma_G E_\gamma^2}{(E_\gamma^2 - E_G^2)^2 + \Gamma_G^2 E_\gamma^2} \text{ mb} \quad (2.7)$$

where x is the fraction of exchange forces present in the nuclear forces (LB 50) and all energies are in MeV.

Brink (Bri 55) has shown that a modified energy-weighted sum of squares of the reduced matrix elements for any multipole moment (summed over levels with a particular total angular momentum J) is also independent of J . Then assuming that the energy dependence of the photoexcitation cross section for any spin states is given by the Lorentzian, the cross section for spin J states is

$$\bar{\sigma}_{\gamma aE1}^J = \frac{g_J}{3} \bar{\sigma}_{\gamma aE1} \quad (2.8)$$

Because of the nuclear-model dependence of the sum rules it is not practical to write a general expression for cross section for other multipoles. Estimates of the strength functions from specific nuclear models have been discussed by several authors, for example for $E1$ in ^{208}Pb (KH 73, Lan 71, Per 70, KBB 70, GGS 66), for $M1$ (Hkw 72, SE 69) and valence model for $E1$ and $M1$ (Lyn 68). In this paper we first present the experimental strength function without invoking specific nuclear models, using the Lorentz line shape for comparison. In Sec. 5 we discuss deviations of the empirical strength function from the Lorentzian shape in the light of some recent models.

Both the extreme statistical model (BW 52, page 645) and the classical damped simple harmonic oscillator model [see Eqs. (2.5), (2.7) and (2.8)] predict that the strength function is independent of J . In both cases the arguments are, in principle, based on the assumption that the wave functions of the highly excited levels contain a large number of configurations. Lynn shows that even in the valency capture model (see Lyn 68, page 329) if the number of configurations (one for each valency transition) contributing to the partial width are large, then the strength function has little dependence on the spins of the levels. The broad distribution of the observed individual reduced widths, i.e., the Porter-Thomas distribution, indicates that these transitions are from complicated levels. Therefore we shall assume J -independence of the strength function and henceforth drop the J superscript. However, it should be borne in mind that the strength function as used in this paper refers to a single J for the states λ .

It is not immediately obvious (except in the case of the extreme statistical model) that \vec{f} should be identical to \tilde{f} . For electric dipole radiation equating $\vec{f}_{0\lambda E_1}(E_\gamma) = \vec{f}_{i\lambda' E_1}(E_\gamma) = \tilde{f}_{i\lambda' E_1}(E_\gamma)$ is tantamount to assuming, following Brink (Bri 55), that the energy dependence of the photoeffect is independent of the detailed structure of the initial state, so that if it were possible to perform the photoeffect on an excited state, the cross section for absorption would have the same energy dependence as for the ground state. Rosensweig has presented plausibility arguments in support of this hypothesis (Ros 68). A thorough experimental verification has yet to be made.

In practice, it is possible to measure $\vec{f}_{0\lambda XL}$ for all E_λ 's but exceedingly difficult if not impossible to obtain $\vec{f}_{i\lambda XL}$ ($i > 0$). On the other hand, one may, in principle, determine all $\vec{f}_{i\lambda XL}$. For E_λ above a particle threshold one can obtain $\vec{f}_{i\lambda XL}$ by detailed balance from the corresponding capture reaction. With this method Allas *et al.* (All+ 64) have shown that in ^{12}C the γ -ray strength functions based on the ground state and the first excited state are similar and depend only on the γ -ray energy. Below the particle threshold one can use the (γ, γ') reaction to obtain $\vec{f}_{i\lambda XL}$ for i near the ground state by measuring the elastic to inelastic scattering ratio as a function of E_λ . However, no such attempt has been made. Confirmation of the compatibility of $\vec{f}_{0\lambda E_1}$ with $\tilde{f}_{i\lambda' E_1}$ for the restricted case where E_λ represents the excitation energy interval at the neutron separation energy and $E_i < 4$ MeV, is obtained from the spectrum average technique discussed in Sec. 3.4. One can, in principle, determine all $\vec{f}_{i\lambda XL}$ by the sequential extraction method described in Sec. 3.3. It yields the functional form (energy dependence) of the $\vec{f}_{i\lambda XL}$ but not their absolute normalization. However, for

the purpose of testing the Brink hypothesis one need only show that the functional forms of $\tilde{f}_{i\lambda XL}$ for all λ and of $\tilde{f}_{0\lambda XL}$ in the energy range $0 \leq E_\gamma \leq E_\lambda$ are the same. Unfortunately, as will be discussed in Sec. 5 these conditions have as yet not been achieved in any one nuclide.

In the absence of a rigorous proof of this hypothesis, it would be admissible to proceed by assuming that it is true, and subsequently to examine the consequences of having made the assumption. However, in this review we will find it convenient in presenting strength functions derived from experiment to maintain the distinction between \tilde{f} and \tilde{f} . But, guided by experimental results discussed in Sec. 3.3, we shall assume that the functional form of $\tilde{f}_{i\lambda XL}$ is independent of the levels involved. For simplicity we write \tilde{f}_{XL} , in referring to photoexcitation from the ground state to levels λ , and \tilde{f}_{XL} in referring to decay transitions from a fixed level λ to final states i .

In Eq. (2.5) the strength function is expressed in terms of the photoabsorption cross section. Because of the competition from other processes it is impractical to measure the photoabsorption cross section below the particle threshold. Instead the elastic or, more often, the quasielastic scattering cross section is usually measured. This can be related to the photoabsorption cross section by

$$\tilde{\sigma}_{\gamma\gamma'XL}^J(E_\gamma) = \tilde{\sigma}_{\gamma aXL}^J(E_\gamma) \frac{\bar{\Gamma}_{\gamma i\lambda XL}^J}{\bar{\Gamma}_{\gamma T\lambda}^J} S \quad (2.9)$$

where the statistical fluctuation factor $S = \overline{\Gamma_{\gamma i\lambda} \Gamma_{\gamma 0\lambda}} / (\bar{\Gamma}_{\gamma i\lambda} \bar{\Gamma}_{\gamma 0\lambda})$ depends on the statistical distribution of the partial widths and the size of the sample. For a sample size, $n_\lambda > 100$, and with a Porter-Thomas distribution of the partial widths, S is 3. It decreases with sample size, becoming unity for $n_\lambda = 1$. The branching ratio $\bar{\Gamma}_{\gamma i\lambda XL}^J / \bar{\Gamma}_{\gamma T\lambda}^J$ can be calculated as discussed in Secs. 2.3 and 3.1.

2.3. Spectral Distributions

The average spectral distribution $\nu_{i\lambda XL}^J(E_\gamma)$ per unit γ -ray energy of primary γ -rays of type X and multipolarity L from an excited level of spin J at an excitation energy E_λ with unit initial population is

$$\begin{aligned} \nu_{i\lambda XL}^J(E_\gamma) &= \frac{\bar{\Gamma}_{\gamma i\lambda XL}^J}{\bar{\Gamma}_{T\lambda}^J} \sum_{I=J-L}^{J+L} \varrho_I(E_i) \\ &= E_\gamma^{2L+1} \frac{\tilde{f}_{XL}(E_\gamma)}{\bar{\Gamma}_{T\lambda}^J} \frac{\sum_{I=J-L}^{J+L} \varrho_I(E_\lambda - E_\gamma)}{\varrho_J(E_\lambda)} \end{aligned} \quad (2.10)$$

where $\bar{\Gamma}_{T\lambda}^J$ is the average total width, and $\varrho_I(E_i)$ is the density of states, at an excitation $E_i = E_\lambda - E_\gamma$, which combine with levels of spin J for emission of radiation of multipole XL .

The average total radiative width is given by

$$\begin{aligned}\bar{\Gamma}_{\gamma T\lambda}^J &= \sum_{XL} \int_0^{E_\lambda} \bar{\Gamma}_{\gamma i\lambda XL}^J \sum_{I=J-L}^{J+L} \varrho_I(E_i) dE_i \\ &= \sum_{XL} \int_0^{E_\lambda} E_\gamma^{2L+1} \tilde{f}_{XL}(E_\gamma) \frac{\sum_{I=J-L}^{J+L} \varrho_I(E_\lambda - E_\gamma)}{\varrho_J(E_\lambda)} dE_\gamma \quad (2.11)\end{aligned}$$

For levels above the particle threshold, $\bar{\Gamma}_{T\lambda}^J$ in Eq. (2.10) includes the total radiative width and the widths for all particle channels.

Information on the level-density distributions needed for these calculations must be obtained from other sources. Excellent recent summaries of the theoretical and experimental situations have been provided by Block (Blo 72), French and Chang (FC 72) and Huizenaga (Hui 72). However, none of the theoretical level-density formulas are adequate near closed shells and at low excitation energies. There have been several attempts to calculate the level densities with combinatorial methods (e.g., HG 69) using shell-model states. Although somewhat more realistic than the free Fermi gas model, these methods suffer from uncertainties in the numbers and energies of the shell-model states included in the calculation.

The J -dependence of the level density is usually assumed to be given by (Bet 36, Blo 72)

$$\varrho_J(E) = \varrho_0(E)(2J + 1)e^{-(J+1/2)^2/2\sigma^2} \quad (2.12)$$

where ϱ_0 denotes the density of levels with $J = 0$ and σ is the spin-cutoff factor. This formula is applicable to both parities and is based on the assumption that the nuclear system can be represented by a system of independent Fermi particles. The derived level density is then a well-defined function of the single-particle level density, which can be defined by means of Laplace transforms. The functional form of $\varrho_0(E)$ and the spin-cutoff factor σ depend on the models used for the single-particle level density and the method used for inverting the Laplace transform (Blo 72). The factorization of ϱ_J into spin-dependent and spin-independent parts depends, in principle, on the assumption that a large number of particles are excited (Eri 60). However, this assumption breaks down, and therefore Eq. (2.12) may not be valid, for energies near the ground state. Even at higher excitation energies the validity of Eq. (2.12) has not been fully investigated. This factorization of the level-density formula into spin-

and energy-dependent terms is extremely useful provided σ is independent of energy. Then for dipole radiation for excitation energies below all particle thresholds, Eq. (2.10) reduces to

$$\nu_{i\lambda X1}(E_\gamma) = 3 \frac{E_\gamma^3 \tilde{f}_{X1}(E_\gamma)}{\bar{\Gamma}_{\gamma T\lambda}} \frac{\varrho_0(E_\lambda - E_\gamma)}{\varrho_0(E_\lambda)} \quad (2.13)$$

which implies that the spectral distribution is independent of the spins of the states involved. The nondependence of $\bar{\Gamma}_{\gamma T\lambda}$ on J follows from Eq. (2.11). The observed total radiation widths of neutron resonances ($E_\lambda \simeq 6$ MeV) show no significant dependence on the spins, $J_0 - \frac{1}{2}$ and $J_0 + \frac{1}{2}$, of s -wave neutron resonances in target nuclei with spin J_0 ranging from 0 to $\frac{7}{2}$ (Lyn 68). This observation provides confirmation that \tilde{f} is independent of J and to some extent supports the validity of Eq. (2.12), although it sheds but little light on the energy dependence of σ , since the spins involved are low.

If we assume that the spin-cutoff factor is energy-dependent then Eq. (2.13) is not valid and both $\bar{\Gamma}_{\gamma T\lambda}$ and $\nu_{i\lambda X1}$ depend on the spin of the states at E_λ . Gilbert and Cameron (GC 65) show that for a free Fermi gas model, $\sigma \propto (E)^{1/4}$. Combinatorial calculations (HG 69) also show that at low excitation energies, in general, low spin levels predominate. Again this can be simulated by making σ energy-dependent. Under these circumstances one must use Eq. (2.10) for the calculation of spectral distributions.

In the theoretical level-density formulas the functional form of ϱ_0 depends on the theoretical model assumed. In this paper, for the analysis in Sec. 3 we need level densities near closed shells and for excitation energies from the ground state to ~ 8 MeV. This is the region where these models are found to be inadequate. From a review of the data available to 1965, Gilbert and Cameron (GC 65) showed that an expression of the type $\varrho_0 \propto e^{2\sqrt{aE}}$ could not be valid simultaneously for the lower levels and for the neutron and proton resonances. On the other hand, they found that a formula of the type $\varrho_0 \propto e^{E/T}$ gave a good fit to the experimental data over the first few MeV of excitation energy. A review of the data shows that the functional forms $\varrho_0 \propto (E - E_0)^{-2} e^{2\sqrt{a(E-E_0)}}$ or $\varrho_0 \propto e^{E/T}$ can be fitted to the known level densities (Gol+ 66, Gro+ 68, 69) up to an excitation energy of ~ 8 MeV. Similar conclusions were drawn by Maruyama (Mar 69), who investigated the functional forms of the level densities needed to fit the neutron yields from the (n, n') reactions in several nuclei. In even-even nuclei the concept of the statistical level density has no validity at an excitation energy below the pairing gap. Therefore in this paper, for excitation energies E above a lower limit E_t approximately equal to the pairing

gap, we adopt the level-density formula Eq. (2.12), for both parities, with

$$\rho_0 = Ae^{E/T} \quad (2.14)$$

where the constants A and T are determined empirically from the known level densities (normalized to zero spin) 1–2 MeV above the ground state and at the neutron threshold. Below E_t the known discrete levels are adopted with their appropriate spins and parities.

3. EXPERIMENTAL METHODS

Four experimental methods for the determination of γ -ray strength functions will be considered. The first, involving *photoexcitation techniques*, leads to determinations of \tilde{f} ; the other three to determinations of \tilde{f} . In the second method, herein called the *spectrum fitting method*, \tilde{f} is found by trial fitting of various forms of strength function in a calculation reproducing the total γ -decay spectral distribution. In the third method, *sequential extraction*, the primary γ -ray spectral distribution is extracted from the data thereby enabling a unique \tilde{f} to be deduced by Eq. (2.13). In the fourth method, called the *high-resolution γ -ray method*, \tilde{f} is found by applying Eq. (2.2) to high-energy γ -rays known, or presumed to be, primaries.

In this section each of the four methods is discussed in turn with attention to its underlying assumptions and inherent experimental limitations. Some of the assumptions are supported by direct experimental evidence but discussion of those experiments is deferred to later sections. At the end of this section we compare the advantages and disadvantages of the various methods.

3.1. Photoexcitation Method

The photoexcitation strength function \tilde{f} may be extracted from photoexcitation experiments in which the energy spread of the incident γ -radiation is greater than the level spacing $D(E_\gamma)$ so that averages over the initial states λ are obtained, as it were, automatically. If available, variable energy incident beams of resolution high enough to resolve individual levels could also be used to obtain radiation widths of such levels from which average values could then be derived to determine the strength function. So far, because of inadequate resolution of variable-energy beams, few experiments have fallen into this category. However, much the same thing is accomplished in several experiments in which high-resolution detectors are used, thereby permitting individual resonances to be examined in spite of poor beam resolution.

In this section the various photoexcitation techniques are described and the extraction of \vec{f} from the measurements is discussed in some detail. Inelastic scattering experiments at individual resonances from which the γ -decay strength function \vec{f} may be determined are also discussed briefly.

Determinations of \vec{f} require that one first obtain $\bar{\sigma}_{\gamma a}$, from which the strength function is deduced with the aid of Eq. (2.5) or related expressions, or that one obtain $\Gamma_{\gamma 0\lambda}$ for individual transitions and then, after averaging over several resonances near E_λ , obtain \vec{f} from Eq. (2.1). In practice, transmission measurements yielding $\bar{\sigma}_{\gamma a}$ directly are usually not feasible because of the much larger cross sections for competing atomic absorption processes and hence one must resort to indirect estimation of $\bar{\sigma}_{\gamma a}$ from measurements of other cross sections such as $\bar{\sigma}_{\gamma n}$, $\bar{\sigma}_{\gamma f}$, $\bar{\sigma}_{\gamma\gamma}$, and $\bar{\sigma}_{\gamma\gamma'}$, various combinations of which dominate $\bar{\sigma}_{\gamma a}$ depending on the nucleus and the energy regime in question.

3.1.1. Measurements above the Neutron Threshold

In nonfissionable heavy nuclei, in the energy range from a few hundred keV above the neutron separation energy to the energy, usually 1–3 MeV higher, where charged particle emission becomes important one has, to a good approximation, $\Gamma_n \gg \Gamma_\gamma$ and hence $\bar{\sigma}_{\gamma a} \simeq \bar{\sigma}_{\gamma n}$. If dominance of dipole radiation is assumed, Eq. (2.5) can then be written

$$\vec{f}_{x1} = \frac{26 \cdot 10^{-8} \bar{\sigma}_{\gamma n} (\text{mb})}{gE_\gamma (\text{MeV})} \quad (3.1)$$

where it is understood that $\bar{\sigma}_{\gamma n}$ is averaged over all levels of appropriate J and \vec{f} is in MeV^{-3} units.

The photoneutron cross section has been measured for most heavy natural element targets (see photonuclear review (FGC 70)). Early measurements (NH 54, FH 56) were made with a broad bremsstrahlung beam and differential analysis was used to extract $\bar{\sigma}_{\gamma n}$ from neutron yields measured with a 4π “Halpern-type” BF_3 counter (GF 67). More recently incident photon beams with energy spreads of 100–200 keV, from positron annihilation in flight (Ful+ 69, Bei+ 69) have resulted in much improved data. Examples of $\bar{\sigma}_{\gamma n}$ data obtained by these methods (FH 62b, Bei+ 69) for targets of ^{206}Pb , ^{208}Pb , and ^{209}Bi are shown in Fig. 2.

In fissionable nuclei above the neutron separation energy the photoabsorption cross section is given to good approximation by

$$\bar{\sigma}_{\gamma a} = \bar{\sigma}_{\gamma n} + \bar{\sigma}_{\gamma f} \quad (3.2)$$

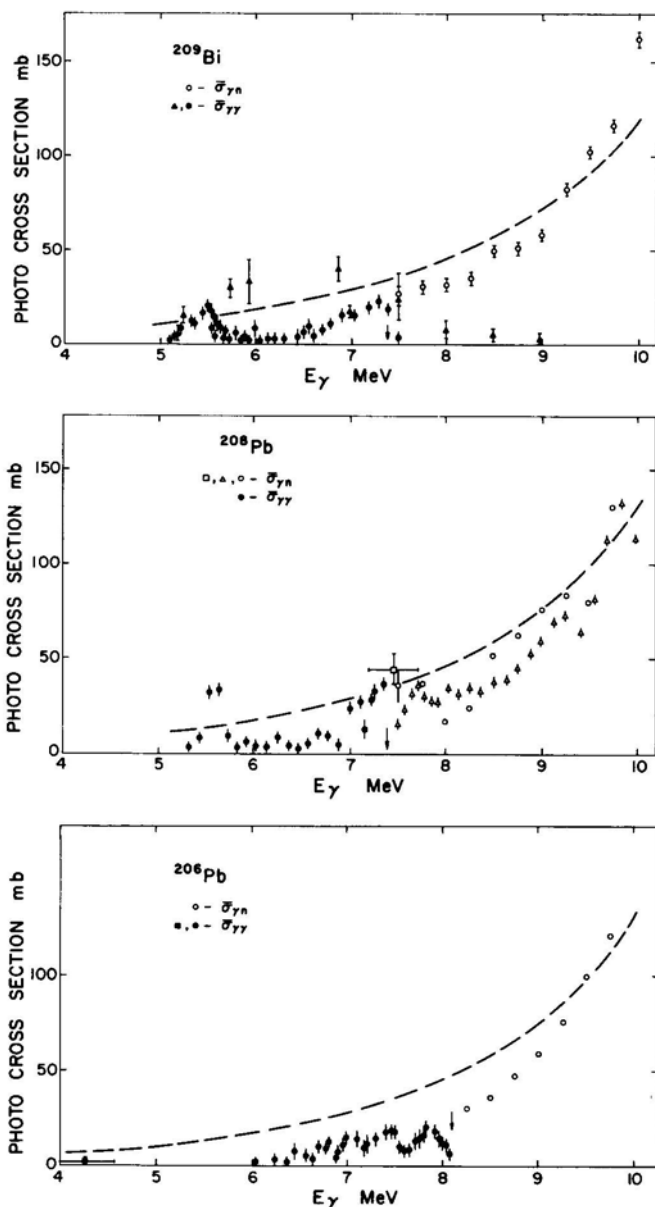


Fig. 2. The photo cross section for Bi and Pb isotopes. The photoneutron cross sections $\bar{\sigma}_{\gamma n}$ of ^{209}Bi , ^{208}Pb , and ^{206}Pb , above the neutron threshold (indicated by the vertical arrow) are indicated by \circ (FH 62b), \triangle (Bei + 69) and \square (Bow + 70). The photoelastic cross sections $\bar{\sigma}_{\gamma\gamma}$ are indicated by \blacktriangle (FH 62a), \blacksquare (Swa 73a), and \bullet (Axe + 63) in ^{209}Bi and ^{206}Pb and (KK 67) in ^{208}Pb . The broken line shows the Lorentzian fitted to the giant dipole resonance with constants given in Table V.

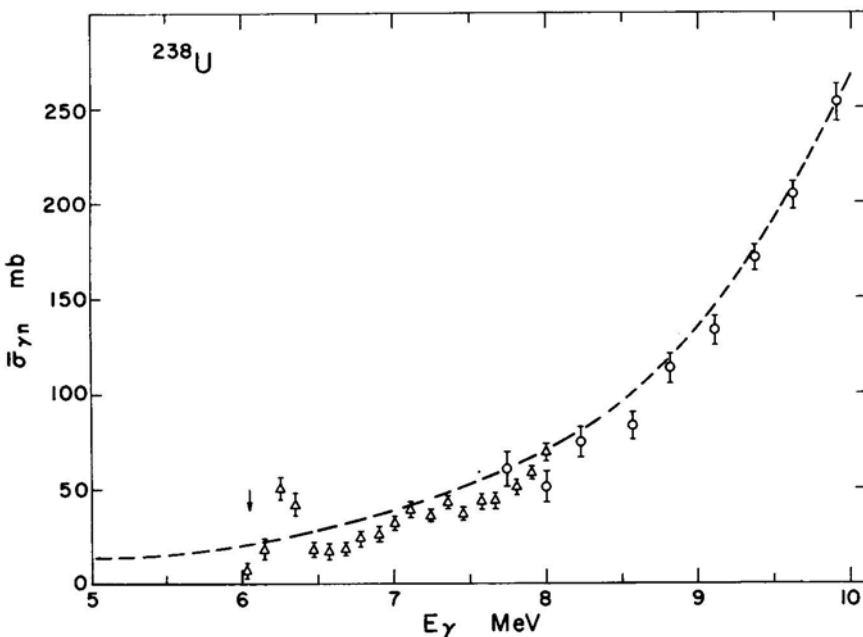


Fig. 3. The photoabsorption cross section $\bar{\sigma}_{\gamma a}$ of ^{238}U from references; Δ , (KM 73) and O, (Ber + 72). For other details see Fig. 2.

The energy dependence of $\bar{\sigma}_{\gamma a}$ for ^{238}U given in Fig. 3 was obtained from the photoneutron and photofission measurements of Bergère *et al.* (Ber + 72) and Knowles and Mafra (KM 73) shown by circles and triangles, respectively.

The γ -ray beam used by Knowles and Mafra (KM 73) was produced by the Compton-monochromator facility (KA 66) at Chalk River Nuclear Laboratories. This device provides a variable-energy γ -ray beam between 3 and 8.3 MeV with energy spread of $\sim 2.5\%$. The source of radiation is an intense line spectrum of maximum energy 8.99 MeV from the $^{58}\text{Ni}(n, \gamma)^{59}\text{Ni}$ reaction produced by a nickel plate located in a region of high flux in a reactor beam tube. Any energy between 3 and 8.3 MeV may be selected by Compton scattering from a wide, curved, aluminum scatter-plate. The geometry is such that γ -radiation impinging on the target, following scattering of a particular source γ -ray from all parts of the scatterer, is monoenergetic and may be varied by changing the position of the target relative to source and scatterer.

In a related high-resolution experiment, (Kno 70) the unscattered nickel γ -rays, Doppler-broadened by thermal motion in source and target

to an effective beam width of 10–18 eV at 5–9 MeV, were allowed to impinge on a ^{238}U target. At energies above about 7 MeV, the level densities in ^{238}U are high enough that more than one $J = 1$ state would be expected to be excited by such a beam, and \vec{f} and fluctuations of \vec{f} could be measured (Kno 70). Below 7 MeV in ^{238}U , and higher energies in lighter nuclei, photoexcitation by a high-resolution beam occurs only through chance overlap between the beam energy and a level energy. Experiments of this type have been most extensively exploited by Israeli workers (Ben + 66, MSW 70). While they provide useful information on the widths and other parameters of isolated levels they do not provide much information on the average behavior of γ -ray strength functions.

A powerful method of studying photoexcitation with high-resolution detectors in a restricted energy range above the neutron separation energy is the so-called threshold photonuclear technique. In this method, which was first used by Bertozzi *et al.* (BST 63) and later developed by others (BSB 66, JS 71), 5–10 MeV electrons from a linac are used to produce bremsstrahlung which is incident on the target under study. The energy of the electrons is adjusted so that the highest-energy bremsstrahlung just exceeds the (γ, n) threshold and hence only neutron transitions to the ground state of the product nucleus are energetically possible. The neutron energy, determined by time-of-flight techniques, can be found very precisely and resonances in the compound nucleus can therefore be observed with good resolution as peaks in the ground-state neutron spectrum. In measurements on isotopes of lead, Bowman *et al.* (Bow + 70) and Toohey and Jackson (TJ 72) have studied the shapes and thus the widths of individual resonances from 0 to 1 MeV above the neutron separation energy. The results of Toohey and Jackson (TJ 72) (Fig. 4) are typical of this technique. By the same methods, the average level spacing between resonances can be determined and the spin and parity of the compound nucleus and hence information on the multipolarity of the absorbed radiation can be obtained by measuring the neutron angular distributions. This, then, is a valuable method for studying properties of individual resonances and for obtaining \vec{f} [with the aid of Eq. (2.5)] in a restricted range above the neutron separation energy.

3.1.2. Measurements below the Neutron Threshold

Below the neutron separation energy and fission threshold, $\bar{\sigma}_{\gamma a}$ is given by

$$\bar{\sigma}_{\gamma a} = \bar{\sigma}_{\gamma\gamma} + \sum_{\gamma'} \bar{\sigma}_{\gamma\gamma'} \quad (3.3)$$

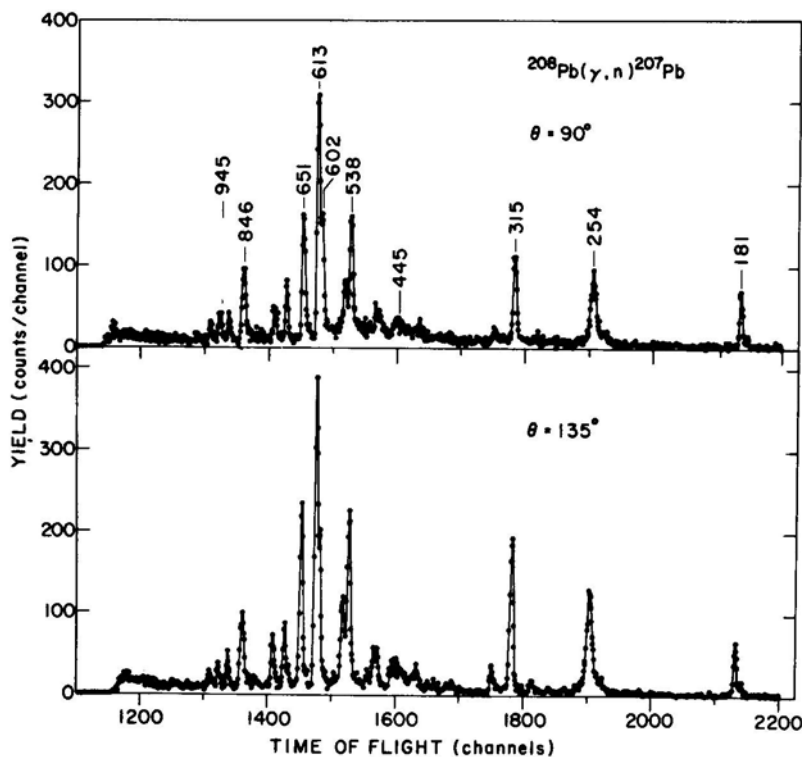


Fig. 4. The threshold photoneutron yield in $^{208}\text{Pb}(\gamma, n)^{207}\text{Pb}$ measured at 90 and 135° (TJ 72) plotted as a function of the neutron time-of-flight. Peaks are labeled with the neutron energy in keV.

and determinations of $\bar{\sigma}_{\gamma a}$ and hence \bar{f} require measurements of the elastics $\bar{\sigma}_{\gamma\gamma}$, and total inelastic scattering cross sections or, alternatively, what in effect amounts to a measurement of $\bar{\sigma}_{\gamma\gamma}$ plus a measurement, or judicious estimate, of the ground-state branching ratio.

For the more common experimental situation in heavy nuclei where the energy spread of the incident γ -ray beam spans many resonances so that the complexity of the inelastic spectrum precludes an accurate measurement of the branching ratio, one may still determine \bar{f} by measuring $\bar{\sigma}_{\gamma\gamma}$ and combining this with an assumed or estimated branching ratio. In the more crude determinations of this kind, the branching ratio has been assumed to be unity but a more realistic value can be derived from the strength function \bar{f} .

The relationship giving \bar{f} in terms of $\bar{\sigma}_{\gamma\gamma}$ and \bar{f} , obtained by combining

Eqs. (2.5), (2.8), (2.9), and (2.11), is

$$\tilde{f}^2(E_\gamma) = \frac{78 \cdot 10^{-8}}{SE_\gamma^4} \bar{\sigma}_{\gamma\gamma} \int_0^{E_\gamma} E_{\gamma'}^3 \tilde{f}(E_{\gamma'}) \varrho_0(E_\gamma - E_{\gamma'}) dE_{\gamma'} \quad (3.4)$$

where $\bar{\sigma}_{\gamma\gamma}$ is in mb and E_γ is in MeV. In solving for \tilde{f} in any particular case, \tilde{f} may be known from γ -decay experiments in the same nucleus or may be adopted from an adjacent nucleus. Alternatively, \tilde{f} can be substituted for \tilde{f} , assuming the Brink hypothesis; Eq. (3.4) then becomes an integral equation solvable for \tilde{f} . If $\bar{\sigma}_{\gamma\gamma}$ is not known below a certain energy, E_{\min} , Eq. (3.4) can still be solved above that energy provided some estimate of \tilde{f} below E_{\min} is available.

Experiments giving information on \tilde{f} below the neutron threshold are listed in Table II. Of these, those using recoil broadening of 7-MeV γ -rays from the $^{19}F(p, \alpha\gamma)^{16}O$ reaction (RM 60, Swa 73b, and Hui+ 62) give values of the strength function at isolated γ -ray energies only. The other three methods yield the elastic scattering cross section over a range of E_γ , from which, in principle, one can determine \tilde{f} with the aid of Eq. (3.4).

One of the more powerful tools for this type of measurement is the bremsstrahlung monochromator (OTA 62) used by Axel *et al.* (Axe+ 63, AMS 70). In this instrument electrons from a betatron are incident on a thin copper foil in which they produce bremsstrahlung with wide energy spread but limited to a narrow forward cone. This beam is directed at the target. Photons in a narrow energy band of the bremsstrahlung spectrum are tagged by observing coincidences between γ -radiation scattered from the target and electrons from the copper foil selected by a wide-angle magnetic spectrometer. The energy resolution of the spectrometer and hence also of the tagged bremsstrahlung radiation is about 100 keV. This device has been used to measure the elastic scattering cross sections of natural lead, radiolead, bismuth, tin, and zirconium (Axe+ 63, AMS 70).

Another effective instrument for subthreshold γ -ray scattering measurements is the Compton monochromator (KA 66) described in Sec. 3.1.1. This facility has been used for elastic scattering measurements on targets of ^{197}Au , ^{205}Tl , natural lead, radiolead (88% ^{206}Pb , 9% ^{207}Pb , 3% ^{208}Pb) and lead enriched to 78% in ^{208}Pb and for self-absorption measurements on natural and radiolead. The scattered radiation is conveniently measured with a NaI detector but measurements are also possible with large volume Ge(Li) detectors. Similar measurements of elastic scattering and self-absorption are in progress at Saclay (Luc+ 72).

Elastic scattering cross sections for ^{206}Pb , ^{208}Pb , and ^{209}Bi , shown by solid points in Fig. 2, are examples of the data that can be obtained by these

TABLE II
Photoexcitation Experiments Below the Neutron Separation Energy

Geometry	Energy range, MeV	Resolution keV	Detector	Target		References
				Scattering	Self-absorption	
1) Recoil broadening	6-7	130	Nal(Tl)	31 elements	5 elements	(RM 60)
	6-7	6.8	Ge(Li)	$^{207,208}\text{Pb}$, ^{209}Bi		(Swa 73b)
	6-7	130	Ge(Li)	^{232}Th , $^{233-238}\text{U}$, ^{237}Np		(Hui + 62)
2) Bremsstrahlung differential analysis	6-20	10%	Nal(Tl)	$^{206,207,208}\text{Pb}$	$^{206,207,208}\text{Pb}$, ^{209}Bi	(FH 62a)
	3-5	6.8	Ge(Li)	$^{206,207,208}\text{Pb}$, ^{209}Bi		(Swa 73a)
3) Bremsstrahlung monochromator	5-19	100	Nal(Tl)	^{90}Zr , Nat-Sn, Nat-Pb, Radio-Pb, ^{209}Bi		(AMS 70) (Axe + 63)
4) Compton monochromator	3-8.3	200	Nal(Tl)	^{205}Tl , ^{197}Au , Radio-Pb	Nat-Pb	(Ear + 73) (KK 67, Bar 69)
		6.4	Ge(Li)	Nat-Pb		(KK 73)
		20	Ge(Li)		Nat-Pb, ^{208}Pb	(Luc + 72)

variable-energy methods (Axe + 63, KK 67, FH 62b, Swa 73a). In ^{206}Pb and ^{209}Bi , and to a lesser extent in ^{208}Pb , the level densities are sufficiently high that several levels λ are included within the monochromator-beam energy spread. However, application of Eq. (3.4) to deduce \tilde{f} , even in ^{206}Pb and ^{209}Bi , is scarcely warranted because, for nuclides this close to the ^{208}Pb closed shell, \tilde{f} , $\varrho(E_\gamma - E_{\gamma'})$, and S (Eq. 3.4) cannot be relied upon to give representative statistical averages. Therefore, strength functions corresponding to $\bar{\sigma}_{\gamma\gamma}$ measurements have been extracted only in the special cases where branching ratios and level densities are also obtained directly from the measurements. In particular Swann's (Swa 73a) measurements with a broad-incident-beam, high-resolution-detector technique permit crude estimates of the strength function at low energies in ^{206}Pb . By observing inelastic and elastic scattering from individual resonances and making angular distribution measurements, he was able to deduce the width of the ground-state transitions and the multipole type. From his results for several neighboring resonances, we have obtained rough values for $\bar{\Gamma}_{\gamma 0\lambda}^J$ and $\varrho_J(E_\lambda)$, and hence \tilde{f} using Eq. (2.1). Similar estimates of \tilde{f} were made for the peak cross sections, $\sigma_{\gamma\gamma}$, in ^{208}Pb at 5.5 and 7.3 MeV (Fig. 2) for which the branching ratios are known (KK 73) to be unity. The results are shown in Fig. 15.

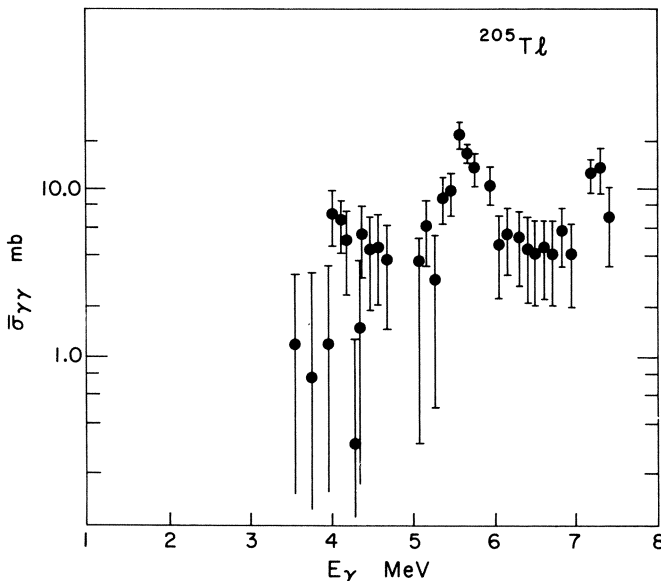


Fig. 5. The elastic scattering cross section $\bar{\sigma}_{\gamma\gamma}$ of ^{205}Tl (Ear + 73).

In ^{205}Tl rather better statistical behavior of the levels is found and for this nuclide the elastic scattering cross section (Fig. 5) has been used (Ear + 73) to obtain \vec{f} with the aid of Eq. (3.4). Because the cross section is unknown below 3.5 MeV, values of \vec{f} for that region were taken to be the same as those of ^{204}Tl . The final curve for \vec{f} is shown in Sec. 4.1, Fig. 16. A similar procedure is used to obtain \vec{f} for ^{197}Au (Fig. 18).

3.1.3. Photoexcitation Measurements Giving \vec{f}

Gamma-decay strength functions \vec{f} may be obtained from spectral distributions of the inelastically scattered γ -radiation (MW 69). The information obtained from such reactions is similar to that obtained from neutron-capture γ -ray spectra. Individual γ -ray k -values (Sec. 1) can be deduced and \vec{f} can in principle be extracted by the spectrum fitting method discussed in the next section. Although this method has not been widely applied, the information obtained is complementary to that obtained by (n, γ) reactions since stable nuclei are not always accessible through the (n, γ) reaction.

3.2. Spectrum Fitting Method

The γ -ray strength function \vec{f} may be obtained by calculating the shape of the spectral distribution with different trial strength functions until good agreement is achieved with the observed shape (Lon 73). This is the only approach that can be used to deduce \vec{f} from γ -ray spectra for which no information is available enabling the primary spectrum to be separated from the secondary and subsequent radiations. Different versions of this method have been used earlier by several groups (e.g., GDP 60, Tro 61, Sta 64, Brz + 71). In heavier nuclei the high-energy part of the γ -ray spectrum from the decay of levels excited by s - and p -wave neutron capture is dominated by $E1$ and $M1$ radiation (Secs. 3.4, 4.2.2). We therefore make the simplifying assumption that only dipole γ -emission is important at all energies. However, no attempt is made to separate \vec{f}_{E1} and \vec{f}_{M1} and the empirical strength function deduced is thus a mixture of both. For the sake of brevity the XL subscript will henceforth be dropped. This assumption, that all radiation is of dipole type, probably leads to serious errors in the deduced strength function at low energies in some nuclei, e.g., in the collective region, in which the predominant mode of decay between low-lying excited states is quadrupole radiation. However, a correction for higher multipole decay would be difficult to formulate in most cases because of ignorance of the

level-structure and γ -decay details above all but the lowest few states. Because of these uncertainties, energies below ~ 2 MeV are ignored in comparing observed and fitted spectral distributions.

3.2.1. Derivation

The strength function \tilde{f} is related to the absolute average primary γ -ray spectral distribution per unit population, $v_{i\lambda}(E_\gamma)$, as discussed in Sec. 2.3 by

$$v_{i\lambda}(E_\gamma) \Delta E_\gamma = 3 \frac{E_\gamma^3 \tilde{f}(E_\gamma) \varrho_0(E_\lambda - E_\gamma) \Delta E_\gamma}{\bar{\Gamma}_{\gamma T\lambda} \varrho_0(E_\lambda)} \quad (3.5)$$

where, for simplicity, we assume a constant spin-cutoff parameter and that the functional form of \tilde{f} is independent of E_λ and J . The average total radiative width is usually known for the resonance region just above the neutron threshold and substituting this in Eq. (3.5) one obtains \tilde{f} in absolute units provided $v_{i\lambda}$ is in absolute units. For excitation regions where $\Gamma_{\gamma T\lambda}$ is not known, it may be calculated from the expression

$$\Gamma_{\gamma T\lambda} = 3 \int_0^{E_\lambda} \tilde{f}(E_\gamma) E_\gamma^3 \frac{\varrho_0(E_\lambda - E_\gamma)}{\varrho_0(E_\lambda)} dE_\gamma \quad (3.6)$$

To calculate the γ -ray spectral distributions one divides the region between the ground state and the initial excitation energy, E_λ , into n intervals, each of width ΔE . Let P_m be the population probability of interval m at excitation $E_m = m\Delta E$. Then

$$P_m = \int_{E_m}^{E_\lambda} v_{m\mu}(E_\mu - E_m) P_\mu dE_\mu \quad (3.7)$$

For unit initial population ($P_\lambda = 1$), the total spectral distribution, $v_{i\lambda}(E_\gamma)$, of primary plus secondary and subsequent γ -rays from an initial excitation E_λ is

$$v_{i\lambda}(E_\gamma = E_m - E_i) \Delta E_\gamma = \Delta E_\gamma \int_0^{E_\lambda - E_\gamma} v_{im}(E_m - E_i) P_m dE_i \quad (3.8)$$

Within the framework of these calculations, a strength function which gives agreement between the observed and calculated $v_{i\lambda}(E_\gamma)$ is selected by trial. Uncertainties in the assumed level-density distributions and in the observed spectral distributions provide the main sources of uncertainty in the \tilde{f} deduced. We now discuss these in more detail.

3.2.2. Level-Density Distributions

Information on the energy dependence of the level-density distributions needed for these calculations must be obtained from other sources. Inadequacies of available level-density expressions were discussed in Sec. 2.3. In the absence of a universally reliable prescription for the energy dependence, it is necessary to make use of the available empirical data for each nucleus of interest. Immediately above the neutron threshold, level densities, for a few spins only, are known from neutron resonance spectroscopy. Up to 1–2 MeV above the ground state, level densities are known from (n, γ) and charged-particle reactions. In particular, spectrum average techniques used in (n, γ) spectroscopy (Sec. 3.4) are valuable in revealing all final states that can be fed by dipole transitions from the resonances (usually *s*-wave) excited. Between these two regions the level-density distributions must be obtained by a suitable interpolation.

3.2.3. Observed Spectral Distributions

Spectral distributions are obtained by unfolding the detector response function from the observed γ -ray spectra. This procedure introduces errors due to uncertainties in the response function and cumulative errors from repeated unfolding operations. In general, the magnitudes of these errors are difficult to assess. The spectra measured with magnetic Compton, magnetic pair, and NaI spectrometers are suitable for obtaining spectral distributions, because their response functions are fairly well known and, for the magnetic spectrometers, of simple, near-Gaussian shape. From spectra obtained with these instruments one obtains the complete γ -spectral distributions $\nu_{i\lambda}(E_\gamma)$ over the energy range covered. High-resolution Ge(Li) single-detector data, on the other hand, yield information on the resolved γ -rays only. Because of the form of the Ge(Li) detector response function (large Compton distribution with sharp total absorption and pair peaks), unfolding of a spectrum to extract unresolved γ -ray intensity is impractical. This difficulty is overcome if one uses a Ge(Li)–NaI coincidence arrangement in Compton-suppression or pair spectrometer modes (Ras + 70).

The uncertainty in $\nu_{i\lambda}(E_\gamma)$ due to the Porter–Thomas fluctuations (PT 56) is

$$\Delta\nu_{i\lambda}(E_\gamma) = \nu_{i\lambda}(E_\gamma) \sqrt{2/m} \quad (3.9)$$

where m is the number of transitions in the γ -ray energy interval. In spectra from nuclei near closed shells, particularly in even–even or even–odd nuclei, there are, often, only a few primary transitions within 2–3 MeV of the upper

limit. Thus γ -ray spectra from the decay of individual excited levels at E_λ , as obtained for example in thermal neutron capture, provide $\nu_{i\lambda}(E_\gamma)$ with large errors $\Delta\nu_{i\lambda}(E_\gamma)$ for E_γ near E_λ . However, for several nuclei better average intensities are available at high energies from resonance-averaged neutron capture γ -ray measurements (Sec. 3.4). At lower γ -ray energies, at least in heavier nuclei, there are many transitions ($\sim 40 \text{ MeV}^{-1}$ at $\sim 5 \text{ MeV}$ in Au) and the uncertainty in $\nu_{i\lambda}(E_\gamma)$ from Porter-Thomas fluctuations is reduced.

3.2.4. Results

Thermal neutron-capture γ -ray spectra (Gro+ 69) measured with a magnetic Compton spectrometer by Groshev *et al.* (Gro+ 58) and magnetic pair spectrometer by Bartholomew and Kinsey (BK 53) were used by Lone (Lon 73) to deduce strength function for several elements. In order to

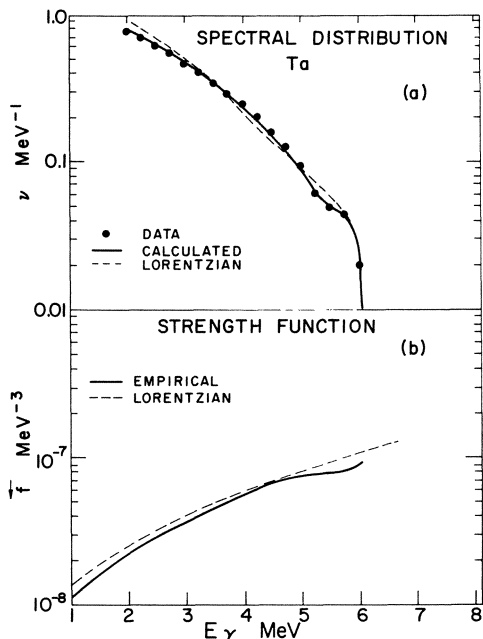


Fig. 6. Comparison of calculated and observed spectral distributions ν and \bar{f} for Ta. The points in (a) show the observed spectral distribution following thermal neutron capture (Gro+ 69) smoothed to remove fine-structure. The spectral distributions shown by the solid and broken curves were calculated from the empirical and Lorentzian strength functions, respectively, (b) with giant dipole resonance and level-density parameters given in Tables V and VI.

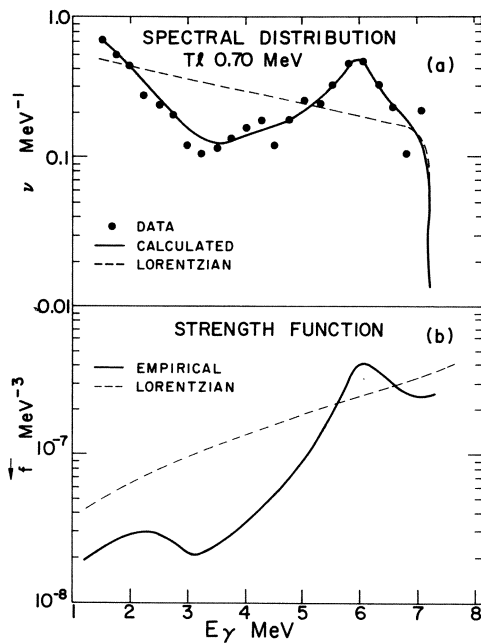


Fig. 7. Comparison of calculated and observed ν and f for Tl. The points in (a) show the observed spectral distribution (Ear + 72b) following 0.7-MeV neutron capture in natural Tl. For other details see Fig. 6.

reduce Porter-Thomas fluctuations, the data were first smoothed by averaging over the γ -ray fine-structure and, for even-even and odd-even nuclei, the intensity information in the high-energy part of the spectrum was augmented by resonance neutron-capture data. For excitation energies above a lower limit E_t (approximately equal to the pairing energy gap) the constant temperature formula, Eq. (2.14), was used for spin-zero level-density distributions. The constants A and T were determined empirically from the known level densities at the neutron threshold and in the region 1–2 MeV above the ground state. Below E_t the known levels were adopted explicitly with their appropriate spins and parities. A similar analysis was also done for the fast-neutron-capture data of Earle *et al.* (Ear + 72b).

A typical fit to the Ta thermal capture γ -ray spectrum is shown in Fig. 6a. The points give the smoothed measured spectrum (Gro + 69). The broken and the solid curves are the fits obtained by using the strength function deduced from the giant dipole Lorentzian tail and by the spectrum fitting method, respectively. These strength functions are plotted in Fig. 6b. As a second example, in Fig. 7a, the points give the spectral distribution

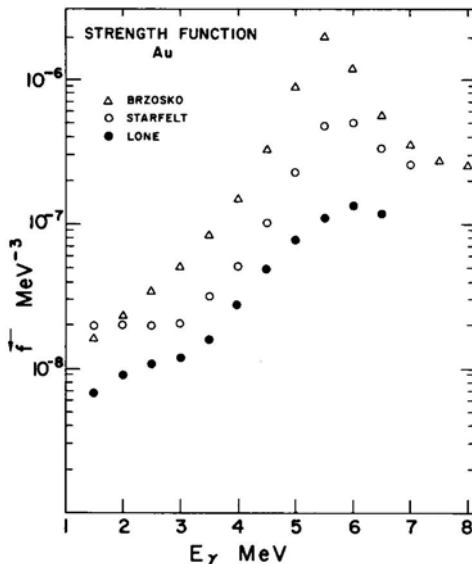


Fig. 8. A comparison of strength functions for Au based on the same spectral distribution showing the sensitivity to level-density parameters. Strength functions extracted with the constant temperature level-density formula with $T = 0.753$ and 0.6 MeV and with the Gilbert and Cameron formula (GC 65) are shown by solid circles (Lon 73), open circles (Sta 64) and triangles (Brz + 71), respectively.

from 700-keV neutron capture in Tl (Ear + 72b). The broken and solid curves show the spectra calculated with \tilde{f} obtained from the tail of the giant dipole resonance and with a trial \tilde{f} , respectively. These strength functions are shown in Fig. 7b.

Starfelt (Sta 64) and Brzosko *et al.* (Brz + 71) also used the spectrum fitting method to investigate \tilde{f} in medium weight and heavier nuclei. Both used a strength function of the form

$$\tilde{f}(E_\gamma) \propto \left[\frac{\Gamma_1 e^{-a(E_\gamma - E_1)}}{E_1[(E_\gamma - E_1)^2 + \frac{1}{4}\Gamma_1^2]} + b \frac{\Gamma_2 e^{-a(E_\gamma - E_2)}}{E_2[(E_\gamma - E_2)^2 + \frac{1}{4}\Gamma_2^2]} \right] \quad (3.10)$$

where the first term is the expression proposed by Lane and Lynn (LL 60) for the giant dipole resonance, and the second term represents a superimposed pigmy resonance ($E_2 \sim 6$ MeV) whose strength is adjusted to give the observed spectral distribution and total radiation width. Starfelt imposes the further constraint that \tilde{f} be constant below 3 MeV. The strength functions for Au deduced by Lone (Lon 73), Starfelt (BS 70a) and Brzosko *et al.* (Brz + 71) are shown in Fig. 8. The serious disagreement between these

deduced strength functions, particularly in absolute magnitude at ~ 6 MeV, is primarily due to the assumed level-density distributions. Starfelt used a constant temperature expression with $T = 0.6$ MeV. Brzosko *et al.* adopted the Gilbert and Cameron (GC 65) expression and parameters. In our recent evaluation (Lon 73), both of these distributions were found to be inadequate for predicting both the resonance level densities (Gol+ 66) and the density of levels below 2 MeV (Gro+ 69, LBT 72). Instead a constant temperature expression with $T = 0.753$ MeV which gives good agreement with these level densities was adopted.

3.3. Sequential Extraction Method

The separation of the primary spectrum from the total decay spectrum can be effected if the spectral distributions of secondary and all subsequent decay radiations are known. In the sequential extraction method, one begins with measured total spectra from each of a complete set of contiguous intervals in excitation energy populated in some experiments as illustrated in Fig. 9. By a procedure described in detail in an earlier paper (Bar+ 70) it is possible, for any interval λ , knowing the detector response function, to construct from the spectra of all lower intervals i the distribution of all secondary and subsequent decay radiation, and hence to unfold the primary

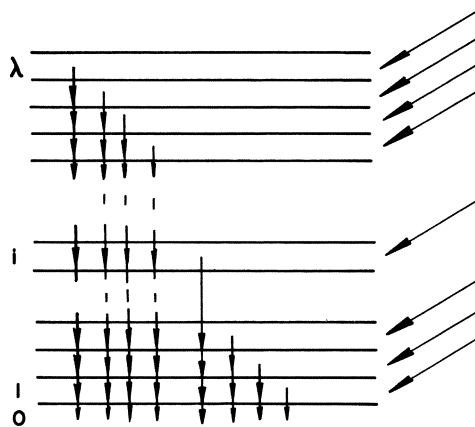


Fig. 9. Schematic showing population and γ -decay of levels in particle reactions. Each interval corresponds to an energy window applied to the coincident particle spectrum. From experiments in which the γ -rays in coincidence with each particle window are recorded, the γ -decay from each interval, comprising primary and all subsequent transitions, are known. From these data, knowing the detector response function, one can solve for the primary spectrum from each interval in sequence, beginning at the lowest.

spectrum $\nu_{i\lambda X_1}(E_\gamma)$ for interval λ . It is assumed as in Sec. 3.2, that the cascade involves dipole transitions only. The primary spectrum so obtained can then be used in the same way to unfold the primary spectrum of interval $\lambda + 1$, and so on. It is a fundamental assumption of the method that the branching ratios for γ -decay from any excitation interval to lower intervals are independent of how the upper interval was populated. This implies the assumption that, on the average, the same distribution in the population of individual levels in each interval is obtained regardless of the mode of excitation or that, if these microscopic populations differ with the mode of excitation then, on the average, the branching ratios are independent of J or of other parameters distinguishing the levels. Once the individual primary spectra are available they can be used to deduce a relative strength function $\tilde{f}_{X_1}(E_\gamma)/\bar{f}_{\gamma T\lambda}$ with the aid of Eq. (2.13) and available level-density information. If $\bar{f}_{\gamma T\lambda}$ is known for any interval, as, for example, when E_λ overlaps the region of known resonances near the threshold, then the absolute value of \tilde{f} can be determined for the region $0 < E_\gamma < E_\lambda$.

The above procedure was followed in analyzing spectra from the $^{197}\text{Au}(d, p\gamma)^{198}\text{Au}$ and $^{181}\text{Ta}(d, p\gamma)^{182}\text{Ta}$ reactions at $E_d = 12$ MeV (Bar + 70). The spectra were measured in coincidence with protons with energies falling within 24 contiguous windows, each 240 keV wide, corresponding to excitation intervals in the product nucleus between 0.8 MeV and the neutron separation energy. Relative strength functions from a selection of primary spectra obtained from the analysis are shown in Fig. 10. Within uncertainties introduced by finite counting statistics and the use of finite

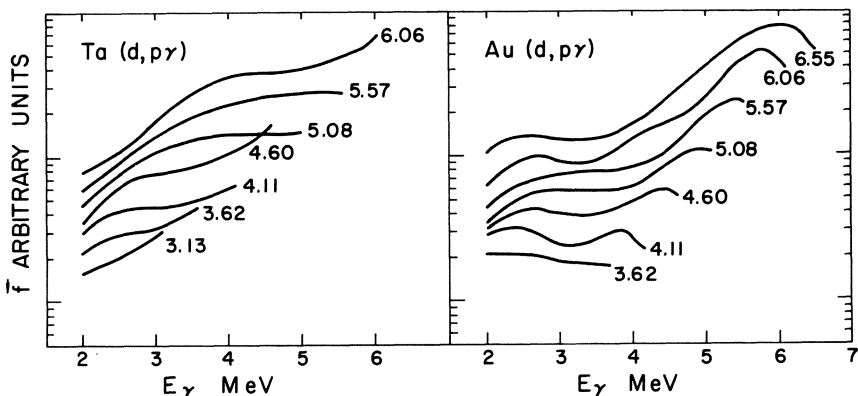


Fig. 10. Relative strength functions $\tilde{f}_{i\lambda}$ for Ta and Au. The curves were obtained by the sequential extraction method from γ -ray spectra measured in the $\text{Ta}(d, p\gamma)$ and $\text{Au}(d, p\gamma)$ reactions (Bar + 70). The numbers on the curves give E_λ in MeV.

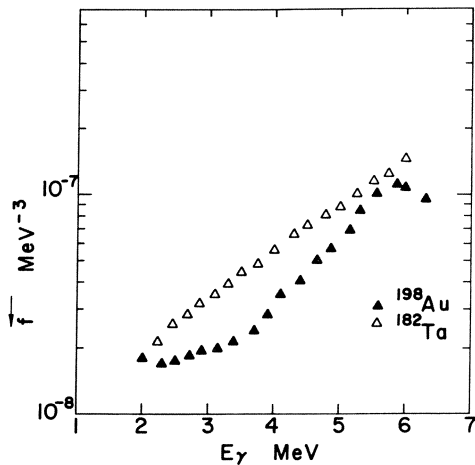


Fig. 11. Absolute strength functions for Au and Ta derived by the sequential extraction method from $(d, p\gamma)$ reactions in Au and Ta (Bar + 70).

energy intervals in the analysis, these and all other strength functions obtained in the calculation have common functional forms for each target. The \tilde{f} obtained by normalizing and averaging these strength functions evaluated absolutely for the interval at the neutron threshold with the aid of Eq. (2.13) and with $\bar{I}_{\gamma T\lambda}$ and $\varrho(E_\lambda)$ estimated as in Sec. 3.2, are shown in Fig. 11.

The sequential extraction method has the distinct advantage of providing a complete strength function \tilde{f} to low energies by an unambiguous analytical procedure. However, the validity of the assumption that the branching ratios for decay from any interval are independent of the mode by which it was populated is open to some doubt and the justification of the method lies largely in its internal consistency and the agreement achieved with other methods. The internal consistency achieved in the application to the $(d, p\gamma)$ reaction (Bar + 70) seems satisfactory as is the agreement between the results of this and other methods as shown in Sec. 4.1. It should be noted, however, that the distributions in J_i of levels in interval i when fed by γ -ray cascade cannot be greatly different from that when the interval is fed directly in the (d, p) reaction because only a small range of angular momentum transfers (the most probable I_n is ~ 3) can occur at $E_d = 12$ MeV, and only one or two cascade steps are sufficient to account for most of the decay from any interval to the ground state. Therefore the assumption of independence of branching ratios on the mode by which the interval was populated seems plausible enough in this application. However, as

discussed in Sec. 4.2.3 when the same excitation interval is populated by different reactions, e.g., $(d, p)E_d = 12$ MeV and $(p, p')E_p = 18$ MeV, large differences in J -distributions, and possibly in other parameters, can result in significantly different spectral distributions.

The conclusion that the strength function $\tilde{f}_{i\lambda}$ derived for each excitation interval λ are the same except for an unknown normalizing factor is important in the support it provides for the Brink hypothesis. But, as discussed in Sec. 2.2, it is not sufficient to establish its validity. For a complete test of the hypothesis it is necessary to establish that this common functional form of the $\tilde{f}_{i\lambda}$ is also consistent with that of $\tilde{f}_{0\lambda}$. This compatibility has not yet been checked in the same nucleus but partial tests will be discussed in Sec. 5.2.

3.4. High-Resolution Gamma-Ray Method

A fourth method of studying the γ -ray strength function involves detection of the individual high-energy primary γ -rays by high-resolution γ -ray spectroscopy with Porter-Thomas fluctuations reduced or eliminated by averaging the γ -ray intensities over many neighboring resonances. The observed average intensity for transitions, E_γ , to a particular final state i must be calibrated in absolute units (photons per initial excitation), whence the average partial radiation width, $\bar{\Gamma}_{\gamma i \lambda}$, can be found if the total radiation width is known. The strength function $\tilde{f}_{i\lambda}$ at the energy E_γ then follows from Eq. (2.2). The method has so far been applied mostly to neutron-capture γ -ray spectra but it can also be applied to other reactions. The measurements of elastically and inelastically scattered γ -rays with good detector resolution (Swa 73a, KK 73) discussed in Sec. 3.1 fall into this class.

Two techniques can be employed to obtain the averaged spectra: (a) by measuring the γ -spectra with a Ge(Li) detector from many individual resonances selected by a high-resolution neutron time-of-flight spectrometer and then averaging over resonances the intensity for each γ -ray (Sam+ 68, Was+ 68, LEB 70), and (b) by measuring the average γ -ray spectra (All 68, BT 70) following bombardment with neutrons with energy spread large enough to span many resonances but small enough to avoid serious smearing of the γ -ray resolution. In the former method, absolute calibrations are made on the γ -rays prior to averaging while in the latter an absolute calibration is made on the observed average intensity. We shall call these (a) the high neutron resolution (HNR) and (b) the low neutron resolution (LNR) spectrum average techniques, respectively.

It should be noted that the averages obtained by the two methods are not necessarily the same. In the HNR method all individual intensities are weighted equally and $\bar{\Gamma}_{\gamma i \lambda}$ is obtained directly while in the LNR method (BT 70) the determination of $\bar{\Gamma}_{\gamma i \lambda}$ from the average intensity is, or may be, complicated. For a thin target the average intensity is proportional to $\bar{\Gamma}_{n\lambda} \bar{\Gamma}_{\gamma i \lambda}$ which is related to $\bar{\Gamma}_{\gamma i \lambda}$ by

$$\bar{\Gamma}_{n\lambda} \bar{\Gamma}_{\gamma i \lambda} = S \bar{\Gamma}_{n\lambda} \bar{\Gamma}_{\gamma i \lambda} \quad (3.11)$$

where S is the fluctuation factor discussed in Sec. 2.2. For a thick target, a more complex relationship applies (BT 70). In Eq. (3.11), if $\bar{\Gamma}_{n\lambda}$ and $\bar{\Gamma}_{\gamma i \lambda}$ are not correlated, one has $S = 1$ and the average absolute intensity is the same as for the HNR method. If, however, the widths are correlated, and assuming $\bar{\Gamma}_{n\lambda}$ conforms to the Porter-Thomas distribution, S can have any value $1 < S \leq 3$ depending on the degree of correlation, and the average absolute intensity obtained by this method then exceeds that from the HNR method. There would appear now to be no strong evidence for $(\bar{\Gamma}_{n\lambda}, \bar{\Gamma}_{\gamma i \lambda})$ correlations in heavy elements (Chr 72). While future investigations may show that some correlating effects are definitely present, it will be assumed in this review that they are small and therefore that the average absolute intensities and hence the strength functions obtained by the HNR and LNR techniques are equivalent.

The HNR technique has the advantage that resonance capture effects can be cleanly separated from direct capture and other nonresonant background but it has the disadvantage that in most attempts to use it to date it has not been possible, because of limitations imposed by neutron intensity, to include enough resonances in the average to remove all Porter-Thomas fluctuations. At the present state of development of these techniques, better smoothing of fluctuations can be achieved with the LNR method, but that method is also limited to regions where level densities are high enough to provide a good statistical sample within the energy spread of the bombarding neutrons. In either method, additional smoothing of Porter-Thomas fluctuations can be achieved by extending the average over several neighboring γ -rays and ascribing the strength so obtained to the mean E_γ .

The HNR technique has been applied to many nuclei (see examples in Table III). In nuclides where final state spins and parities are already known, $E1$ and $M1$ γ -rays can be identified and information on the corresponding strength function obtained. Where the $J\pi$ are not known, it has been possible only to establish the distribution of intensities for "dipole" radiation. High-resolution, HNR, data are used to establish reliable intensity averages and estimates of the energy dependence of the relative

TABLE III

Relative Strength Functions from High-Resolution γ -Ray Methods

For each residual nucleus in the first column the energy range covered in the experiment and the number of γ -rays of $E1$, $M1$, or $E2$ type are shown in the next three columns. In the fifth column a smooth energy dependence is indicated by "Lorentzian" or n in E_γ^n and a peak structure by giving the energy of the peak in MeV. In the sixth column the technique, low neutron resolution (LNR) or high neutron resolution (HNR), is indicated and for the latter the number of resonances in the average are shown in brackets.

Residual nucleus	E_γ range, MeV	Multipole	No. of transitions	Energy dependence, n , or peak energy, MeV	Technique	Reference	
^{239}U	3.3–4.1	$E1$	13	3.7	HNR(9)	(BT 72)	
		$M1$	9	3.7			
	3.0–4.0	$E1$	9	3	HNR(23)		
	3.6–4.7	$M1$	4	3			
^{206}Tl	4.0–4.8	$E2$	4	3	(Was + 71)		
	4.5–6.5	$E1$	12	Peak \sim 5.5			
	4.0–6.5	$M1(E2)$	12	Peak \sim 6			
	5.1–6.5	$E1$	79	5			
^{198}Au		$M1$	3	5	LNR	(LBT 72)	
	4.78–6.51		97	Peak \sim 6			
	6.2–8.0	$E1$	8	Lorentzian			
	6.0–8.0	$E1$	9	5			
^{196}Pt	4.8–6.0	$E1$	44	5	{ LNR HNR(22) }	(Was + 68)	
		$M1$	10	5			
		$E1$					
			50				
^{182}Ta					LNR	(HGR 71)	
^{176}Lu	5.05–6.05				HNR(10)	(LBT 72)	
			37		(Was + 69)		
					HNR(15)	(WCT 70)	

^{166}Ho	5.4–6.2	$E1$	22	Lorentzian 7.2 5	{ LNR (BT 70)
	5.7–6.1	$E1$	9		
	5.7–6.2	$M1$	8		
^{168}Gd	5.6–7.9	$E1$	18	Lorentzian 3 7.5	{ LNR (BT 70)
	6.1–7.0	$M1$	4		
	6.25–8.5	$E1$	20		
^{166}Gd	6.25–7.4	$M1$	7	{ LNR 5 7	{ LNR (Smi+ 72)
	4.0–6.0	$E1$	24		
		$M1$	13		
^{163}Sm		$E2$	18	{ LNR 5 7	{ LNR (Smi+ 72)
	4.0–6.0	$E1$	21		
		$M1$	16		
^{150}Sm	5.4–7.7	$E1$	31	{ LNR 5 5	{ LNR (BS 70b)
	5.6–7.0	$M1$	12		
	5.5–7.6	$E1$	23		
^{148}Sm	6.7–7.0	$M1$	4	{ LNR 5 5	{ LNR (LP 71)
	4.75–6.5	$E1$	14		
		$M1$	17		
^{124}Sb	5.0–6.8	$E1$	11	{ HNR(4) 5 5	{ HNR(12) (LP 71)
	6.5–9.3	$M1$	15		
	5.5–6.6	$E1$	12		
$^{119,121}\text{Sn}$	6.5–7.5	$M1$	15	{ Peak $E_\gamma \sim 8.5$ 3 Peak $E_\gamma \leq 5.5$	{ LNR (BL 70)
	6.8–9.0	$E1$	12		
	4.1–7.0	$M1$	14		
^{106}Pd			145	{ Peak ~ 7.7 5 3, Peak ~ 6	{ LNR (Rim+ 70)

intensity at the high-energy end of capture γ -ray spectral distributions for strength function determinations by the spectrum fitting method (Sec. 3.2). These data are separately identified in the strength functions plotted in Sec. 4.1.

The LNR technique has been developed and exploited most vigorously by the Argonne group (BT 70). In their technique the sample under study is surrounded by ^{10}B and placed in a region of high flux near the reactor core. The ^{10}B absorbs the thermal neutrons so that the neutron spectrum reaching the sample consists of the epithermal component which has a $1/E$ energy dependence. The neutron flux in the $1/E$ tail is such that resonance capture can be observed for s -wave and some p -wave resonances; there is no sharp cutoff but the effective energy spread of the neutrons responsible for most of the captures is about 2 keV beginning at thermal energies. This energy spread is sufficient to include a large number of resonances in most heavy elements of interest. By close examination of the γ -ray line-shape, which is broadened by the neutron energy spread, it is possible to establish whether or not a particular high-energy γ -ray is

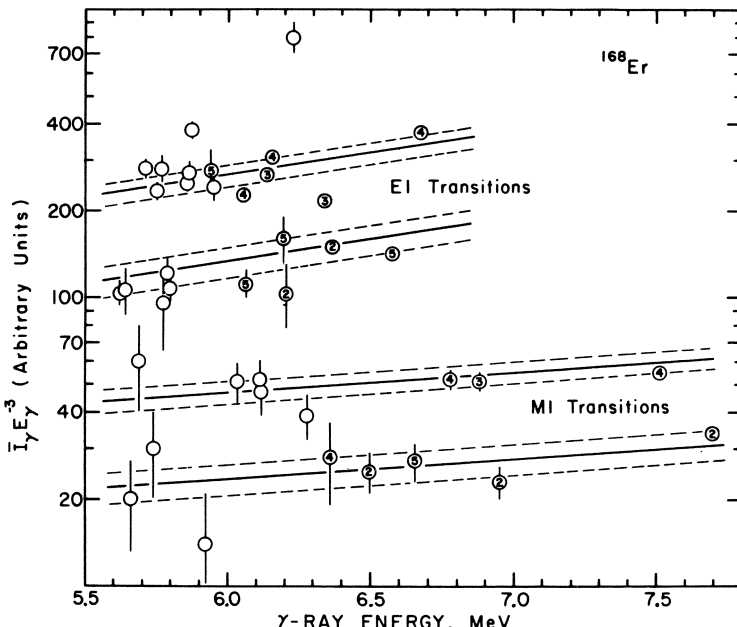


Fig. 12. Average reduced γ -ray intensities in ^{168}Er obtained by the low-neutron-resolution technique (BT 70). The upper two curves are for $E1 \gamma$ -rays, the lower two for $M1 \gamma$ -rays. Known final-state spins are shown in the circles. The estimated limits of uncertainty from Porter-Thomas fluctuations are shown by the broken lines.

emitted in a primary transition. Bollinger and Thomas (BT 70) have shown that the technique is useful in determining the multipolarity of the γ -rays and is also sensitive to the spins of the final states, specifically whether the final state spin J_i is $J_0 \pm \frac{1}{2}$ or $J_0 \pm \frac{3}{2}$, where J_0 is the target spin. The latter effect follows simply from counting the number of transition paths by which states of a particular J_i can be reached by primary transitions of a given multipolarity from the resonances excited by *s*-wave capture. Figure 12 for ^{168}Er (taken from BT 70) illustrates the quality of the results obtained with this technique. The figure shows the partial separation of γ -rays according to final state spins, 3 and 4 or 5 and 2 (the alternatives available for dipole transitions following *s*-wave capture on a $J_0 = \frac{7}{2}$ target), and according to γ -ray multipolarity. At energies below about 5.8 MeV in this target the energy resolution is not sufficient to resolve all γ -rays and the clear separation into bands disappears. Similar data have been obtained for a large number of other nuclei as shown in Table III.

Most published distributions such as Fig. 12 provide only relative strength function information, but with suitable calibration they can be compared with absolute strength function data or with the prediction of the Lorentzian shape (Bol 68). Absolute calibrations can be obtained by normalizing the total average intensity for several high-energy lines to the average for lines in the thermal-capture spectrum for which an absolute calibration is available. The validity of this procedure has been justified by Bollinger (BT 72).

The LNR technique has also been used by Allen and Bird (AB 68) to study the energy dependence of the γ -ray strength function in gold. In this work the broad neutron beam, extending between 10- and 60-keV neutron energy, is obtained from the $\text{Li}(p, n)$ reaction by a time-of-flight technique. Although this type of neutron source provides some flexibility in the energy and width of the neutron beam available, it suffers from low beam intensity and from neutron background problems.

A promising technique for LNR average resonance measurements employs reactor neutrons filtered with a scandium filter (SM 68) or iron filter (CWG 73). The scandium device provides an external neutron beam with 800 eV full width at half maximum at 2 keV. It has been used by Greenwood and collaborators (GR 71, Gre+ 69, HGR 71) for the study of γ -ray spectra from a number of heavy nuclei including Ta, Hf, W, and Pb. A drawback of this method is that the 800-eV beam spread may sometimes be too narrow to encompass a sufficiently large number of resonances to completely smooth out Porter-Thomas fluctuations. There may also be intensity limitations compared to the ^{10}B filter method. Reduced intensities for Ta obtained with the scandium filter are shown in Fig. 13

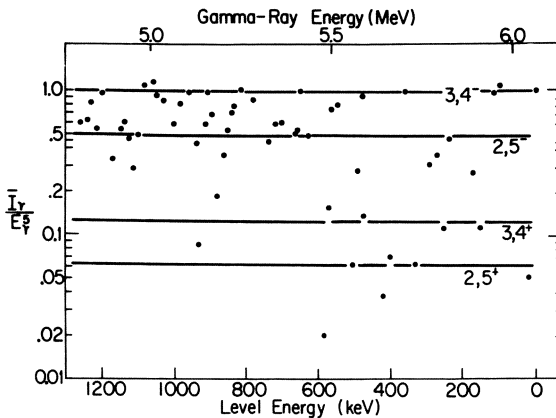


Fig. 13. Average reduced γ -ray intensities for ^{182}Ta obtained by the low-neutron-resolution technique (HGR 71). The upper two curves are for $E1$ transitions and the lower two for $M1$ transitions. Final-state spins and parities are indicated on each line.

(HGR 71). The iron filter device provides a 25-keV beam 4 keV wide (CWG 73).

The value of the average-resonance method lies in the facility it provides to examine the strengths of individual γ -rays, to test that they are primaries, and to distinguish between multipoles. In Table III, for example, one sees a clear indication that the spectra above 5 MeV are dominated by $E1$ radiation in nuclei at the heavy end of the table; the ratio of the number of $M1$ γ -rays to $E1$ γ -rays gradually grows with decreasing Z , becoming roughly unity at Sm and greater than unity, in general, for still lighter nuclei. A disadvantage, at the present state of the art, is the small energy range covered. In particular, below 5 MeV individual lines become difficult to resolve in most elements in Table III and the multipolarity and primary assignments become difficult to establish. The table shows that the energy dependence of the $E1$ radiation width is widely represented by any power between E_γ^3 and $E_\gamma^{7.5}$ with most cases conforming to the E_γ^5 dependence expected from the Lorentzian (Axe 62). The $M1$ dependence similarly varies widely with some evidence of peaking.

3.5. Comparison of Methods

Below the neutron separation energy, none of the four methods described in Secs. 3.1–3.4, at least insofar as it has been possible to exploit them to date, stands out as clearly superior for studying γ -ray strength functions. All have advantages and disadvantages and to a large degree

they complement one another. Above the separation energy most strength function information has been derived from photoexcitation data. The quantity measured in each method, and parameters needed for strength function extraction, are summarized in Table IV. Strength functions derived by the various methods are compared in Sec. 4.1.

The photoexcitation method is the only one providing $\tilde{f}(E_\gamma)$. By suitable angular and polarization correlation measurements it is possible to distinguish $E1$, $M1$, and higher multipoles although these techniques have as yet been little used in this application. For a substantial region above the neutron threshold a measurement of $\bar{\sigma}_{\gamma n}$ gives a good approximation to the total absorption cross section, $\bar{\sigma}_{\gamma a}$, required for the calculation of $\tilde{f}(E_\gamma)$, but for precise results one must correct for the total cross section for γ -emission, $\bar{\sigma}_{\gamma T}$, and, where applicable, for charged-particle emission cross sections. Below the neutron threshold, transmission measurements to obtain $\bar{\sigma}_{\gamma a}$ are difficult if not impossible because of competition from electron scattering and absorption processes. In this region one usually measures the elastic or, more precisely, in most cases a quasielastic cross section $\bar{\sigma}_{\gamma \gamma}$, from which one can estimate $\bar{\sigma}_{\gamma a}$. The latter estimate involves, among other things, the branching ratio for decay by the quasielastic channel, evaluation of which poses a serious difficulty for the method because it requires prior knowledge of the γ -decay strength function, $\tilde{f}(E_\gamma)$. So far, the photoexcitation method has given much strength function information above the threshold but below the threshold it has yet to be applied extensively over the full range of targets and excitation energies of which it is capable.

The spectrum fitting method has the advantage that it can provide an empirical strength function for a wide energy range from near zero to the initial excitation energy used in the experiment. However, the strength function extracted depends strongly on the form of the level-density formula used in the calculation. Not only can uncertainties in $\varrho(E)$ affect the form of the strength function but also its absolute value. The absolute value is also affected by uncertainties in the value adopted for the average total radiation width, $\bar{\Gamma}_{\gamma T \lambda}$. A fundamental assumption used in the spectrum fitting method is that the same form, but not necessarily the same absolute magnitude, of strength function, \tilde{f} , governs decay from each excitation interval. Strong support for this assumption is given by the sequential extraction method. It is also assumed that the spectral distribution contains only dipole radiation. A serious weakness of the spectrum fitting method is that it provides no means of uniquely separating multipoles so that the strength function obtained is a composite of the $E1$ and $M1$ strength

TABLE IV

Gamma-Ray Strength Function Parameters

For each method listed in column (1) are given the input experimental data (column 3), data required from other sources (column 4), and parameters derived (column 5).

Method	Section	Experimental data	External data	Derived parameters	Remarks
Photoexcitation (γ, n)	3.1	$\bar{\sigma}_{\gamma n}$	$\bar{\sigma}_{\gamma T}, \bar{\sigma}_{\gamma p}, \dots$	$\bar{f}, E1/M1$	^a
(γ, γ)		$\bar{\sigma}_{\gamma\gamma}$	$\bar{F}_{\gamma\omega}, \bar{F}_{\gamma T\lambda},$ $\varrho(E_\lambda), S, \bar{F}_{\gamma T\lambda}$	$\bar{f}, E1/M1$	^a
Spectrum fitting	3.2	$\nu_{\ell\ell}(E_\lambda = E_B)$	$\varrho(E), \bar{F}_{\gamma T\lambda}$	\bar{f}	
Sequential extraction	3.3	$\nu_{\ell\ell}(0 < E_\lambda < E_B)$	$\varrho(E), \bar{F}_{\gamma T\lambda}$	\bar{f}	
High-resolution γ -ray	3.4	I_γ	$\varrho(E_\lambda), \bar{F}_{\gamma T\lambda}$	$\bar{f}, E1/M1, p$	^b

^a Multipolarity identified by subsidiary polarization correlation measurements.

^b Primary nature of radiation, p , verified from line-shapes and energy shifts in keV neutron capture.

functions. It can be assumed with some confidence that this empirical strength function conforms closely to the $E1$ strength function at high energies in the mass region $182 < A < 208$ but this assumption becomes less reliable toward lower energies and in certain other regions of the table where $M1$ radiation competes well with $E1$ radiation (Secs. 1, 4.2.2).

The sequential extraction method, like the spectrum fitting method, provides a complete strength function over the full energy range available to the experiment and like that method it depends strongly on level-density and total radiation-width information obtained externally. However, sequential extraction is the only method in which the form of \tilde{f} can be solved for directly, for all initial excitation energies, E_λ , a very valuable property. The same uncertainties, concerning the multipole content of the extracted strength function, apply as for the spectrum fitting method. An important assumption of the sequential extraction method is that the branching ratios for γ -decay from any excitation interval to lower intervals are the same whether the upper interval was populated by the initiating reaction or by γ -decay from higher intervals. This presupposes that the strength function is independent of spin (see Sec. 2.2) and other parameters of the levels involved, a supposition that is open to question and, hopefully, eventual verification.

The high-resolution γ -ray method is essentially the only method in which average reduced width of individual γ -rays can be studied; such studies are also possible in the photoexcitation method but, as yet, few measurements of this kind have been made. The method provides means for assigning multipole type and of testing whether γ -rays are primary or occur later in the cascade. Both the average reduced widths and multipole assignments become unreliable when γ -rays are not well-resolved. With detectors now available, this limits the method to the high-energy end of the spectrum; i.e., to ≥ 5 MeV approximately in (n, γ) experiments in most heavy elements. The method requires a knowledge of the level density and total radiation width at the initial excitation energy and also a calibration of the absolute intensity for at least one γ -ray in the spectrum. The last quantity has proved difficult to obtain directly.

4. PROPERTIES OF GAMMA-RAY STRENGTH FUNCTIONS

Basic data in the form of photoexcitation cross sections or neutron capture γ -ray spectra, necessary for the determination of γ -ray strength functions, are available for most heavy elements but the extraction of

strength functions is often thwarted, particularly below the neutron threshold, because a knowledge of branching ratios, multipolarities, or level densities is lacking. Because of the usually greater strength of $E1$ radiation as compared to $M1$ and higher multipoles (Secs. 1, 4.2.2) most of the data presented below have to do with the $E1$ strength function, much less with the $M1$ strength function, and little with higher multipoles. Indeed, in many examples it has not been possible to separate $E1$ from the other multipoles and the strength function must be understood as being mostly $E1$ with smaller but unknown contributions from other types of radiation. In a few examples (Sec. 4.2) the multipoles have been specifically identified.

Because of the above limitations we are unable to present a complete overview of the dependence of even the $E1$ strength function on E_γ and A . Nor will we attempt a complete review of all the fragmentary strength function information that can be extracted. Instead, we have selected some of the more complete examples. These show the degree of agreement between the various methods of Sec. 3 and also, in spite of the gaps in our knowledge, suffice to sketch the general overall trends of the strength function with E_γ and A and more importantly to show some of the detailed structure.

4.1. General Properties

In this section we show the overall energy dependence of the strength function as obtained by the various methods of Sec. 3. All available photo-excitation strength function data for a given target are plotted together on a diagram for \bar{f} and similarly all available \tilde{f} data are plotted together. Where \bar{f} and \tilde{f} strength functions are available for the same element, they are usually shown in adjacent diagrams in the same figure. In all figures, the strength function derived from the Lorentzian line is shown as a basis for comparison. The giant dipole resonance parameters used for the Lorentzian calculation are given in Table V. It is important to note that with few exceptions, the strength functions are absolute; no arbitrary normalizations have been applied.

In order to properly assess the agreement achieved among the various experimental strength functions and between these and the Lorentzian-based curves, one requires some appreciation of the uncertainties associated with each. Some general remarks on this question will be made here and particular remarks appropriate to individual determinations will be made in connection with the element by element review to follow.

All methods are, of course, susceptible to uncertainties from finite counting statistics and, in the high-resolution method in particular, there

TABLE V
Giant Dipole Resonance Parameters

For each nucleus in the first column, the giant dipole resonance width, the peak energy, and the peak cross section of the first component are shown in the next three columns. The width, the peak energy, and the peak cross section of the second component are shown in the fifth, sixth, and seventh columns.

Nucleus	Γ_{G_1} , MeV	E_{G_1} , MeV	σ_{0G_1} , mb	Γ_{G_2} , MeV	E_{G_2} , MeV	σ_{0G_2} , mb	Reference
^{238}U	2.90	10.96	301	4.52	14.04	369	(Ber + 72)
Bi	4.8	13.8	537				(GL 57)
^{208}Pb	4.05	13.42	640				(Bei + 69)
Tl	4.6	14.0	648				(GL 57)
Hg	4.5 ^a	14.0 ^a	405 ^b				
Au	2.9	13.15	255	4.0	13.90	365	(FW 58)
Pt	4 ^a	14.0 ^a	446 ^b				
Ir	4 ^a	14.0 ^a	443 ^b				
Re	4 ^a	14.0 ^a	428 ^b				
W	2.29	12.59	211	5.18	14.88	334	(Ber + 69b)
Ta	1.94	12.59	171	4.98	15.13	265	(BBV 68)
Er	2.9	12.0	225	5.0	15.45	260	(Ber + 69a)
Eu	2.75	12.33	155	5.83	15.79	222	(Ber + 69b)
Sm	4.25	12.77	155	4.6	15.46	260	(Ber + 69a)
Sb	4.5 ^a	15.2 ^a	254 ^a				
^{119}Sn	4.81	15.54	253				(Ful + 69)
^{117}Sn	5.02	15.66	254				(Ful + 69)
In	5.24	15.63	266				(Ful + 69)
Zr	4.0	16.65	211				(Lep + 71)

^a Interpolation.

^b Sum rule.

may be an additional statistical uncertainty from Porter-Thomas fluctuations owing to averaging over too small a number of resonances. In all determinations where f can be extracted point by point from the original measurements, the vertical error bars shown in Figs. 15 to 25 will reflect these statistical uncertainties only. The horizontal bars show the energy

range of the γ -rays contributing to the average. In the spectrum fitting and sequential extraction methods, the statistical uncertainties tend to be reduced because the intervals, ΔE_i , over which spectra are averaged are relatively large (usually > 0.1 MeV). But more important, because of the iterative nature of these methods, realistic estimates of the statistical uncertainties are difficult to carry through. Therefore, for strength functions derived by these two methods error bars have been omitted.

Systematic errors are in general not indicated in the figures. In determinations of f from the photoneutron cross section, systematic errors may be introduced by failing to take proper account of competing photon scattering cross sections. In the methods of Secs. 3.2, 3.3, and 3.4, systematic

TABLE VI
Resonance and Level-Density Parameters

Product nucleus	E_B , MeV	$\bar{I}_{\gamma T \lambda}$, meV ^a	$\varrho_0(E_B) \times 10^4$ MeV ⁻¹ ^b	T , MeV	E_t , MeV
²⁰⁴ Tl	6.54	640.0 ± 70.0	0.078 ± 0.04	0.897	0.0
²⁰⁰ Hg	8.028	205.0 ± 11.0	0.4 ± 0.1	0.858	1.5
¹⁹⁸ Au	6.5	125.2 ± 11.0	0.75 ± 0.1	0.753	0.0
¹⁹⁶ Pt	7.92	110.8 ± 18.0	1.4 ± 0.3	0.717	1.5
¹⁹² Ir	6.14	73.9 ± 3.2	4.3 ± 0.6	0.575	0.0
¹⁸⁷ Re	5.95	51.7 ± 5.4	1.8 ± 0.4	0.555	0.0
¹⁸⁶ Re	6.23	54.3 ± 4.0	2.7 ± 0.4	0.556	0.0
¹⁸⁷ W	5.25	64.0 ± 10.0	0.6 ± 0.3	0.629	0.0
¹⁸³ W	6.5	60.0 ± 7.0	0.9 ± 0.2	0.637	0.0
¹⁸² Ta	6.06	55.7 ± 5.0	1.5 ± 0.2	0.582	0.0
¹⁶⁸ Er	7.771	86.3 ± 0.8	1.8 ± 1.0	0.6	1.0
¹⁵² Eu	6.305	85.4 ± 7.0	15.0 ± 6.0	0.55	0.0
¹⁵⁰ Sm	7.987	60.6 ± 2.0	3.3 ± 1.0	0.6	1.2
¹²² Sb	6.807	94.0 ± 13.0	0.63 ± 0.3		
¹¹⁶ In	6.784	74.0 ± 4.7	0.5 ± 0.2		

^a Ref. (Gol+66).

^b *s*-wave resonance density $\varrho_0 = \varrho/(2J_0 + 1)$, where J_0 is the target spin, Ref. (Gol+66); for ¹⁸⁷Re Ref. (SNG 71).

errors of 10–50% may be introduced by adopting an incorrect value for $\bar{\Gamma}_{\gamma T \lambda}$ and in the method of Sec. 3.4 a further uncertainty of about the same size is associated with $\varrho_0(E_\lambda)$ (Gol+ 66). The level-density parameters and $\bar{\Gamma}_{\gamma T \lambda}$ are given in Table VI. By far the most important systematic error affecting strength functions obtained from photoexcitation below the neutron threshold and by the spectrum fitting and sequential extraction methods is introduced through the nuclear temperature, T , used for the level-density estimate, Eq. (2.14). The temperature is obtained from known level densities at the neutron threshold and from the region below ~ 2 MeV. The latter density is least certain and, in general, available estimates provide only a lower limit. At high γ -ray energies, $E_\gamma \geq 4.5$ MeV, the error in \bar{f} arising from a systematic error in T may be estimated from

$$\Delta \bar{f} \approx -E_\gamma \bar{f} \frac{\Delta T}{T^2} \quad (4.1)$$

For example, in Au for which we derive $T = 0.753$ MeV, a 20% decrease in T increases \bar{f} at 6 MeV by a factor of ~ 3 . This strong dependence of \bar{f} on T is shown graphically in Fig. 8, Sec. 3.2. Thus for \bar{f} obtained by methods of Secs. 3.2 and 3.3, for which no error bars are shown, the systematic uncertainty far exceeds any possible statistical errors.

Uncertainties in Γ_G , E_G , and σ_{0G} entering the Lorentzian prediction for f through Eqs. (2.5), (2.7), and (2.8), introduce uncertainties in the absolute value of the Lorentzian prediction sometimes by as much as a factor of 2. Therefore failure to achieve agreement in absolute magnitude between the Lorentzian curves and the experimentally determined strength functions is much less significant than departures in functional form.

4.1.1. Nuclei with $Z \geq 82$

(a) ^{238}U , ^{232}Th . The strength functions \bar{f} for ^{238}U and ^{232}Th have been calculated from $\bar{\sigma}_{\gamma n}$ and $\bar{\sigma}_{\gamma f}$ measurements (Ber+ 72) as described in Sec. 3.1. The results above 8 MeV in ^{238}U are shown in Fig. 14 where they are plotted with the results of Knowles and Mafra (KM 73) below that energy. The relatively low values of \bar{f} near threshold may not be significant because, in this region where $\bar{\sigma}_{\gamma n}$ varies rapidly with energy, systematic errors in the correction for beam spread may be appreciably larger than the statistical error bars shown on the points. The overall agreement with the Lorentzian-based curve is good. Similar good agreement is found in ^{232}Th (Ber+ 72, MKG 72).

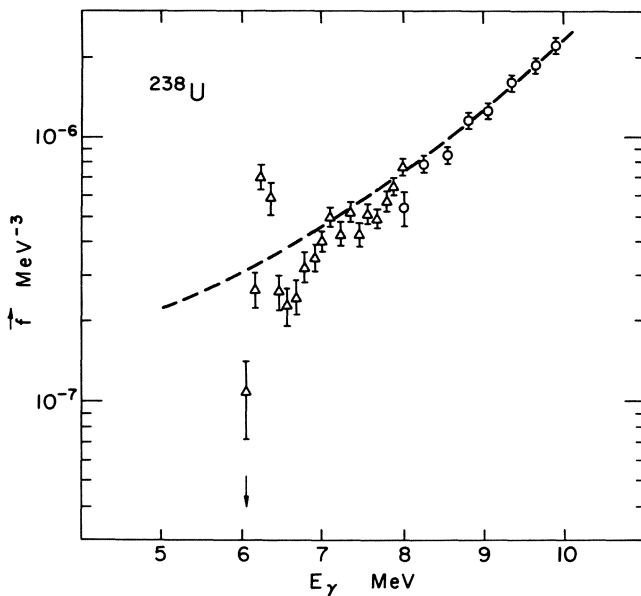


Fig. 14. The strength function \hat{f} for ^{238}U . The \triangle and \circ points are from the $\bar{\sigma}_{\gamma a}$ measurements (KM 73) and (Ber + 72), respectively, shown in Fig. 3. The broken line is derived from the Lorentzian curve fitted to the giant dipole resonance with constants given in Table V. The arrow indicates the (γ, n) threshold.

(b) Pb, Bi . Strength functions \hat{f} for ^{206}Pb , ^{207}Pb , ^{208}Pb , and ^{209}Bi have been calculated from the $\bar{\sigma}_{\gamma n}$ and $\bar{\sigma}_{\gamma\gamma}$ measurements as described in Sec. 3.1. The open circles and triangles in Fig. 15 are from the $\bar{\sigma}_{\gamma n}$ measurements of Fuller and Hayward (FH 62b) and Beil *et al.* (Bei + 69), respectively. The open square at 7.6 MeV in ^{208}Pb is obtained by averaging the ground-state radiation widths of $J = 1^-$ resonances from the $\bar{\sigma}_{\gamma n}$ measurements by Bowman *et al.* (Bow + 70). The level spacing used, $D = 0.04$ MeV, is obtained from the (n, γ) measurements of Allen and Macklin (AM 71) assuming that half of the observed $J = 1$ resonances are 1^- . The closed squares and circles are \hat{f} calculated from the photoelastic scattering cross sections of Swann (Swa 73a) and Khan and Knowles (KK 67), respectively. Only a limited number of points are obtained below the neutron separation energy because strength functions calculated from $\bar{\sigma}_{\gamma\gamma}$ are limited to those few measurements discussed in Sec. 3.1 for which branching ratios and level densities are known. The parity of the levels have not been measured. Above the neutron separation energy the smoothed empirical strength function is in good agreement with that derived from the Lorentzian.

4.1.2. Nuclei with $73 \leq Z < 82$

Strength functions for nuclei in this mass range have been obtained from all the methods discussed in Sec. 3. The $M1$ contribution for γ -ray energies >4.5 MeV following s -wave neutron capture is believed to be small (Sects. 3.4 and 4.2.2) and therefore the empirical strength functions are essentially f_{E1} in this region. Below 4.5 MeV the multipole purity of the strength function is less certain.

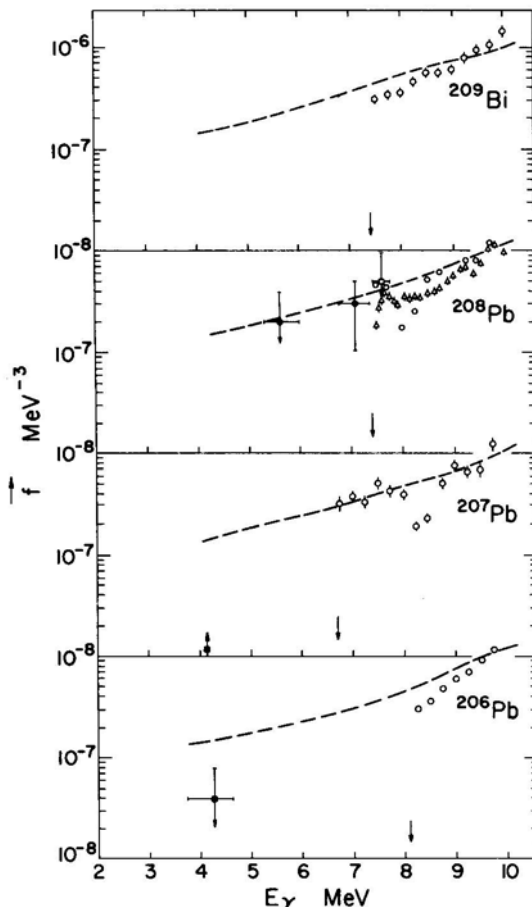


Fig. 15. Strength functions \hat{f} for ^{209}Bi , ^{208}Pb , ^{207}Pb , and ^{206}Pb . Above the neutron separation energies, shown by arrows, the points are calculated from $\bar{\sigma}_{\gamma n}$ measurements, some of which, \circ (FH 62b), \triangle (Bei + 69) and \square (Bow + 70) are shown in Fig. 2. The data points \bullet in ^{208}Pb and \blacksquare in $^{207,207}\text{Pb}$ are from $\bar{\sigma}_{\gamma\gamma}$ measurements (KK 67) and (Swa 73a) respectively. Other details are as in Fig. 14.

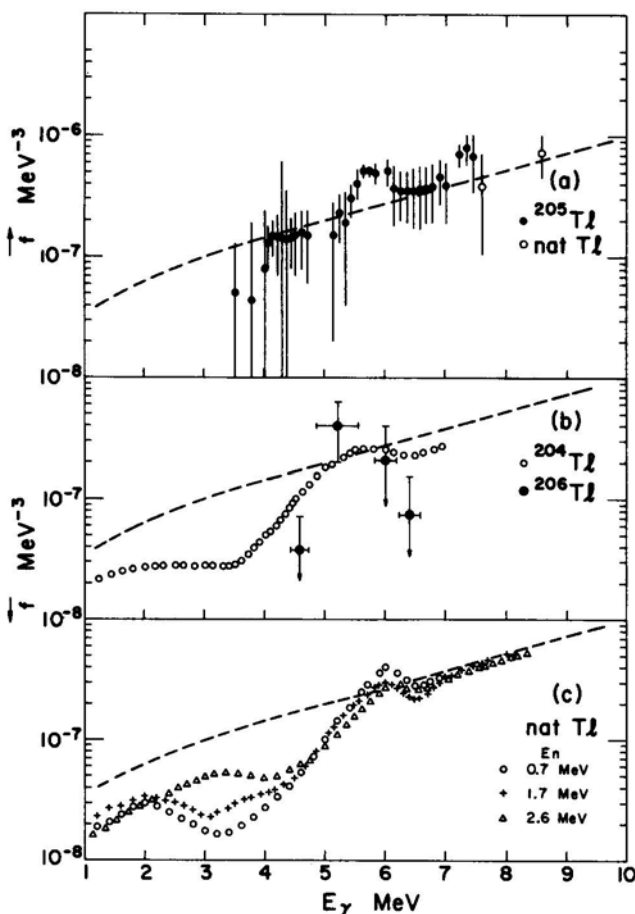


Fig. 16. Strength functions for Tl. (a) The solid circles show \bar{f} in ^{205}Tl calculated from $\bar{\sigma}_{\gamma\gamma}$ (Ear + 73) shown in Fig. 5 and the open circles from $\bar{\sigma}_{\gamma n}$ (GL 57). (b) The closed circles are from resonance (n, γ) data (Ear + 72a) and the open circle from thermal (n, γ) data (BK 53). (c) The strength functions obtained from fast-neutron capture data (Ear + 72b). The broken curves are derived from the Lorentzian.

(a) Tl . Strength functions for isotopes of Tl are shown in Figs. 16a, b, and c. The solid points in (a) give \bar{f} for ^{205}Tl from the photoelastic scattering measurements (Ear + 73). The open circles in (a) are values of \bar{f} for natural Tl (70% ^{205}Tl) from photoneutron cross sections (GL 57).

Strength functions \bar{f} from neutron-capture reactions are shown in (b) and (c). The open circles in (b) show \bar{f} for ^{204}Tl obtained by the spectrum fitting method from thermal neutron capture γ -ray data (BK 53) and the

solid circles are obtained by the high-resolution γ -ray method from individual γ -ray transitions in ^{206}Tl following resonance neutron capture in ^{205}Tl (Ear + 72a). In (c) three strength functions obtained by fitting the spectral distribution following ~ 0.7 MeV (\circ), ~ 1.7 MeV (+), and ~ 2.6 MeV (\triangle) neutron capture in natural Tl are shown. For $E_\gamma > 4$ MeV these have similar form. However, below 4 MeV, the shape of \bar{f} is found to depend on the excitation energy.

Relative to \bar{f} derived from the Lorentzian tail, the strength functions in all three isotopes and for both photoexcitation and capture reactions show a marked irregularity, i.e., a small resonancelike structure at ~ 6 MeV and a pronounced dip below 5 MeV (see Sec. 4.2.2). When uncertainties in f arising from uncertainties in level-density parameters and, in the Lorentzian curve, from uncertainties in giant dipole resonance parameters are allowed for, the absolute magnitudes of the strength function and the Lorentzian above 6 MeV are not significantly different.

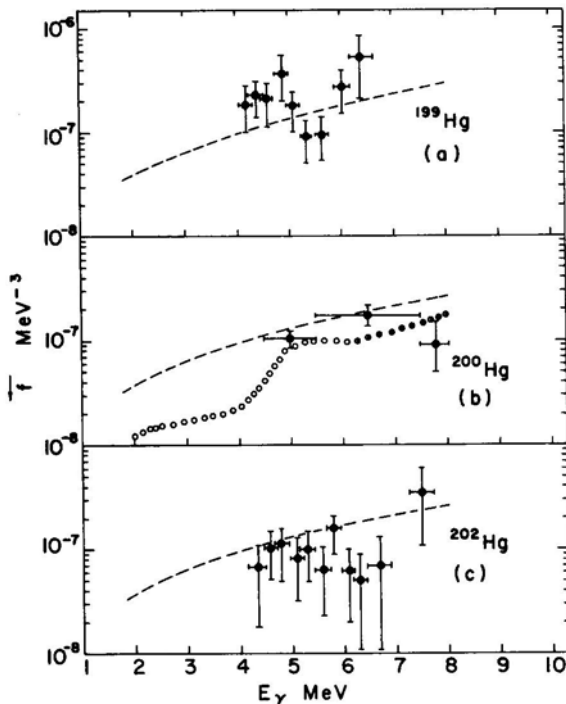


Fig. 17. Strength functions for Hg. The solid circles in a, b, and c are from resonance (n, γ) data (LEB 73). In (b) the open and half-filled circles are from (n, γ) thermal (Gro + 69) and resonance data (LEB 73), respectively.

(b) *Hg*. The strength functions for ^{199}Hg , ^{200}Hg , and ^{202}Hg are shown in Fig. 17a, b, and c. The solid points are obtained by averaging the high-resolution γ -ray absolute intensities, from neutron capture in resonances (LEB 73), over the energy interval shown by the horizontal bars. The open circles in (b) are strength functions for ^{200}Hg obtained by spectrum fitting the γ -ray distributions from thermal neutron capture (Gro+ 69). The energy dependence of the strength function shown by half-filled circles was obtained from epithermal neutron capture (LEB 73). The general shape of this strength function (open circles) is the same as in the Tl isotopes, i.e., there is a dip with respect to the Lorentzian below 5 MeV. Unfortunately, the data for both ^{199}Hg and ^{202}Hg are neither extensive nor precise enough to confirm this trend. The maximum (scarcely prominent enough to be called a pigmy resonance) seems to be at ~ 5 MeV, somewhat lower in energy than in Tl.

(c) *Au*. Strength functions for isotopes of gold above 4.8 MeV have been extracted by each of the four methods discussed in Sec. 3. Thus their mutual consistency can be tested.

The strength function \tilde{f} for ^{197}Au shown by solid points in Fig. 18a has been deduced from $\bar{\sigma}_{\gamma\gamma}$ measurements (Bar 69) as described in Sec. 3.1. Above the (γ, n) threshold (8.1 MeV) \tilde{f} obtained from $\bar{\sigma}_{\gamma n}$ measurements is shown by open circles (FW 58) and triangles (Ful+ 62). The \tilde{f} for ^{198}Au , shown by the open circles in (b) and (c), was extracted by the spectrum fitting method from γ -ray distributions obtained from capture of thermal neutrons (Gro+ 69) and ~ 2.6 MeV neutrons (Ear+ 72b), respectively. The solid triangles in (b) show \tilde{f} obtained by the sequential extraction method (Bar+ 70) and the solid circles by the high-resolution γ -ray method from individual γ -ray intensities following capture of neutrons from a ~ 2 keV broad beam (LBT 72). Each of the solid circles was obtained by further averaging over γ -rays in a 250-keV-wide interval.

In the region of overlap, $E_\gamma > 4.8$ MeV, the strength functions obtained from all four methods are consistent. At 6 MeV the absolute magnitude of \tilde{f} is consistent with the Lorentzian tail (broken curve), however, below 5 MeV the empirical strength functions depart significantly below the Lorentzian.

There is a shallow maximum or pigmy resonance peaking at ~ 6 MeV in ^{197}Au and ^{198}Au .

(d) *Pt, Ir, Re, W*. The strength functions for these elements shown by open circles in Figs. 19a-d were deduced by fitting spectral distributions of γ -rays following thermal neutron capture in the natural elements (Gro+

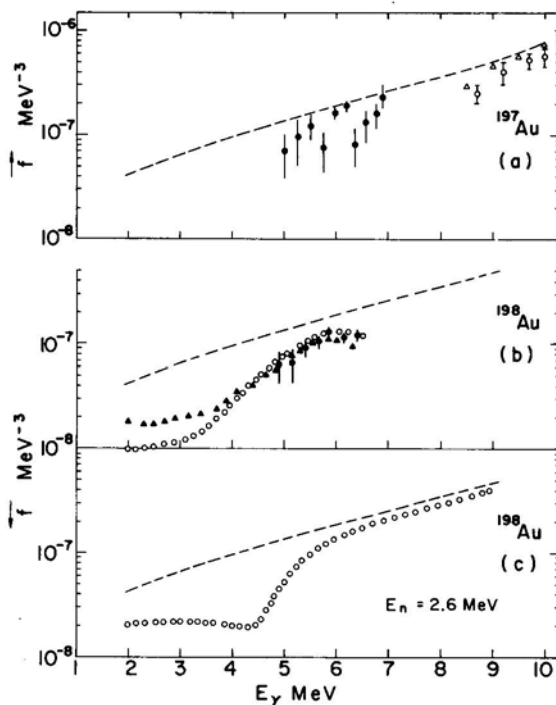


Fig. 18. Strength functions for Au. (a) The solid circles are from $\bar{\sigma}_{\gamma\gamma}$ (Bar 69), points above 8 MeV are from $\sigma_{\gamma n}$, \circ (FW 58) and \triangle (Ful+ 62). (b) The points \circ , \blacktriangle , and \bullet are from the spectrum fitting method—thermal (n, γ) data (Gro+ 69), the sequential extraction method— $(d, p\gamma)$ data (Bar + 70) and the high-resolution method (LBT 72). (c) Open circles \tilde{f} from spectrum fitting method. Other details are as in Fig. 14.

69). For the even–even ^{196}Pt nucleus the energy dependence of \tilde{f} in the 6.2–7.9-MeV region (half-filled circles) was obtained from the relative intensities of the average partial radiation widths observed by Bollinger and Thomas (BT 67). The solid point for ^{196}Pt was obtained by averaging partial radiation widths of 9 γ -rays between 6.0 and 7.9 MeV observed from twenty-two $J = 1^-$ resonances (Sam+ 68).

The solid point for ^{188}Re was obtained by averaging reduced partial widths of 53 γ -rays in the region $4.8 < E_\gamma < 5.9$ MeV following thermal neutron capture (She+ 72).

The solid point in W was obtained from intensities of 7.302- and 7.413-MeV γ -rays in ^{184}W following 2-keV neutron capture (GR 71). The level spacing $D = 28.7$ eV for resonances of spin 1 was used. In the energy

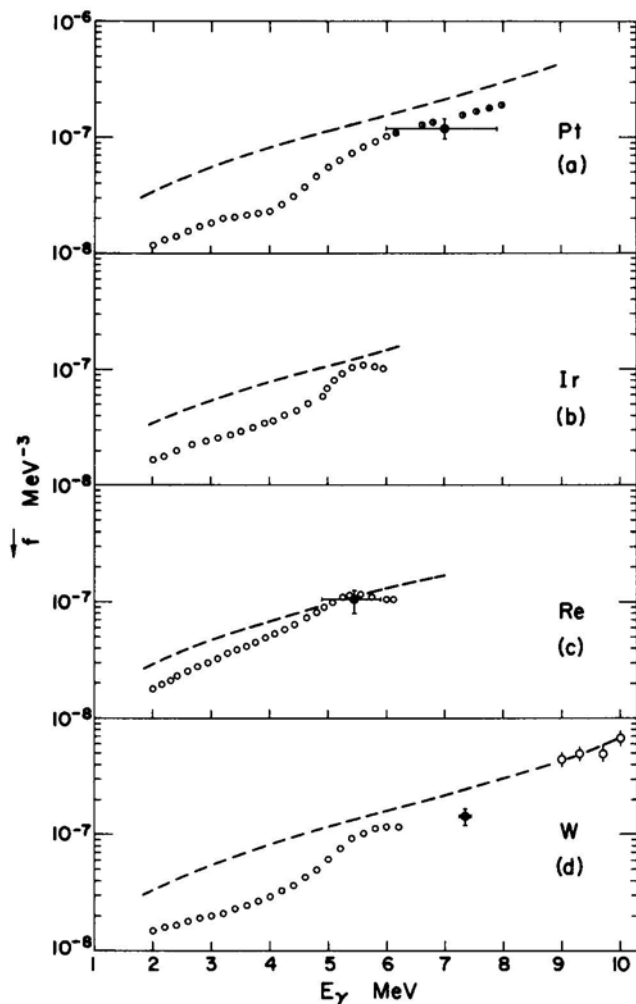


Fig. 19. Strength functions for Pt, Ir, Re, and W. The open circles in (a) to (d) below 8 MeV are from fitting of spectra from thermal neutron capture (Gro+ 69). In (a) the energy dependence of \tilde{f} shown by half-filled circles was obtained from (BT 67 see text). The solid points are from high-resolution method, Pt (Sam+ 68), Re (She+ 72) and W (GR 71). In (d) the open circles above 8 MeV are from $\bar{\sigma}_{\gamma n}$ (Ber+ 69b). Broken curves are from Lorentzians.

range 9 to 10 MeV the strength functions \tilde{f} for natural W have been obtained from $\bar{\sigma}_{\gamma n}$ (Ber + 69b).

The strength functions in these elements also show features similar to those in Hg, Au, and Tl, i.e., relative to the Lorentzian tail, there is a dip in the empirical strength function below 5 MeV and a hint of a pigmy resonance in Ir and Re.

(e) *Ta*. The consistency of form of the strength function \tilde{f} obtained by the different methods discussed in Sec. 3 can also be demonstrated for Ta. The strength functions for ^{182}Ta shown by the open circles in Fig. 20a and by open circles and triangles in Fig. 20b were obtained by fitting spectral distributions of γ -rays following capture of thermal neutrons (Gro + 69) and neutrons of 0.7 and 2.6 MeV (Ear + 72b), respectively. Above 6.2 MeV the strength function shown by the open triangles has an uncertainty of about a factor of 2 owing to poor precision of the data in this energy region. The strength function, given by solid triangles in Fig. 20a, was obtained from $(d, p\gamma)$ measurements using the sequential extraction method (Bar + 70) and the solid points with error bars are obtained from the individual γ -ray intensities following capture of a \sim 2-keV-broad beam of neutrons (LBT 72). In order to reduce the Porter-Thomas fluctuations at each point,

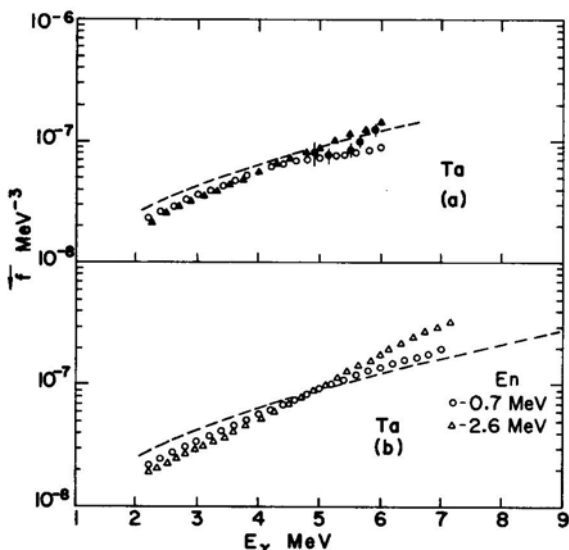


Fig. 20. Strength functions for Ta. (a) The points \circ , \blacktriangle , and \bullet have the same meaning as in Fig. 18b. (b) The points \circ and \triangle are obtained by the spectrum fitting method from fast-neutron capture data (Ear + 72b).

additional averaging was carried out over all γ -rays in a 250-keV interval. The strength functions obtained from the different methods are consistent within the uncertainties inherent in each method.

In overall form the empirical strength function for Ta is very similar to the Lorentzian tail of the giant dipole resonance with no sign of a pigmy resonance.

4.1.3. Nuclei with $55 < Z < 73$

Strength functions \tilde{f} above the neutron separation energy can be obtained from $\bar{\sigma}_{\gamma n}$ measurements in natural isotopes of many nuclei in this region. These cross sections, in the energy range from the neutron threshold to well above the giant dipole resonances, have been measured for example in Ba, La, Ce, Pr (Bei+ 71), Ce, Sm, Eu, Er, Lu (Ber+ 69a), Eu, Gd, Ho (Ber+ 69b), and Tb (BBV 68). However, below the neutron threshold there is little or no information from which values of \tilde{f} can be obtained.

Strength functions \tilde{f} can be obtained from the spectrum fitting method, however, because of the presence of both $E1$ and $M1$ radiation in the spectra, the empirical strength functions extracted lose much of their significance. In Fig. 21a, b, and c, \tilde{f} obtained from $\bar{\sigma}_{\gamma n}$ are shown by open circles, above 8 MeV for natural samples of Er (Ber+ 69a), Eu (Ber+ 69b) and Sm (Ber+ 69a), respectively. The open circles below 8 MeV are obtained by the spectrum fitting method from the thermal neutron capture spectra (Gro+ 69). The solid points in (a) show \tilde{f}_{E1} obtained from average neutron capture data (BT 70), as discussed in Sec. 3.4. The absolute normalization was obtained by comparing the average reduced intensities with those observed in thermal capture (Ras+ 69). The uncertainties arising from this calibration are shown by the error bars. In (b) the solid points are obtained by averaging individual γ -ray intensities (without regard to multipole type) from thermal capture (SH 68). In (c) the solid points are from the relative intensities of $E1$ γ -rays following average neutron capture (BS 70). The absolute normalization was obtained as in Er.

In Er and Eu the Lorentzian is in good agreement with the data. In Sm there is an apparent discrepancy which, in view of inherent uncertainties, may not be significant.

The strength functions from different methods for any one element are consistent among themselves and follow the general form of the Lorentzian curve.

The functional form of \tilde{f}_{E1} for $^{156,158}\text{Gd}$ (BT 70) is compared with the Lorentzian in Fig. 22. The solid curve which is the best fit through the data points deviates slightly ($\sim 20\%$ at 7.5 MeV) from the Lorentzian. Between

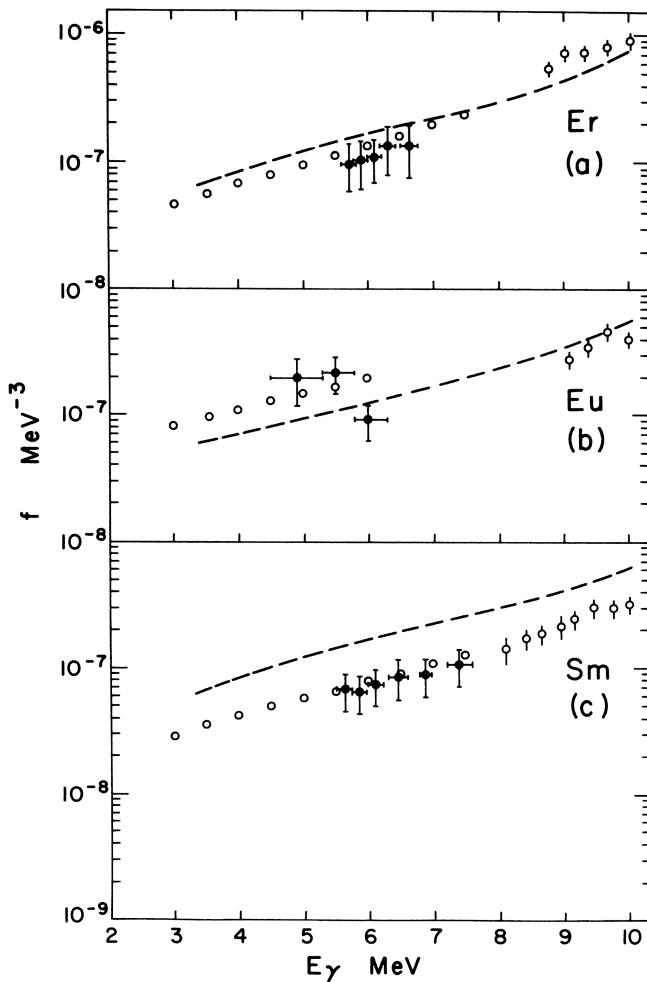


Fig. 21. Strength functions for Er, Sm, and Eu. The open circles above 8 MeV are from $\bar{\sigma}_{\gamma n}$, Er and Sm (Ber+ 69a) and Eu (Ber+ 69b). Below 8 MeV the open circles are obtained by the spectrum fitting method from thermal capture data (Gro+ 68, 69). The solid circles are obtained by the high-resolution method from (a) (BT 70), (b) (SH 68), and (c) (BS 70). The broken curves are from the Lorentzian.

7.5 and 8 MeV the empirical \tilde{f}_{E_1} appears steeper than that derived from the Lorentzian.

Similar local deviations from the Lorentzian have been observed in other nuclei in this mass range (see Table III). Several $M1$ transitions have been identified in the spectra from average resonance capture.

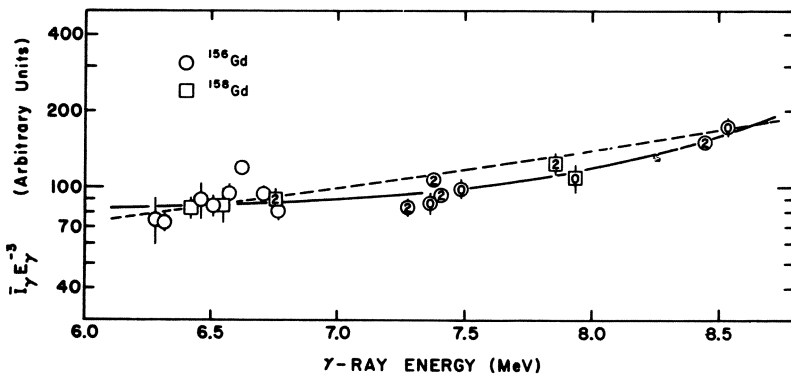


Fig. 22. The relative strength function for $^{156,158}\text{Gd}$ (BT 70). The numbers within some of the points are the spins of final states. The solid line is the best fit through the points and the broken line is derived from the Lorentzian.

4.1.4. Nuclei with $40 < Z \leq 55$

The γ -ray spectral distributions from (n, γ) and $(d, p\gamma)$ reactions in Cs, I, and Sb (see Sec. 4.2.2) contain a bump similar to those for nuclei near Pb. Because of the difficulty in obtaining reliable estimates of level densities both near the neutron threshold (because of unidentified p -wave resonances) and at lower excitation energies, we have not attempted to extract \tilde{f} by the spectrum fitting method. However, Starfelt (Sta 64), using both Newton's level-density formula (New 56) and the constant temperature level-density formula, had concluded that \tilde{f} in Cs exhibits a small peak at ~ 5.5 MeV. Brzosko *et al.* (Brz+ 71), using the Gilbert and Cameron (GC 65) level-density formula, have also extracted strength functions from spectral distributions observed in (p, γ) and (n, γ) reactions. They conclude that "echo-resonances" in \tilde{f} at 7, 8, 6.8, 6.5, and 6 MeV are required to fit the data in Ag, In, Sb, I, and Cs, respectively. Unfortunately, as discussed in Secs. 2.3 and 3.2, the Gilbert and Cameron formula does not give reliable estimates of level densities and therefore the strength of these echo resonances would appear to require further verification when better level densities are available.

In Fig. 23, \tilde{f}_{E1} and \tilde{f}_{M1} for ^{122}Sb obtained from the resonance neutron capture data of Lottin and Paya (LP 71) are shown. The basis for the identification of $E1$ and $M1$ transitions used by these authors is the separation of the average γ -ray intensities into two groups (see Sec. 3.4). The ratio $\tilde{f}_{E1}/\tilde{f}_{M1}$ is about 3. Similar conclusions were drawn by Bhat *et al.* (Bha+ 70).

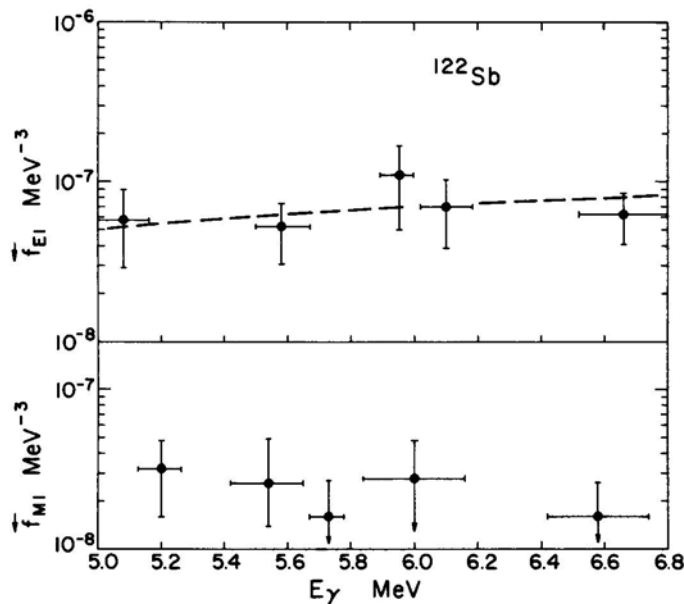


Fig. 23. Strength functions for ^{122}Sb . The points are from the neutron-resonance capture data (LP 71). The broken curve is from the Lorentzian.

The large uncertainty in the data preclude any investigation of a structure in \bar{f} .

The form of \bar{f}_{M1} derived from the average neutron capture γ -rays in Sn isotopes (Bol 70) is shown in Fig. 24. There is a suggestion of a peak at ~ 8.5 MeV. In Fig. 25 \bar{f}_{E1} and \bar{f}_{M1} for ^{116}In from neutron capture in seven

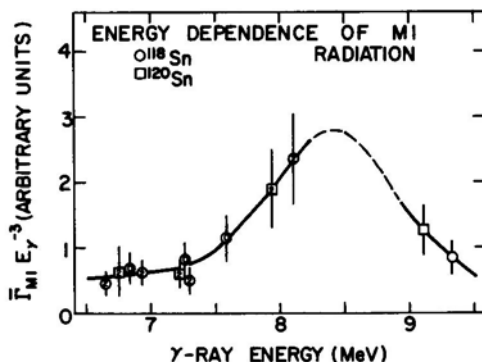


Fig. 24. The relative $M1$ strength function for $^{118,120}\text{Sn}$ (Bol 70). The numbers within the points refer to the final state spins, and the solid curve represents a best fit through the points. The broken curve is interpolated.

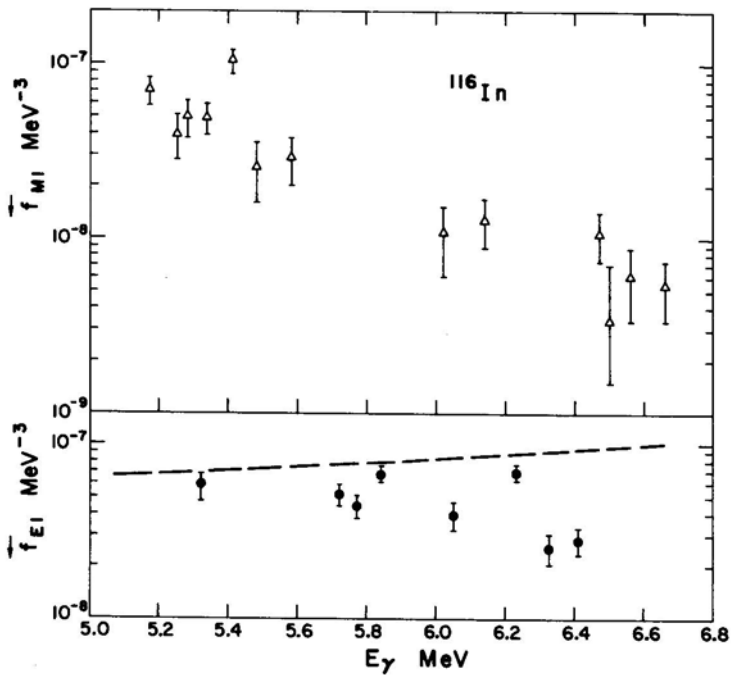


Fig. 25. The $M1$ and $E1$ strength functions for ^{116}In . The points are from neutron resonance capture (LEB 70). The broken curve is from the Lorentzian.

resonances (LEB 70) are shown. The $E1$ and $M1$ γ -rays were identified from the known spins and parities of final states. The \bar{f}_{E1} is almost constant, however, \bar{f}_{M1} shows an energy dependence apparently peaking below 5.4 MeV. Stefanon *et al.* (Ste+ 72) also investigated γ -rays above 5.4 MeV from 31 resonances in ^{115}In ; their data confirm the above trends in f . Although the apparent peaks in \bar{f}_{M1} in In and Sn are at different energies, it is interesting to note that transitions in these peaks feed states ~ 1.5 MeV above the ground state in both cases.

The general form of (dipole) strength functions in ^{90}Zr and Sn is presented in the next section (see Figs. 26-28) in connection with discussions of substructure. While the original measurements (AMS 70, Win+ 70) included no determination of multipolarity, these curves are similar in overall form and absolute magnitude to those derived from the Lorentzian. Although this is consistent with the presence, if not a preponderance, of $E1$ transitions it cannot be construed as evidence that the substructure peaks are $E1$.

4.2. Detailed Properties

From the general shapes of the γ -ray strength functions described in Sec. 4.1 it is clear that they are not always smoothly varying but may possess more or less prominent irregularities or gross-substructure involving many transitions and, sometimes, extending over a range of nuclei. Single-line (microstructure) effects which, by definition, deserve no attention in a treatment concerned with average behavior are in general smoothed out in these curves. However, at closed shells, particularly in ^{208}Pb , the average approach is scarcely appropriate even at 5–8 MeV and some attention to individual transitions is essential for an adequate appreciation of the overall trends of the substructure.

Much experimental effort has been expended in investigating the nature and origin of the strength function irregularities or, more precisely, of the γ -ray structures to which they give rise in the observed spectra. Chronologically, it was in such experiments (e.g., LS 65) that the spectral irregularities were originally demonstrated to arise from the strength function and not some other parameter such as the level density. The justification of the spectrum fitting and sequential extraction methods, in which uniformly varying statistical level densities are assumed and irregularly varying strength functions are derived, depends in part on prior knowledge established by these experiments.

In this section we review the results of some of the more important experiments revealing substructure. Since some irregularities show up more clearly in one type of reaction than in others, it will be convenient to subdivide the discussion by the reactions used. We will also, for directness of presentation, frequently discuss the irregularities as properties of the spectra rather than of the underlying strength functions.

4.2.1. Photoexcitation Reactions, Local Substructure

Gross structure has been observed in the photoabsorption cross section of a number of nuclei above the neutron separation energy. In all cases, averaging is over many resonances so that the major irregularities in strength are not attributable to statistical fluctuations. We now discuss the evidence for some of these substructures and their significance.

(a) ^{90}Zr , Sn . Substructure appears in the photon strength functions \vec{f} of ^{90}Zr and Sn, Figs. 26 and 27, respectively, which we have obtained by applying Eq. (2.5) to the total photon cross section reported by Axel *et al.* (AMS 70). The 70-keV γ -beam resolution used in these measurements

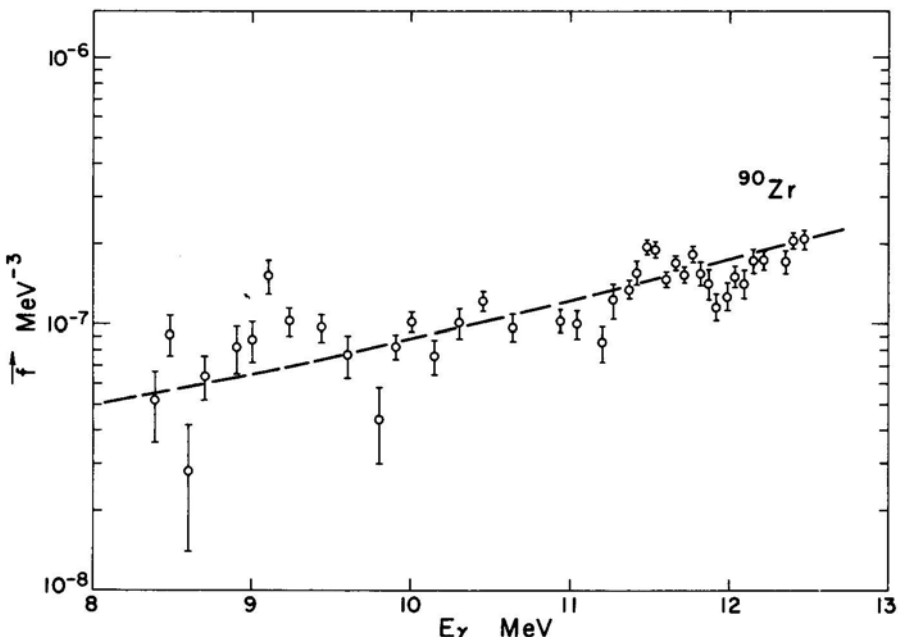


Fig. 26. The strength function \vec{f} for ^{90}Zr . The points are calculated from $\bar{\sigma}_{\gamma a}$ (AMS 70). In estimating $\bar{\sigma}_{\gamma a}$ it was assumed that the elastic photon scattering above 8.68 MeV was due to ^{90}Zr only. The broken curve is derived from the Lorentzian.

is sufficient to average over many resonances. In ^{90}Zr , below the effective (γ, p) threshold at 10.6 MeV, only photon elastic and inelastic scattering contribute to the cross section; the neutron threshold is at 12 MeV. Above 10.6 MeV, $\sigma_{\gamma p}$ must be taken into account in estimating the photon strength function. For this estimate the $\bar{\sigma}_{\gamma p}$ were obtained (AMS 70) by detailed balance from (p, γ) measurements in ^{89}Y (ORR 66, ORW 67, Mas+ 69). Of particular interest is the substructure in ^{90}Zr between 11.2 and 11.8 MeV, since this structure has been inferred previously from (p, γ) measurements (ORR 66). As emphasized by Axel *et al.* (AMS 70) the increase in the photon interaction near 11.5 MeV cannot be ascribed to the photo-proton cross section alone but is the combined result of $\sigma_{\gamma T}$ and $\sigma_{\gamma p}$.

It is pointed out by Axel *et al.* (AMS 70) that the strength shown in Fig. 27 involves only the even isotopes of Sn because in the odd isotopes neutron emission is allowed, and dominates over photoemission. Prominent substructure has also been observed in the photon strength functions of ^{119}Sn and ^{117}Sn in measurements of the ground-state photoneutron cross section $\bar{\sigma}_{\gamma n_0}$ near 7.8 MeV by Winhold *et al.* (Win+ 70; see however, JS 73).

These are shown in Fig. 28 along with the extrapolated Lorentzian line (Ful + 69). The peaks have widths of several hundred keV and include many individual levels. Because photon emission is relatively weak, $\bar{\sigma}_{\gamma n_0}$ provides a good approximation to $\bar{\sigma}_{\gamma a}$ and gives a good measure of \vec{f} . The authors point out that the decrease in $\sigma_{\gamma n_0}$ above 7.8 MeV in ^{119}Sn might be due to p -wave neutron emission but that explanation cannot account for the corresponding decrease in ^{117}Sn where the threshold is higher. They compare these results with the quasielastic scattering data of Axel *et al.* (AMS 70) for natural Sn near 8 MeV (see Fig. 27) and conclude that since the widths and general shapes are similar, all the isotopes of Sn, even as well as odd, must exhibit this characteristic structure near 8 MeV.

(b) ^{209}Bi , $^{206-208}\text{Pb}$. Fluctuations of the elastic cross section $\bar{\sigma}_{\gamma\gamma}$ and strength function \vec{f} in ^{208}Pb and neighboring nuclei, shown in Figs. 2 and 15, cannot be identified for certain as either gross substructure or statistical fluctuations because the level spacing is large and the statistical

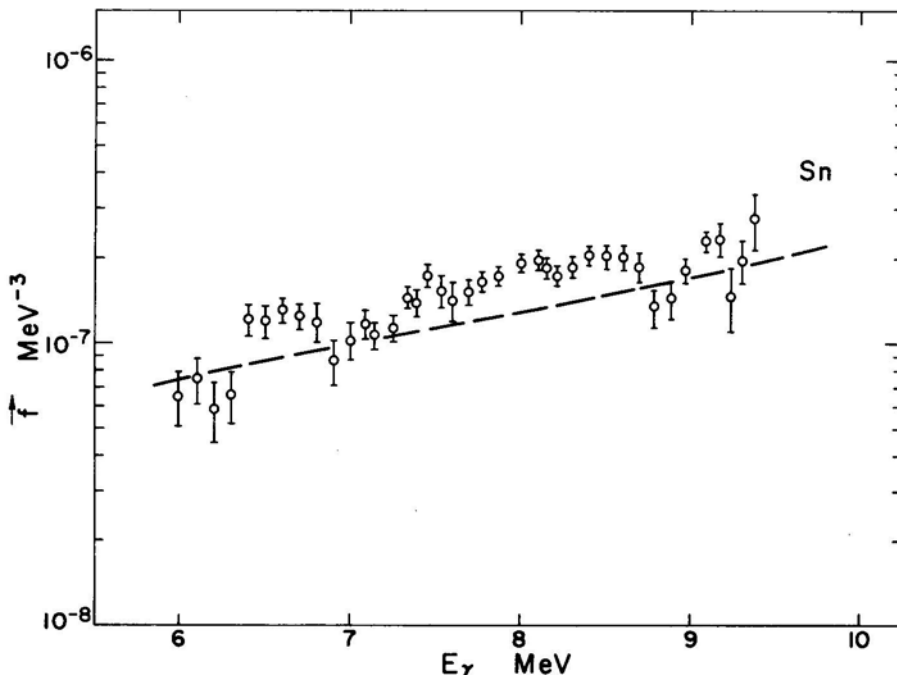


Fig. 27. The strength function \vec{f} for Sn. The points are calculated from $\bar{\sigma}_{\gamma a}$ (AMS 70). In estimating $\bar{\sigma}_{\gamma a}$ it was assumed that only those isotopes contribute which have photoneutron thresholds above E_γ , that these isotopes have equal cross sections, and that photon partial widths follow a Porter-Thomas distribution.

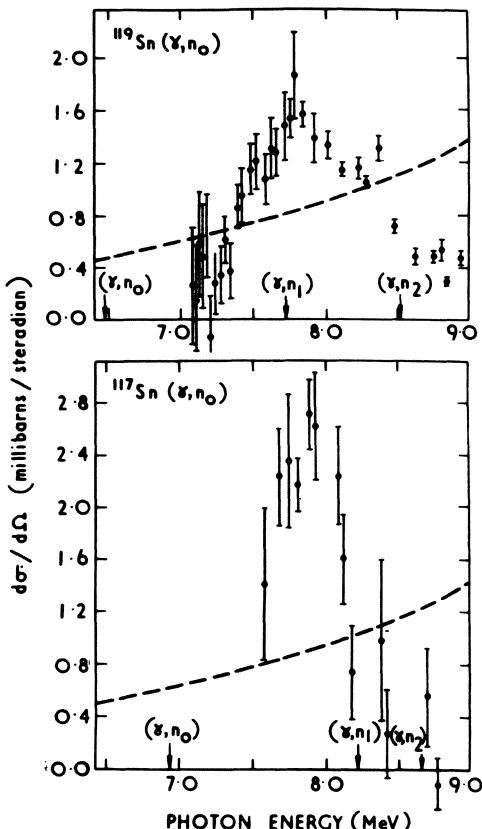


Fig. 28. Differential cross section measurements for $^{119}\text{Sn}(\gamma, n_0)$ and $^{117}\text{Sn}(\gamma, n_0)$ (Win + 70).

sample size small. For example, the strength function below 7 MeV in ^{208}Pb (Fig. 15), obtained by averaging the few available individual transitions shows, within the wide limits of uncertainty, no evidence of substructure. On the other hand, $\bar{\sigma}_{\gamma\gamma}$ for ^{206}Pb and ^{209}Bi , obtained with moderate resolution (Fig. 2) shows considerable fluctuations which may represent a real substructure, especially if many transitions are involved in each peak. Perhaps a more definite substructure effect is indicated by the low values of \vec{f} relative to the Lorentzian in ^{206}Pb and ^{207}Pb at 4.2 MeV in Fig. 15 and by the complete absence of dipole photoabsorption below 5.0 MeV in ^{208}Pb (Swa 73a). This is undoubtedly just a continuation of the step effect in f at ~ 4.5 MeV in elements between Tl and W (Figs. 16–19). This effect is discussed further in Sec. 4.2.2. A concentration of $M1$ strength is evident in the threshold photoneutron cross section and angular distribution

measurements on ^{208}Pb by Bowman *et al.* (Bow+ 70) and Toohey and Jackson (TJ 72). Bowman *et al.* report seven 1^+ states in ^{208}Pb between 7.5 and 8.5 MeV which combine to give a total $M1$ width of 52 eV. These measurements are only partly supported by Toohey and Jackson who conclude, because of uncertainty in identifying the outgoing neutrons as p or s -plus- d wave, that only two of the seven can be unambiguously assigned 1^+ . For the same reason, some of the peaks between 602 and 846 keV, assigned by Bowman *et al.* (Bow+ 70) are probably not $M1$. Toohey and Jackson set a minimum integrated width of 20 eV for the $M1$ strength detected.

According to the shell model, the strength of the $M1$ excitation in ^{208}Pb is mostly contributed by spin flips from $i_{13/2}$ to $i_{11/2}$ for neutrons and from $h_{11/2}$ to $h_{9/2}$ for protons. If the $i_{13/2}$ and $h_{11/2}$ orbits contain more than one particle (Coh 71), the $M1$ strength can be enhanced to several times the single-particle value. Weiss (Wei 70) estimates a total $M1$ width of 100 eV, of which 43 eV is for the $i_{13/2}$ neutrons and 57 eV for the $h_{11/2}$ protons. However, spin-dependent forces between the excited particles and the residual nucleus can cause polarization effects (BM 69, page 388) which can reduce the single-particle magnetic moments by two and thus the $M1$ radiation widths by 4. With polarization included then, the total $M1$ strength can be between 25 and 50 eV. Thus the observed total width 20–50 eV could account for any amount between all the strength to less than half. Polarization, as well as reducing the strength, can cause a splitting in its distribution (GGS 66). Thus an $M1$ strength of 20 eV between 7.5 and 8.5 MeV might be accompanied by a like amount at lower energy. In the $^{208}\text{Pb}(e, e')$ reaction, $M1$ peaks at 7.9 MeV, $\Gamma_{\gamma_0} = 43$ eV and 6.2 MeV, $\Gamma_{\gamma_0} = 11$ eV have been observed (Fag+ 73). In the $^{208}\text{Pb}(\gamma, \gamma)$ reaction an $M1$ transition at 7.20 MeV, $\Gamma_{\gamma_0} = 0.8$ eV has been identified (MSW 70). A considerable amount of additional strength is known to be present (KK 67, KK 73, Sec. 5.3). Any one of these transitions, if $M1$, together with the $M1$ strength already observed would account for all $M1$ strength predicted by shell-model calculations.

Concentrations of $M1$ strength in $^{206,207}\text{Pb}$ (Bow+ 70) and of $E2$ strength in ^{207}Pb (Bow+ 70) and ^{208}Pb (Bus+ 72) are also reported.

(c) ^{238}U . A further example of substructure is that shown at 6.2 MeV in the photon strength function \vec{f} of ^{238}U (KM 73) (Fig. 14). The peak, ~ 300 keV wide, is located at the fission threshold, just above the neutron separation energy, and is prominent in both the photoneutron and photo-fission cross sections. Angular distribution measurements of the fission

yield show the 6.2 MeV peak to have a $\sin^2 \theta$ distribution, θ being the angle between the fission fragment direction and the incident beam direction. In the theory of fission discussed by Albertson and Forkman (AF 65) low-energy states with $J\pi = 1^\pm$ near the fission threshold can be described by exit channel quantum numbers $K = 0$ and $K = 1$ and should display photo-fission angular distributions $\sin^2 \theta$ and $2 - \sin^2 \theta$, respectively (KM 73). On this basis one associates the prominent peak at 6.2 MeV with the $K = 0$ exit channel and the underlying continuum with the $K = 1$ exit channel (KKC 70). However, this interpretation of fission yield substructure in terms of exit channels does not account for the corresponding substructure in the γ -ray strength function which concerns the entrance channel. A possible explanation is that photoabsorption over the 300-keV-wide energy interval containing the substructure takes place through at least two channels of comparable strength, each involving levels of spin $J = 1$. The most natural interpretation for these two channels is that they correspond to electric and magnetic dipole photoabsorption, the electric dipole absorption being associated with the substructure and the magnetic dipole with the underlying continuum.

4.2.2. Nucleon Transfer Reactions, 5.5-MeV Radiation

An outstanding feature common to many of the strength functions in Figs. 15–19 (Bi to W) is the irregularity below ~ 6 MeV. This takes the form of a small “pigmy” resonance at 5.5 MeV in some nuclei, and a more or less abrupt decrease below 5 MeV in all nuclei in the range $182 < A \leq 206$. This feature gives rise to a bump ~ 1 MeV wide at ~ 5.5 MeV in the γ -ray spectra from (n, γ) , $(d, p\gamma)$, and (γ, γ') reactions which was originally referred to as the “anomalous” bump (see historical remarks, Sec. 1). A similar but weaker bump is found in spectra from the region $108 \leq A \leq 134$ and evidence for a similar effect in (p, γ) reactions has been reported (Brz+ 71).

In this section we review experiments contributing to the understanding of the 5.5-MeV bump and relate the results to properties of the strength function. The fast neutron capture and $(d, p\gamma)$ reactions together provide a means of studying the 5.5-MeV bump over a wide range of excitation energy from ~ 5 MeV, where some evidence of the effect begins to appear, to ~ 4 MeV above the neutron separation energy, above which the effect becomes progressively obscured by the more intense γ -rays from the $(n, n'\gamma)$ reaction. Because of low energy resolution, (one is generally restricted to the use of NaI detectors by available γ -ray intensities in fast-

neutron capture and in $(d, p\gamma)$ particle-gamma coincidence measurements) detailed information about γ -rays comprising the bump is generally not obtained in those reactions. Fortunately, thermal and resonance neutron capture γ -ray spectra can be studied with high-resolution spectrometers and some information on the properties of individual γ -rays in the bump can be obtained. However, such measurements are limited to a narrow region of excitation energy, at most 100 keV wide, above the neutron separation energy. Examples of resolved lines in the bump from resonance capture in ^{205}Tl are shown in Fig. 29 (Ear+ 72a).

(a) Origin of the 5.5-MeV Radiation. The experimental results which we shall now discuss show that the 5.5-MeV bump γ -rays are primary, that they are emitted in the decay of resonances of the compound nucleus, and that the bump is not a consequence of local level-density irregularities but must be, as portrayed in Sec. 4.1, a strength function effect.

The 5.5-MeV bump has been shown to consist of primary radiation by application of the Ritz combination principle to neutron capture γ -rays aided by knowledge of the level scheme gained from other reactions. This has been particularly successful in fitting thermal neutron capture γ -rays from the bump region in $^{203}\text{Tl}(n, \gamma)^{204}\text{Tl}$ and $^{205}\text{Tl}(n, \gamma)^{206}\text{Tl}$ (Wei+ 69) and in $^{197}\text{Au}(n, \gamma)^{198}\text{Au}$ (Joh+ 66), and resonance neutron capture γ -rays in $^{205}\text{Tl}(n, \gamma)^{206}\text{Tl}$ (Ear+ 72a). Other examples of decay-scheme-fitting in the $182 < A \leq 206$ mass region have been compiled (Gro+ 69). In an elaboration of this approach, γ -ray coincidence measurements have been used to show that at least 45% of the bump γ -rays in the $^{199}\text{Hg}(n, \gamma)^{200}\text{Hg}$ thermal neutron capture spectrum are primaries (Bar+ 67). A still more convincing confirmation of the primary nature of the bump γ -rays is obtained in resonance neutron capture where it has been possible to show in several instances that the energies of bump γ -rays obey $E_\gamma = E_{\gamma 0} + E_n$, where $E_{\gamma 0}$ is the γ -ray energy corresponding to thermal capture. Similar shifts in E_γ or distortions of the resonance-averaged γ -ray line-shape obtained with the LNR technique (Sec. 3.4) can be used to establish primary assignment. By such methods the predominance of primary radiation has been demonstrated above ~ 5 MeV in Au (AB 68, LBT 72) and above ~ 4.7 MeV in Ta (HGR 71, LBT 72).

That the 5.5-MeV-bump γ -rays are emitted in γ -decay from resonances is evident (ELB 69) from many results, such as illustrated by the 2.800- and 3.048-keV resonances in Fig. 29, in which the fine-structure intensities fluctuate strongly from one resonance to the next while the overall bump shape is preserved. Were the bump a nonresonant, direct-capture effect,

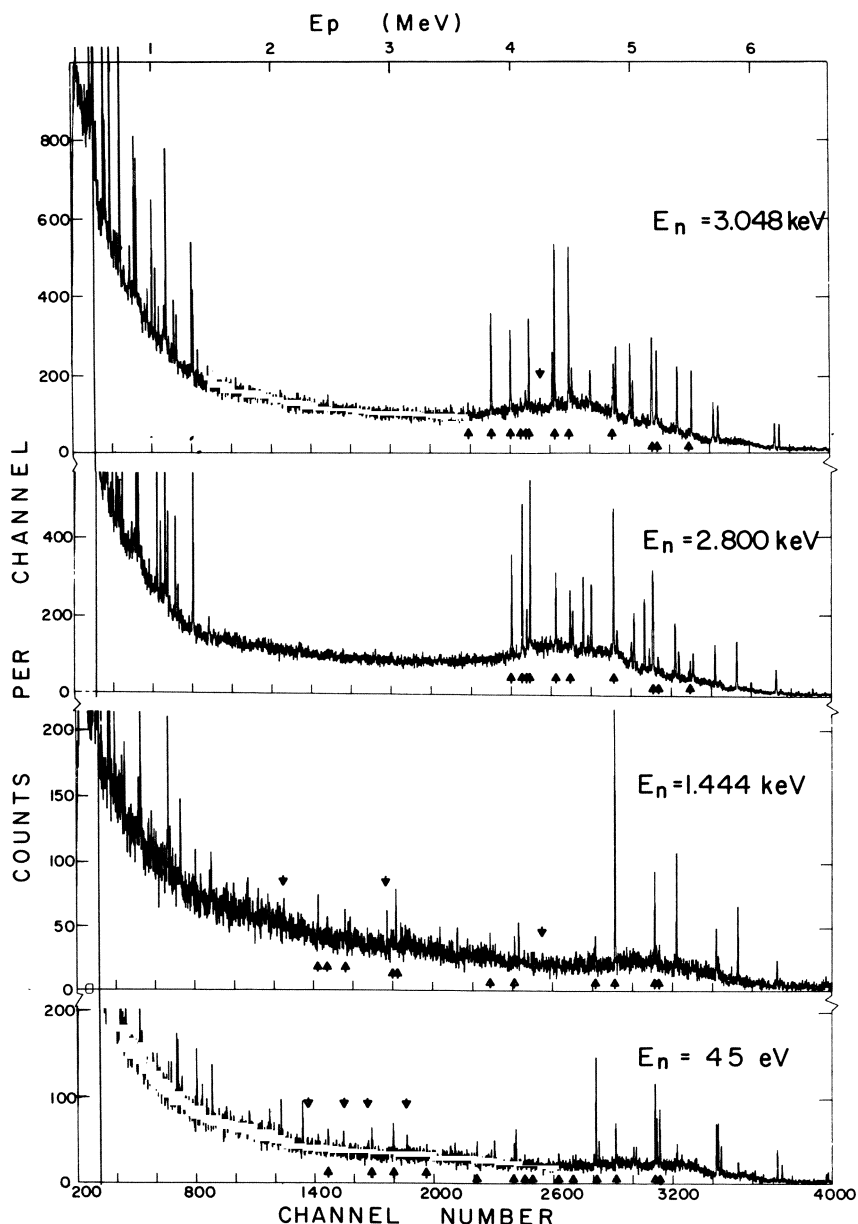


Fig. 29. High-resolution Ge(Li) spectra from neutron capture at neutron energies E_n in four resonances in the $^{205}\text{Tl}(n, \gamma)^{206}\text{Tl}$ reaction (Ear + 72a). The upper two are s -wave and the lower two p -wave resonances. Arrows under the curves indicate second-escape peaks of γ -rays known to be primaries. Arrows above the curves indicate γ -rays which may be either primaries or secondaries. The scale E_p gives the second-escape peak energy.

a uniform intensity pattern would persist over this narrow region of E_n . Furthermore, the partial capture cross section for production of the bump radiation in resonances is orders of magnitude larger than the prediction (LL 60) of ~ 0.1 b for direct capture near lead.

Evidence that the 5.5-MeV bump radiation does not arise in primary transitions to a special group of levels at $(E_\lambda - 5.5)$ MeV was first given by Bergqvist *et al.* (BS 62, LS 65). As mentioned in Sec. 1, these authors showed that the center of gravity of the bump in Au does not change with E_λ for neutron bombarding energies, E_n , in the range $0 < E \leq 4$ MeV.* Similar effects are shown in Fig. 30 (Ear+ 72b) which displays γ -ray spectra observed in fast capture in Tl with $0.7 \leq E_n \leq 2.6$ MeV. The same invariance of the center of gravity of the bump with E_λ is shown in the region below E_B by the series of γ -ray spectra from $^{197}\text{Au}(d, p\gamma)^{198}\text{Au}$ (Fig. 31) (Bar+ 70). Clearly, with the final state E_i fed by the bump ranging over $0 < E_i < \sim 5$ MeV, as it does in the fast-neutron capture and $(d, p\gamma)$ experiments in Au, the possibility of involvement of special levels in a narrow region of excitation energy is eliminated. From Eq. (2.10) the most likely remaining variable able to account for the bump is then \tilde{f}_{XL} . Closer inspection, however, shows that explanations involving nonuniform level densities and smooth, Lorentzian-like, strength functions cannot be so easily dismissed because, as E_λ increases both in the $(d, p\gamma)$ and fast-neutron capture reactions, the angular momentum transferred increases and the distribution of J for levels E_λ changes. The resonance-averaged primary spectrum is thus in reality given by $\sum_J v_{iXL}^J$ and it is conceivable that nonuniform distributions of levels in spin or parity at $(E_\lambda - 5.5)$ MeV might be matched with the changing J -distributions as E_λ increases to provide a 5.5-MeV bump, even with a smooth Lorentzian-type strength function. However, our attempts to reproduce the observed spectra by calculation from the known J -distribution and with plausible assumptions for the nonuniform spin and parity distributions at $(E_\lambda - 5.5)$ MeV and assuming a Lorentzian-type \tilde{f} have not met with success. Therefore, the simpler explanation involving an irregular \tilde{f} is preferred. This is also sup-

* In a recent study (Jai 72) of resonance neutron capture in Au, it is claimed that an intense cluster of γ -rays at ~ 6.25 MeV following capture with thermal and 4.9-eV neutrons does not persist in capture in the range $80 < E_n < 830$ eV and therefore that this radiation must result from Porter-Thomas fluctuations. This confirms earlier conclusions (BS 62, Was+ 68), about the four γ -rays in this group; however, it does not support the suggestion (Jai 72) that the entire bump in Au, which comprises some 100 γ -rays between 4 and 6.5 MeV and persists over several MeV of excitation energy, has a similar explanation.

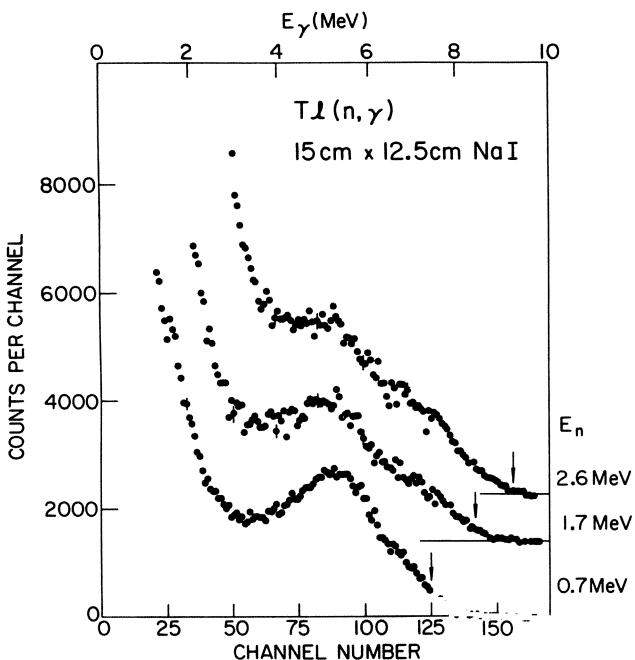


Fig. 30. Background-subtracted NaI spectra from neutron capture in natural Tl (Ear + 72b). Neutron energies, E_n , are indicated at the right of each curve. The upper energy-limit for each spectrum is shown by an arrow. The sharp increase in counts at low energies is caused by the intense γ -rays from the $(n, n'\gamma)$ reaction.

ported, of course, by the available results for the photoexcitation strength function, \vec{f} , which show evidence of the pigmy resonance in Figs. 16 and 18 and some evidence for the step below ~ 4.5 MeV in Figs. 15 and 16.

Most of the above discussion has been concerned with the bump in the region $182 < A \leq 206$. In the lighter region $108 \leq A \leq 134$, the bump is weaker and uncertainties in $\varrho(E)$ greater. In the latter region, it has not been possible to ascribe the bump to the strength function with the same confidence, but the behavior of the observed spectra with E_λ (LS 65, Bar + 70, see also Fig. 33) suggests that essentially the same phenomena are at work.

(b) Properties of the 5.5-MeV Radiation. We here discuss experiments that show that the bump γ -rays are largely of $E1$ type and we review the dependence of the detailed shape of the bump on Z , N , and E_λ .

The well-known fact that the high-energy $E1$ radiation ($E_\gamma > \sim 4.5$ MeV) is generally stronger than $M1$ radiation, except in isolated cases or limited regions of A (see Sec. 1), provides no guide to the multipole type predominating in the 5.5-MeV bump. Indeed, it is quite plausible to suppose (Sta 64) that this feature is a manifestation of a collective $M1$ giant resonance (Mot 60). However, as we now show, all evidence, at least in the $182 < A \leq 206$ region, points to $E1$ radiation.

In ^{206}Tl , the energies, parities, and some spins of the states $E_i < 2$ MeV fed by bump γ -rays in the $^{205}\text{Tl}(n, \gamma)$ reaction have been well studied (LD 70). On the basis of this information it is possible to conclude (Ear+ 71)

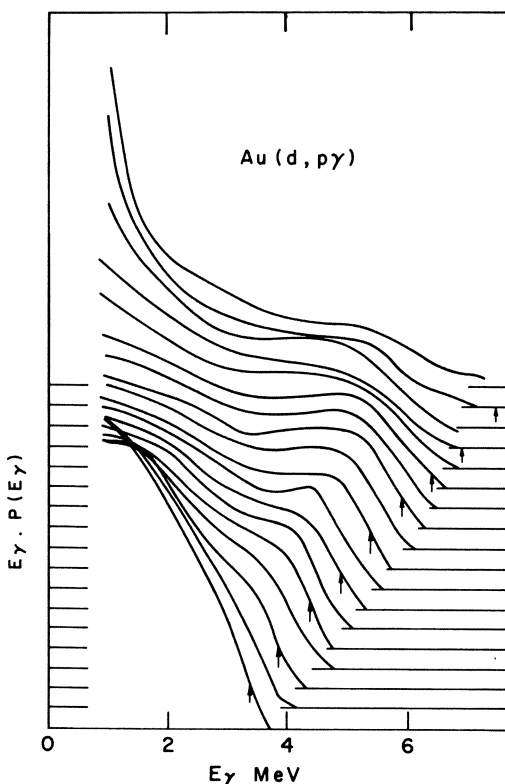


Fig. 31. Background-subtracted, smoothed, NaI spectra normalized to equal area, from the $^{197}\text{Au}(d, p\gamma)^{198}\text{Au}$ reaction (Bar + 70). Curves are plotted as a function of channel energy. The ordinate is counts per channel times channel energy. Each spectrum was obtained in coincidence with a proton energy window ~ 0.24 MeV wide as indicated in Fig. 9. The upper energy limits of various spectra are indicated by arrows; the neutron separation energy is ~ 6.5 MeV.

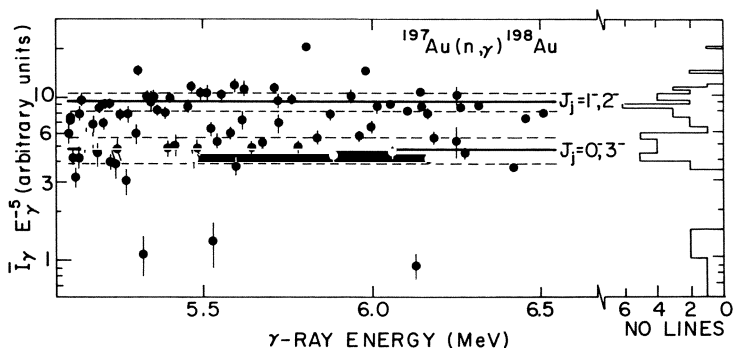


Fig. 32. Average reduced γ -ray intensities for ^{198}Au obtained by the low-neutron-resolution method (LBT 72). See Fig. 12 for further explanation of curves. The histogram on the right shows the distribution of points on the intensity scale.

that all of the strong-bump γ -rays from the s -wave resonances $E_n = 2.800$ and 3.048 keV in Fig. 29 are of $E1$ type. The γ -rays feeding the same levels following p -wave capture for resonances at $E_n = 45$ eV and 1.444 keV in the same figure, are by the same arguments $M1$ and show a less pronounced bump (see also Ear+ 72a).

In ^{200}Hg at least 85% of the γ -rays above ~ 4.5 MeV following thermal neutron capture in ^{199}Hg have been shown to be $E1$ by coincidence and polarization correlation measurements (Bar+ 67, BGE 67).

In ^{198}Au (LBT 72), Fig. 32, and Ta (HGR 71), Fig. 13, the LNR high-resolution γ -ray technique (Sec. 3.4) has been used to identify $E1$ and $M1$ radiation in the bump. In both cases a predominance of $E1$ radiation was found. Similar conclusions have been reached by this technique in other nuclei (Table III) and also, on the basis of the known spins and parities of the states involved, in Re (She+ 72).

In the mass region $108 \leq A \leq 134$, the γ -ray assignments are, in general, less certain. However, Lottin and Paya (LP 71) have shown that in $^{122},^{124}\text{Sb}$ the γ -rays between 5 and 6.8 MeV are equally distributed between $M1$ and $E1$ type. Similar results are found in ^{116}In and ^{106}Pd (see Table III).

The progressive diminution of the irregularity in f with decreasing Z between Pb and Ta in Figs. 15–20 is shown rather more dramatically by the sequence of smoothed γ -ray spectra for the $(d, p\gamma)$ reaction Fig. 33a, c and the (n, γ) reaction Fig. 33b, d (Bar+ 70). All curves correspond to $E_\lambda \approx E_B$. This mass dependence of the 5.5-MeV radiation is presented quantitatively for the $182 \leq A \leq 208$ region in Fig. 34. Part (a) of this figure shows the integrated strength between 1 and 6 MeV for both the experimental f and the Lorentzian-based curve. This shows that the strength

in this energy region is roughly half that predicted from the giant dipole tail. The total ground-state radiation width for levels of a particular J of γ -rays comprising the 5.5-MeV bump, as given by the sum between 4 and 6 MeV, is shown in Fig. 34b. This quantity, as typified by the value of ~ 25 eV for Au, is considerably less than previous estimates, ~ 90 eV (BS 70), because of readjustments incorporating more realistic level densities (see Sec. 3.2, Fig. 8). In Fig. 34c we present a measure of the irregularity as percent deviation of the energy-weighted strength function from the Lorentzian cross section. To obtain these points, the energy-weighted spectrum-fitted strength functions (Figs. 16-20) were shifted until equal deviations occurred above and below the smooth Lorentzian, and the integrated

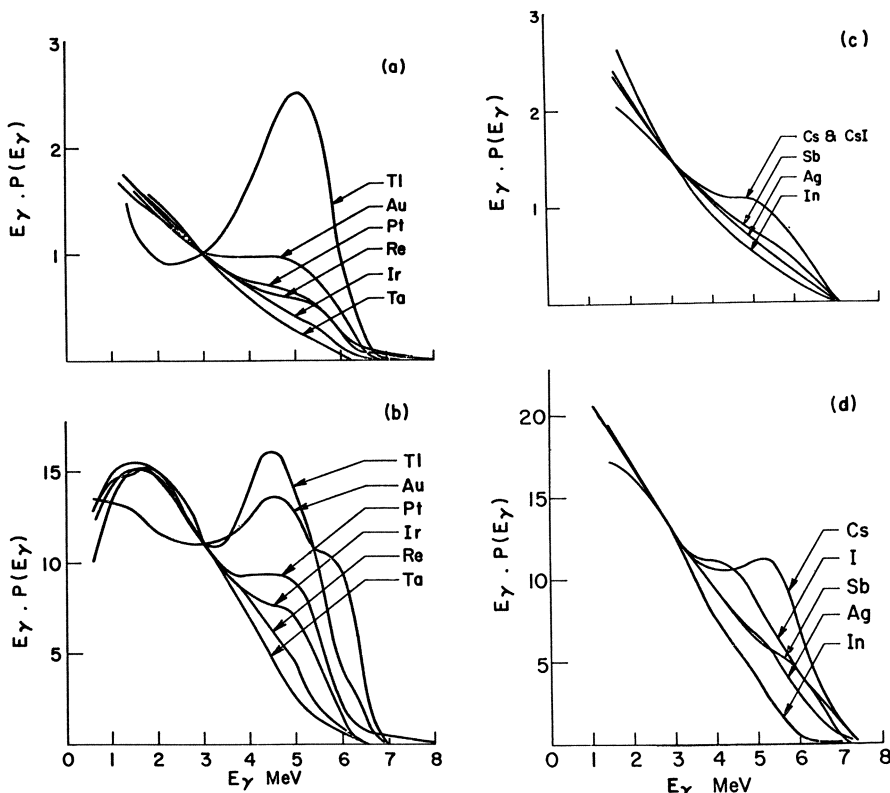


Fig. 33. Spectral shapes from $(d, p\gamma)$ and (n, γ) reactions. Background-subtracted, smoothed, NaI spectra are arbitrarily normalized at 3 MeV for (a), (c), the $(d, p\gamma)$ reaction and (b), (d) the (n, γ) reaction with thermal neutrons, for the target elements shown. The abscissa and ordinate are channel energy and counts per channel times channel energy, respectively.

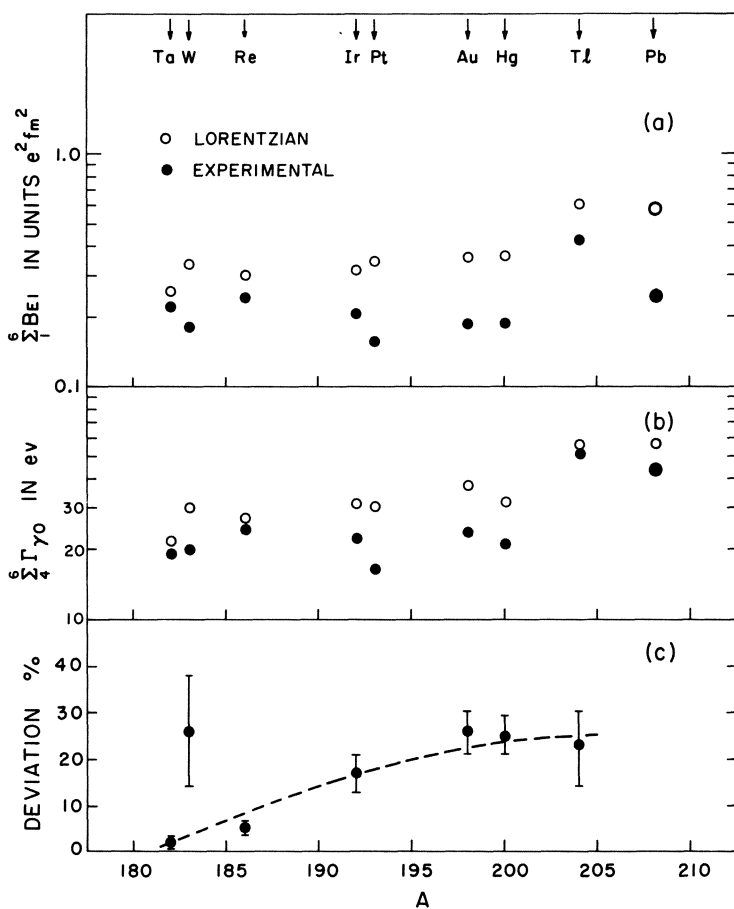


Fig. 34. Assessment of the dipole strength below 6 MeV in nuclei Ta to Pb. (a) The sum of E_1 reduced widths of levels of a particular J between 1 and 6 MeV in $e^2 fm^2$ units. The $B_{E1}(e^2 fm^2)$ per unit excitation energy interval (BM 69, p. 382), averaged over all possible spin combinations, is equal to $0.956 \times 10^6 f_{E1}(\text{MeV}^{-3})$. (b) Total ground-state γ -ray width of levels of a particular J in the γ -ray bump region, 4–6 MeV. (c) Percent deviation of the observed energy-weighted strength function from that derived from the Lorentzian. Target elements are identified at the top of the figure.

deviation below the crossover energy was computed. The error bars represent uncertainties from Porter–Thomas fluctuations. Apart from tungsten, for which the fluctuations are large, all points fall near a smooth curve increasing with A . In ^{208}Pb itself (Fig. 15), Porter–Thomas fluctuations prevent a meaningful estimate of the deviation but, from Fig. 34a and b, it would appear that the behavior in Pb represents a normal continuation

of that in the lighter nuclei. This conclusion is at variance with an earlier impression that in spite of the apparent close connection of the irregularity with the ^{208}Pb closed shell, ^{208}Pb itself presented a glaring anomaly. That notion was engendered partly by the absence of a strong bump at 5.5 MeV in the thermal neutron (n, γ) spectrum from natural Pb (Gro+ 69) and in ($d, p\gamma$) spectra above the neutron threshold (Bar+ 70), but more by the seemingly low value of $\sum_4^6 \Gamma_{\gamma_0}$ of only ~ 40 eV from photoexcitation experiments in ^{208}Pb as compared to the once current higher values, ~ 200 eV, for all levels which decay to the ground state by $E1$ radiation in Au and neighboring nuclei (BS 70).

Inspection of Figs. 16-19 shows that within the errors, no consistent variation of the position or magnitude of the strength function irregularity can be associated with even or odd values of N .

Some differences in the shapes of the strength functions with E_λ ($E_\lambda = E_B + E_n$) are evident in the curves of Fig. 16c and Fig. 20b, and between the curves of Figs. 18b and c. Similarly, below the threshold, some differences in functional form are shown by the curves of Fig. 10. It is not clear, in view of the large possibilities for systematic error (Sec. 4.1) whether any of these trends represent a real dependence of f on E_λ . The most significant trend is perhaps the smoothing of the irregularity with increasing E_λ in Tl (Fig. 16). But even this is not supported by a similar trend in Ta (Fig. 20). Therefore it seems prudent to conclude that more careful measurements are needed before any dependence on E_λ can be inferred with confidence.

4.2.3. Other Reactions

In this section we consider several experiments whose results cannot yet be completely reconciled with the essentially consistent, though fragmentary, picture of strength functions derived from studies with (γ, γ) , (n, γ) and $(d, p\gamma)$ reactions presented in Secs. 4.2.1 and 4.2.2. The experiments in question involve $(n, n'\gamma)$, $(p, p'\gamma)$ and $(\mu^-, x\bar{n}\gamma)$ reactions in which the observed γ -ray spectra in general fail to show the 5.5-MeV bump seen in the other reactions. A typical example of this effect in the $182 \leq A \leq 208$ range is provided by the γ -ray spectrum observed by Bergqvist *et al.* (Ber+ 66a) following 7.5-MeV neutron bombarding of Au (Fig. 35). The γ -ray spectrum from the (n, γ) reaction with 0.3-MeV neutrons shown in the same figure exhibits the usual bump at ~ 5.5 MeV while the $(n, n'\gamma)$ spectrum shows no sign of it.

It is a weakness of most $(n, n'\gamma)$ measurements that it has not been possible, because of insufficient intensity, to isolate narrow intervals in

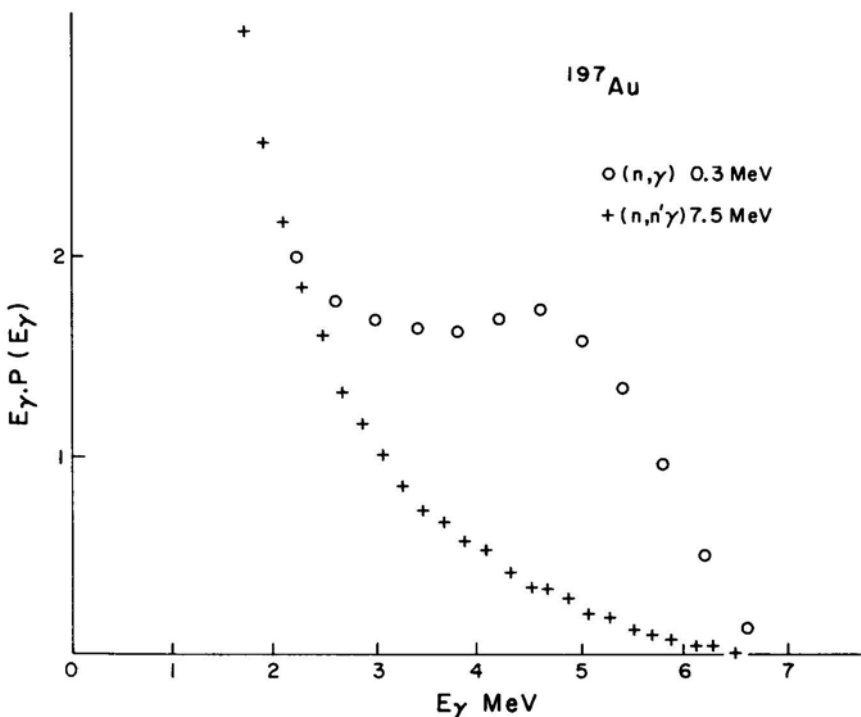


Fig. 35. Comparison of NaI spectra from the (n, γ) and $(n, n'\gamma)$ reactions on ^{197}Au . The abscissa and ordinate are channel energy and counts per channel times channel energy, respectively (Ber + 66a).

excitation energy by imposing energy selection on the inelastic neutrons. In the absence of this energy gating, the γ -ray spectrum observed is the sum over the spectra from all energetically possible excitations weighted according to the partial cross section for excitations of those regions. This need not necessarily obscure the 5.5-MeV radiation, since this radiation is emitted essentially independently of E_λ , but details of the γ -ray spectrum are likely to be smeared compared to what would be obtained if spectra in coincidence with neutrons in a narrow energy band could be measured. This lack of energy definition on the outgoing particle, so difficult to avoid in $(n, n'\gamma)$ experiments, may be overcome in the $(p, p'\gamma)$ reaction where energy gating is easier. However, it has been shown (Lon + 72) in the $^{195}\text{Pt}(p, p'\gamma)$ reaction with the energy of the p' particles well-defined by suitable energy windows, that there is still no evidence for the 5.5-MeV bump in the coincident γ -ray spectra. We have found the results, shown on the right-hand side of Fig. 36, to be common to Tl, Au, and other targets

in the $182 < A < 206$ mass range. Figure 36 also shows for comparison, spectra from the $^{194}\text{Pt}(d, p\gamma)^{195}\text{Pt}$ reaction in which the same regions of excitation in ^{195}Pt are gated. These clearly show the presence of a 5.5-MeV bump. From these results we conclude that the absence of the bump in the $(n, n'\gamma)$ experiments (Fig. 35) is probably real, i.e., not simply a consequence of the absence of gating on the inelastic neutrons.

A further difference noted in γ -ray spectra from the $(n, n'\gamma)$ reaction as compared to the reactions considered earlier is the presence of a 4.1-MeV radiation in the γ -spectra from targets near lead. This effect has been observed in $\text{Pb}(n, n'\gamma)$ (Ber + 66a), $^{206}\text{Pb}(n, n'\gamma)$ (Ber 70), $^{208}\text{Pb}(n, n'\gamma)$ (Ber + 66b, NMH 70) and $^{209}\text{Bi}(n, n'\gamma)$ (Ber + 66a). Figure 37 shows an example of the results in $^{206}\text{Pb}(n, n'\gamma)$ where the effect is particularly pronounced. It is well established from high-resolution γ -ray data in $^{208}\text{Pb}(n, n'\gamma)$ that the 4.1-MeV γ -ray is a secondary emitted in the decay of the 4.07-MeV 2+ state (NMH 70), a conclusion supported by the observation of a strong neutron group feeding that level (Ber + 66b, Ste + 65). It seems likely that the same interpretation should apply to the other spectra where this radia-

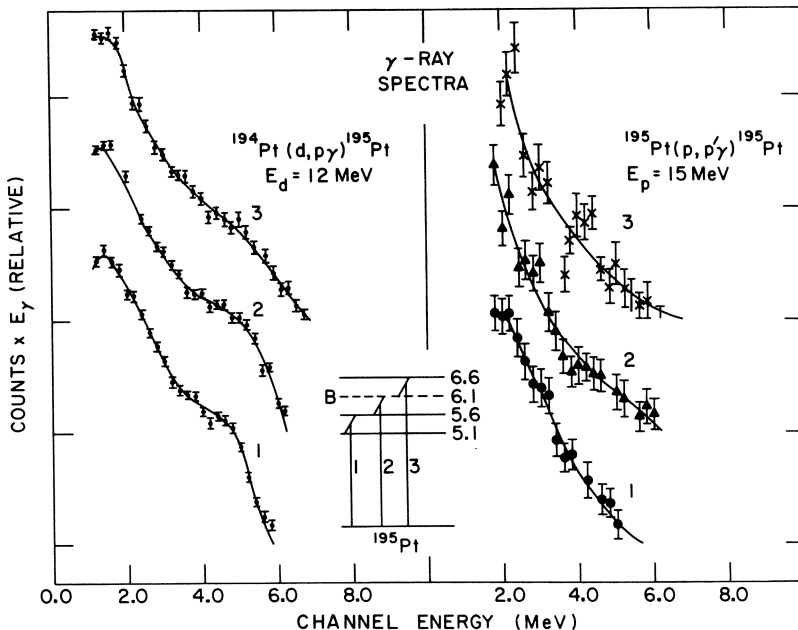


Fig. 36. Comparison of NaI γ -ray spectra from the $^{194}\text{Pt}(d, p\gamma)^{195}\text{Pt}$ and $^{195}\text{Pt}(p, p'\gamma)$ reactions (Lon + 72). The final state energy intervals are indicated in the inset decay scheme. The broken line, B, indicates the neutron separation energy in ^{195}Pt . The abscissa and ordinate are channel energy and counts per channel times channel energy, respectively.

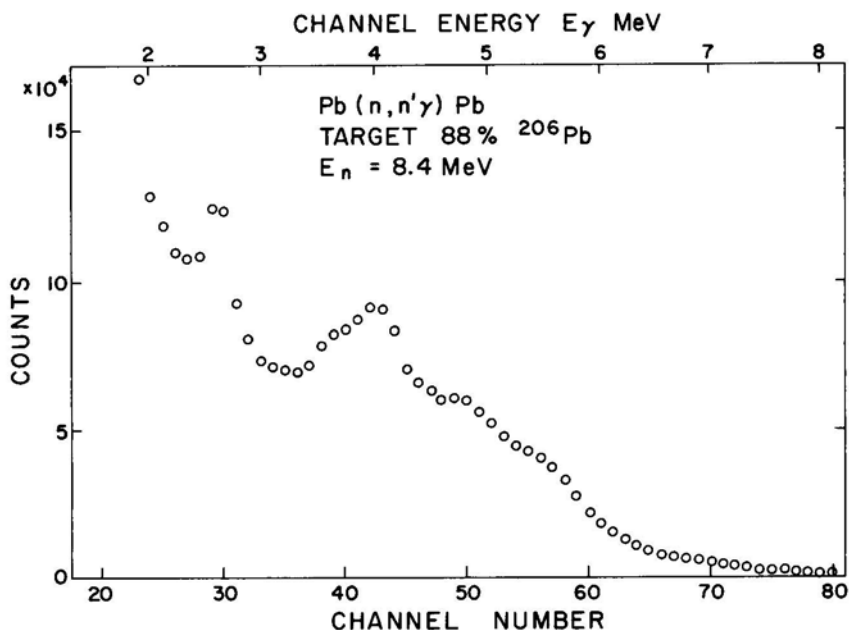


Fig. 37. NaI spectrum of γ -rays from the $\text{Pb}(n, n'\gamma)\text{Pb}$ reaction (Ber 70).

tion is seen. Therefore this 4.1-MeV radiation is, in a sense, extraneous to the present topic of strength functions which concerns the primary decay spectrum.

Another type of reaction in which the overall spectrum shape near 5.5 MeV can be investigated is the (μ^-, xny) reaction. Gamma-ray spectra following this reaction have been studied in Bi, ^{208}Pb , radiogenic Pb, Au, Ag, and Zr targets (EB 71). These spectra are complicated by formation of several product nuclei in each reaction, corresponding to the emission of zero, one, two, etc., neutrons, and by a wide (and largely unknown) energy distribution in the final nucleus prior to γ -emission. Nevertheless, the γ -ray spectra are of interest because as in the $(n, n'\gamma)$ spectra, there is no 5.5-MeV bump and, for Bi, radiogenic Pb, and Au targets, a γ -ray or group of γ -rays centered at ~ 4.1 MeV is clearly evident (Fig. 38).

In an attempt to explain the absence of the 5.5-MeV reaction in the $(n, n'\gamma)$ experiments, three alternatives have been considered (Ber + 66a):

- a. An isotope effect. The $(n, n'\gamma)$ reaction excites the target of mass A while the (n, γ) reaction excites the final nucleus $A + 1$.
- b. An angular momentum effect. The (n, γ) reaction involves relatively

low l -values, ≤ 3 for $E_n < 4$ MeV, while the $(n, n'\gamma)$ reaction at $E_n \sim 8$ MeV can in general involve much higher l -transfers.

- c. A reaction mechanism effect. For example, the (n, γ) reaction might involve excitation of only a few valence nucleons while the $(n, n'\gamma)$ reaction might involve primarily collective core excitations.

Alternative (a) was ruled out by Bergqvist and co-workers (Ber+ 66a) from examination of spectra from natural targets containing both even and odd isotopes. It is now even more effectively ruled out by observations (Sec. 4.2.2) that the 5.5-MeV bump, when present, is independent of N and by the evidence of Fig. 35 which shows the bump in $(d, p\gamma)$ but not in $(p, p'\gamma)$ for the same N .

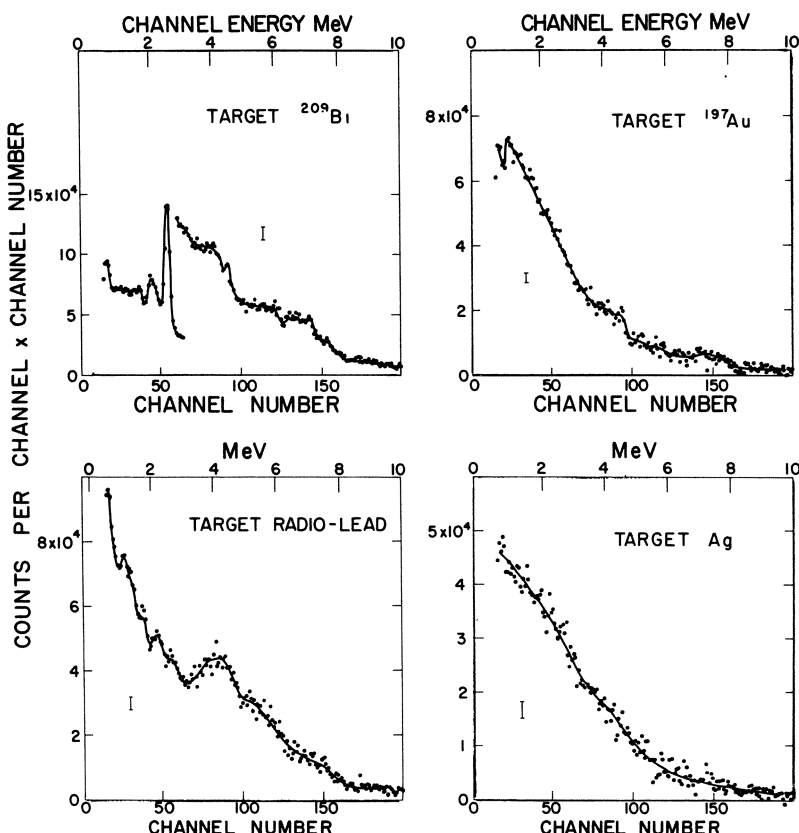


Fig. 38. Background-subtracted NaI spectra of γ -rays from the $(\mu^-, xn\gamma)$ reaction (EB 71). The radiolead target contained 88% ^{206}Pb , 9% ^{207}Pb , and 3% ^{208}Pb . Vertical arrow bars near each curve are representative of uncertainties from counting statistics.

Under alternative (b) it is necessary to postulate a scarcity of high-spin states at $E_\lambda = 5.5$ MeV that can be fed by dipole transitions from the high-spin levels in which the nucleus is left at E_λ following emission of the n' neutron. Thus for $E_n = 7.5$ MeV as in Fig. 35, assuming the peak of the distribution of inelastic neutrons occurs at ~ 1 MeV, we expect the residual nucleus to be excited to roughly 6.5 MeV and subsequent 5.5-MeV γ -emission to feed states near 1 MeV. At the latter energy, because of the spin-cutoff effect, there may be very few states of high J and hence few γ -rays near 5.5 MeV could appear, regardless of the form of \tilde{f} . In considering this possibility Bergqvist *et al.* (Ber + 66a) noted that, while the initial J -distribution at E_λ after inelastic scattering by 7.5-MeV neutrons would, on the basis of Hauser-Feshbach calculations, be expected to be wider than that following fast-neutron capture, about one third of the states would nevertheless have the same J . They further surmised that if the absence of the 5.5-MeV bump was caused by a shortage of high-spin states at ~ 1 MeV, inelastic scattering at a higher bombarding energy should give a γ -ray spectrum more similar to that from neutron capture. To test this, they increased E_n to 8 MeV but again observed no bump. They therefore rejected alternative (b) in favor of (c). Recently, we have made a calculation of the spectral distribution assuming an energy-dependent spin-cutoff as discussed in Sec. 2.3. The results for $E_\lambda = 6$ MeV, given in Fig. 39, show that while a bump is obtained for low J , it does disappear progressively as J increases. Similar results are obtained at 8 MeV. Thus we conclude that alternative (b) cannot be ruled out. A somewhat similar conclusion was reached by Brzosko *et al.* (Brz + 69).

To explore alternative (c), we note that it implies that two more-or-less independent types of levels must coexist in the resonance region, those favored in neutron transfer and those favored in inelastic scattering and μ^- -capture, and that these two types of levels must be associated with different strength functions, \tilde{f} . The difference between the two classes might again be simply a matter of the average J . However, unlike (b) where the level distribution with J is suspect, here we assume that \tilde{f} is J -dependent. Alternatively, some other parameter could give rise to different γ -decay strength functions.

In one attempt to shed more light on this possibility (Bar + 69, Bar 69), the $^{207}\text{Pb}(p, p'\gamma)^{207}\text{Pb}$ reaction was studied at bombarding energies exciting, in ^{208}Bi , isobaric analog resonances (IAR) of various well-localized (MKB 67) neutron particle-hole states in ^{208}Pb . It was recognized that inelastic proton emission from these IAR's would lead to states in ^{207}Pb with large components in their wavefunctions corresponding to configurations in

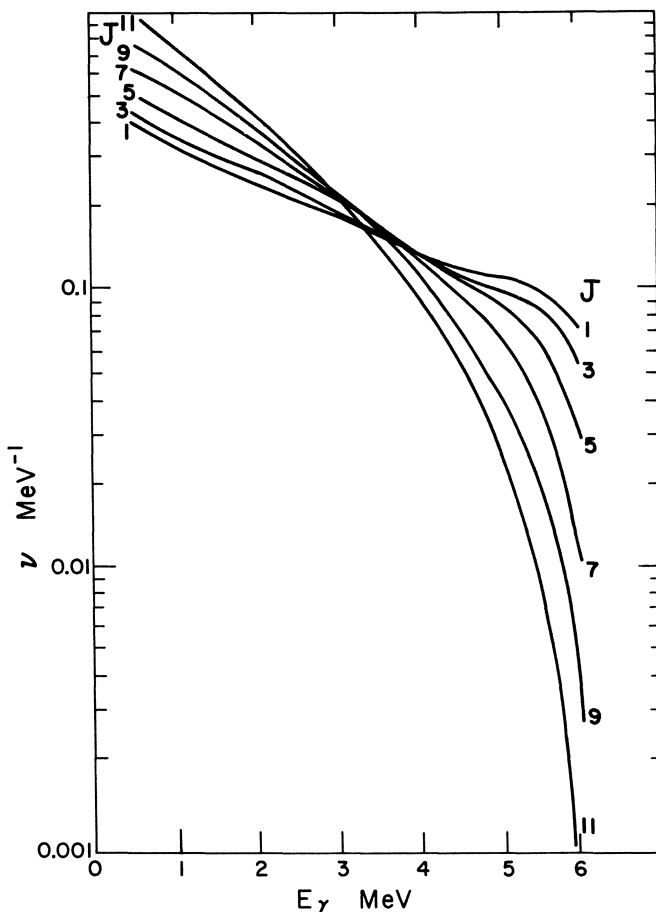


Fig. 39. Gamma-ray spectral distributions calculated with an energy dependent spin-cutoff parameter $\sigma(E) = \sigma(E_0)(E/E_0)^{1/4}$. Each curve is identified with spin J of the initially excited state.

which the particle-hole in question was coupled to a second neutron hole, forming a one-particle-two-hole state. Since many of the latter states would be precisely the type that might be expected to be excited strongly as doorway states in neutron-transfer reactions in ^{207}Pb , it was felt that the observation of a 5.5-MeV bump in $^{207}\text{Pb}(p, p'\gamma)^{207}\text{Pb}$ via the IAR that was similar in size and shape to that found in the $^{206}\text{Pb}(d, p\gamma)^{207}\text{Pb}$ reaction would be evidence at least of a simple doorway mechanism in the neutron transfer reaction. However, at the same time, to support alternative (c), it would be necessary to find *no* bump at off-IAR bombarding energies in

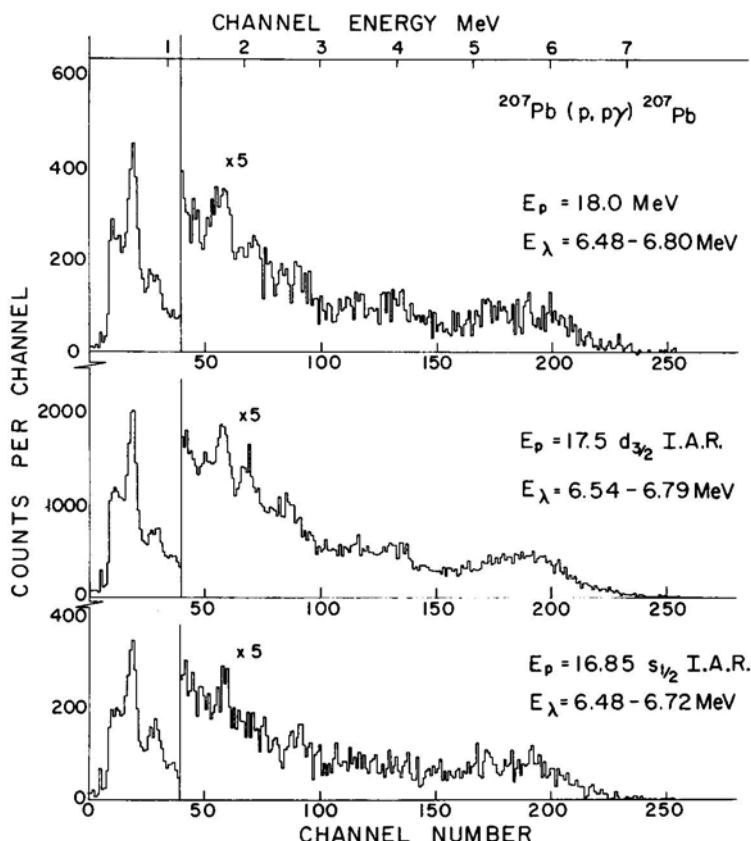


Fig. 40. Background-subtracted NaI spectra of γ -rays from the $^{207}\text{Pb}(p, p'\gamma)^{207}\text{Pb}$ reaction. Proton bombarding energies are indicated by E_p , and the excitation energy intervals in the residual nucleus by E_λ . The uppermost curve represents excitation in ^{208}Bi above the particle-hole IAR region. The lower two curves represent the excitation of isobaric analog resonances (IAR) corresponding to the $d_{3/2}p_{1/2}^{-1}$ and $s_{1/2}p_{1/2}^{-1}$ neutron particle-hole states in ^{208}Pb .

accordance with the usual $(p, p'\gamma)$ spectra as in Fig. 36 or with the $(n, n'\gamma)$ spectra. The results, presented in Fig. 40, show that a 5.5-MeV bump *does* appear in spectra following bombardment at the $s_{1/2}p_{1/2}^{-1}$ and $d_{3/2}p_{1/2}^{-1}$ isobaric analog resonances but an equally strong bump also occurs with bombardment at $E_p = 18$ MeV, well above the IAR region. Hence no definitive support for alternative (c) can be claimed.

In another attempt to explore alternative (c), differences in $\bar{\Gamma}_n$ were sought for levels just above threshold in ^{195}Pt excited by $^{194}\text{Pt}(d, p)$ and

$^{195}\text{Pt}(p, p')$ reactions (Lon + 72). It was hypothesized that if alternative (c) were true, then the type of resonance favored in neutron transfer might on the average tend to have larger neutron widths than those participating in inelastic scattering and this property might be correlated with the differences in γ -ray spectra. It was found, however, that while the $\bar{\Gamma}_n$ associated with the (d, p) reaction were indeed larger by a factor of about 6 than those associated with the (p, p') reaction, these results and the differences in γ -spectra in Fig. 36 could be accounted for by the dissimilarities in J -distributions and it was therefore not necessary to seek further differences between the resonances favored in the two types of reaction.

In summary, it would appear that while alternative (c) is not ruled out, it is not necessary to assume anything more complicated than (b). It can be said in favor of (c), however, that it is well known in the lighter elements and at low excitations in heavy elements, that (d, p) reactions favor shell-model type states while scattering reactions tend to excite collective states. It might be assumed therefore that some tendency in this direction persists into the resonance region and indeed the presence of the 4.1-MeV radiation suggests that higher collective band members may also be strongly excited. On the other hand, this picture of more or less distinct types of resonance is contrary to the extreme statistical model of the compound nucleus; it would violate the Porter-Thomas distribution, for example. Much firmer evidence would therefore be required to establish such a radical departure (Lan 72b).

5. DISCUSSION

5.1. General

From diverse fragments of information, obtained from several experimental methods, it has been possible to gain a rough overview of the absolute strength function for $E1$ radiation and, less completely, for $M1$ radiation, in the range $2 < E_\gamma < 10$ MeV as a function of A in heavy elements. Almost no information is available on higher multipoles. Except for the limited range $\sim 5 < E_\gamma < \sim 8$ MeV in some elements, separation of $E1$ and $M1$ strength functions has not been achieved. Outside this range it is necessary either to make do with a composite (all multipoles) strength function or to assume from known systematics that $E1$ radiation will, on the average, be somewhat stronger than $M1$ and therefore tentatively adopt the composite strength function as purely $E1$.

In elements where several isotopes have been examined, the strength functions are found to be roughly similar in form and magnitude from isotope to isotope. In Ta, Au, and Tl, where measurements have been made as a function of initial excitation energy, E_λ , the decay strength function, $\tilde{f}_{i\lambda}$, maintains roughly the same functional form in the range $\sim 3.5 < E_\lambda < E_B + 4$ MeV.

5.2. Compatibility of Strength Functions

Agreement among the three methods yielding \tilde{f} is, within the errors, satisfactory. In the two low-resolution γ -ray methods, spectrum fitting and sequential extraction, both the functional form and absolute magnitude of \tilde{f} depend crucially on the form and scale of the level-density function used. Good agreement between these methods and the high-resolution γ -ray method for $E_\gamma > 5$ MeV occurs largely because the most accurate estimates of the level densities at low energies, $E_i < (E_B - 5$ MeV), are obtained as a byproduct of the latter method. Failure to detect *all* the levels of required spin and parity at low excitation energies has been a source of error in earlier level-density determinations from other reactions. On the other hand, good agreement between the spectrum fitting and sequential extraction methods in the range $E_\lambda < 5$ MeV, where they stand alone as the only methods giving \tilde{f} , does not necessarily indicate good absolute reliability for either method because in the excitation energy region concerned, $(E_B - 5$ MeV) $< E_\lambda < E_B$, both methods make use of level densities obtained by interpolation.

The present studies present an opportunity to compare the photo-excitation strength function and the γ -decay strength function. Within the limited energy ranges in the two examples, Au and Tl, wherein energy overlap of \tilde{f} and \tilde{f}' occurs (albeit in neighboring isotopes) there are, within the errors, no significant differences in form or magnitude between these strength functions. Most noticeable is the tendency of \tilde{f}' in Tl (Fig. 16a) not to follow the sharp decrease with decreasing E_γ below 5 MeV shown by \tilde{f} in Figs. 16b and c. This may be merely a statistical fluctuation or possibly the result of a systematic error introduced in the measurements or analyses of either \tilde{f} or \tilde{f}' . On the other hand, it may be real, e.g., it may be a true isotopic difference or, as suggested by the cross section (Fig. 5) it may be a local substructure effect that the spectrum fitting and sequential extraction methods for \tilde{f}' do not resolve.

For a valid test of the Brink hypothesis it is necessary, as pointed out in Sec. 2.2, to establish that $\tilde{f}_{0\lambda}$ and all the $\tilde{f}_{i\lambda}$ have the same functional form

in the same nucleus. The necessary data for a complete test are not at hand but a comparison of $\tilde{f}_{0\lambda}$ for ^{197}Au with the internally compatible $\tilde{f}_{i\lambda}$ from sequential extraction in ^{198}Au (Fig. 18) shows reasonable consistency in the small range, 5–6.5 MeV, where they overlap. Fair compatibility between $\tilde{f}_{i\lambda}$ for a limited range of E_λ above the neutron threshold in $^{204,206}\text{Tl}$ and $\tilde{f}_{0\lambda}$ for ^{205}Tl is also shown in Fig. 16 but the necessary demonstration of common form for the $\tilde{f}_{i\lambda}$ for all E_λ is lacking in this case. However, these partial tests, together with the partial demonstration by Rosensweig (Ros 68) using ^{196}Pt resonance-average γ -ray data, support the Brink hypothesis as a good working hypothesis in heavy elements. It is unclear over what range of E_λ this hypothesis might remain even approximately true. There are some suggestions of a gradual, but consistent, smoothing of $\tilde{f}_{i\lambda}$ with increasing E_n in Tl (Fig. 16) but, as discussed earlier, these differences are scarcely significant in view of the possible systematic errors.

5.3. $E1$ Strength Function

In most elements far from closed shells, f_{E1} is in fair agreement in form and magnitude with that predicted from the Lorentzian both above and below the neutron threshold. In elements between Ta and Pb, f_{E1} usually falls below the Lorentzian curve for $E_\gamma < 6$ MeV (Fig. 34). Near closed shells there are strong irregularities in f_{E1} . In extreme cases, e.g., Tl (Fig. 16) there is a small but definite pigmy resonance at ~ 5.5 MeV, but more markedly in all nuclei in the range $182 \leq A \leq 208$ there is rapid decrease of strength for $E_\gamma < 4.5$ MeV as compared to the Lorentzian. The 5.5-MeV bump in the γ -ray spectra from these elements is more a result of this sharp step than of any pigmy resonance that may or may not be present. Other evidence for coarse substructure is found near the 82-neutron and 50-proton closed shells. Thus, while the E_γ^5 -law (Axe 62) provides a reasonably good approximation to the energy dependence for $E1$ radiation in the range $5.5 < E_\gamma < 8$ MeV in most nuclei, it should not be regarded as an appropriate standard for intensity comparison below 5.5 MeV, as has been a frequent practice in the recent literature.

Because of the proximity to closed shells of elements exhibiting the 5.5-MeV γ -ray bump, attempts to explain that effect have all naturally assumed a part to be played by shell structure. It has also seemed appropriate to invoke simple models of the capture mechanism which might be valid near closed shells. It was early established (LL 60) from a consideration of the partial capture cross sections involved, that the 5.5-MeV bump in elements near Pb cannot be a result of direct capture or of channel, i.e.,

valency (Lyn 68, p. 236) capture. It was natural therefore to consider (Bar+ 70) that the next most complicated process, viz., doorway capture, might be responsible. In this process, one pictures the incoming nucleon undergoing a two-body interaction exciting a nucleon from the core to some higher orbit while itself dropping to a bound orbit thereby forming a two-particle-one-hole ($2p1h$) "doorway state" (BF 63). Near closed shells the particle-hole (ph) excitation would for most, but not all, orbitals of interest introduce a parity change. In nuclides near ^{208}Pb many of the unperturbed ph energies for neutrons cluster near 5.5 MeV; those for protons somewhat higher. Hence γ -decay of the doorway state which would occur by ph annihilation might be expected to give rise to the 5.5-MeV $E1$ radiation. Furthermore, because the second excited particle might occupy any unfilled orbit consistent with the energy balance and selection rules, a mechanism is provided for the 5.5-MeV radiation to be emitted over a wide range of E_λ , as observed. In a real nucleus the $2p1h$ state would of course be mixed with other states near the same energy. What is needed to complete this picture is a mechanism providing significant $E1$ strength at 5.5 MeV or, in other words, enabling these simple configurations to dominate over all others in the transition matrix elements.

This problem has been addressed by Lane (Lan 71), who found a promising clue in a certain zero-range ph calculation of Pal, Soper, and Stamp (PSS 64). This calculation indicated that in ^{208}Pb the $s_{1/2}p_{1/2}^{-1}$ neutron ph state would be uncoupled from the other ph states in the process by which most of the $E1$ strength is pushed up into the giant resonance. This suggested that the $s_{1/2}p_{1/2}^{-1}$ particle-hole could act as the required doorway in neutron-transfer reactions. Furthermore, the estimates of Pal *et al.* ascribed a total ground-state width, $\Sigma\Gamma_{\gamma 0} \simeq 200$ eV, to states near 5.5 MeV with large $s_{1/2}p_{1/2}^{-1}$ components. This width was in good agreement with estimates (BS 70) for the total ground-state width in the pigmy resonance in Au.

Recent developments suggest that the doorway picture, at least in so simple a form, may not provide an appropriate basis for describing the 5.5-MeV phenomenon. The evidence is as follows:

(a) *Re-evaluated ground-state width:* Present strength functions show between 4 and 6 MeV, for levels of a particular spin J that $\Sigma\Gamma_{\gamma 0} \simeq 25$ eV (Fig. 34) instead of ~ 90 eV in Au and not so much a bunching of strength at 5.5 MeV as a dip below that energy. (Sec. 4.2.2).

(b) *Experimental test for $2p1h$ states:* An attempt to show that ph annihilation in $2p1h$ configurations was instrumental in 5.5-MeV γ -emission, by selectively exciting such configurations through isobaric analog resonances in the $^{207}\text{Pb}(p, p'\gamma)^{207}\text{Pb}$ reaction was inconclusive (Sec. 4.2.3).

(c) *Recent particle-hole calculations:* A recent study of *ph* calculations with finite-range forces in ^{208}Pb by Khanna and Harvey (KH 73) shows that the $s_{1/2}p_{1/2}^{-1}$ neutron particle-hole state is not uncoupled from other, *ph* configurations as a general rule. The lowest state, which appears at ~ 4.5 MeV in these calculations, does carry a significant fraction ($\sim 1.5\%$) of the total $B(E1 : 0^+ \rightarrow 1^-)$ strength while states in the next ~ 2.5 MeV above it carry essentially none. This lowest state thus provides the basis for a small pigmy resonance. However, although composed of 83% neutron *ph* structures, this state appears “collective” insofar as none of its *ph* components contributes an intensity $\geq 15\%$. The calculations predict a second grouping of *E1* strength between 7 and 8 MeV. The distribution of *E1* strength predicted is shown in Fig. 41 where it is compared with the measurements of Knowles (KK 73). The agreement in integrated strength below 7.4 MeV is satisfactory. Other *ph* calculations (KBB 70, Per 70) give somewhat similar results. The calculations (KH 73) also show that

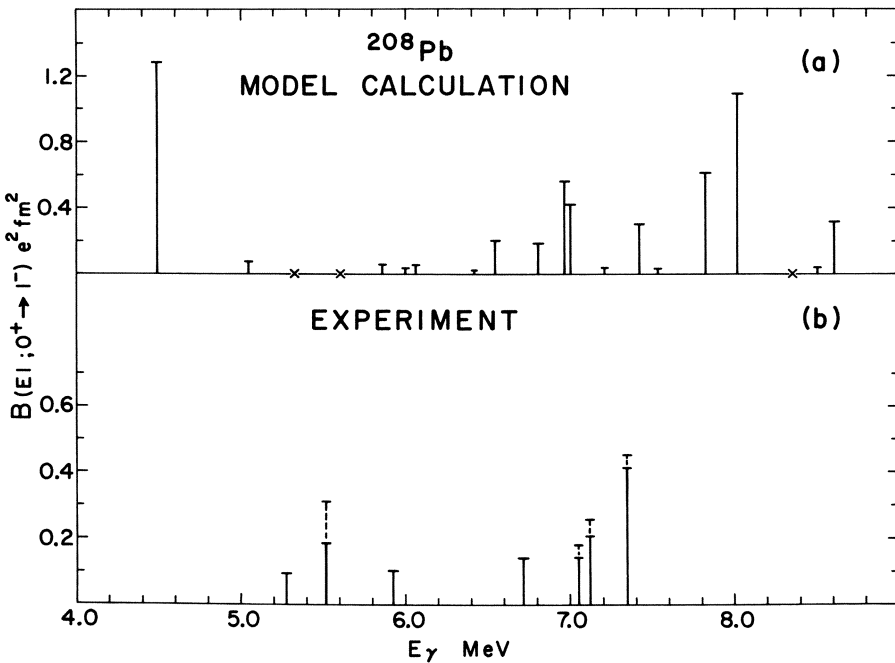


Fig. 41. Theoretical and experimental values of $B(E1; 0^+ \rightarrow 1^-)$ in ^{208}Pb . (a) Model calculations (KH 73) with realistic single-particle energies and Gaussian interaction with Gillett admixture. The spurious center-of-mass state is projected out and lies at zero energy. The crosses indicate dipole states with negligible strength. (b) $B(E1; 0^+ \rightarrow 1^-)$ calculated from the measured widths in $^{208}\text{Pb}(\gamma, \gamma)$. The dashed bars show the limits of precision, caused mainly by uncertainties in corrections for self-absorption (KK 73).

the $s_{1/2}p_{1/2}^{-1}$ neutron ph -states have their largest intensities ($\sim 20\%$) in states that carry little $E1$ strength, a result also, at least qualitatively, in accord with observations (Ear + 70). The $s_{1/2}p_{1/2}^{-1}$ and $d_{3/2}p_{1/2}^{-1}$ fragments moreover are not well localized but are distributed over several MeV above the lowest state (KH 73).

On the basis of the Khanna–Harvey calculations one must conclude that there is no single ph doorway to account for the bump radiation at 5.5 MeV and that, because of the wide spreading, a description in terms of multiple doorways is probably not appropriate. The pigmy resonance at ~ 4.5 MeV and the second clumping at ~ 7.5 MeV appear in the calculations to arise from the difference of ~ 2 MeV between the mean unperturbed energies of neutron- ph and proton- ph states. The step in the strength function at ~ 4.5 MeV appears to arise simply because the redistribution of the $E1$ strength under the residual particle–hole interaction leaves a finite amount distributed downward from the giant resonance to roughly the energy of the lowest unperturbed ph state, where there is an abrupt decrease to zero strength for lower excitation energies. As A decreases below ^{208}Pb this sharp break becomes progressively more diffuse causing a gradual diminishing of the 5.5-MeV bump with decreasing A . A similar step effect is to be expected near other closed shells or wherever shell structure introduces a similar parity gap in the unperturbed $E1$ ph energies.

The Brink hypothesis is consistent with the above particle–hole description insofar as it is possible to couple the ph states of the Khanna–Harvey calculations to any excited state of the core thereby displacing the whole distribution upward in excitation energy.

The above arguments against the appropriateness of the doorway formalism in accounting for the 5.5-MeV bump say nothing, of course, about its suitability for describing other phenomena. Indeed, evidence for doorway states in neutron scattering (New 72) and in photoexcitation reactions (BBB 71) above the neutron threshold in ^{208}Pb seems unassailable. Also the success of the valency model near $A = 100$ (Mug 72) is evidence for a nonstatistical behavior closely related to doorway states (Lan 72a).

5.4. $M1$ Strength Function

The information on the energy dependence of the $M1$ strength is more fragmentary than that for $E1$ radiation. Predictions of the peaking of $M1$ strength (Mot 60, Bri 63, SE 69) have not been very specific about the energies at which maximum strength should be found in different A . The

experimental evidence suggests peaking of $M1$ strength between 7.5 and 8.5 MeV in ^{208}Pb (Bow+ 70), Ba and Sn (Bol 70), at 7.7 MeV in ^{106}Pd (BT 70) and ≤ 5.5 MeV in ^{116}In (LEB 70). In many other nuclei, resonance-averaged measurements show an E_{γ}^5 energy dependence for $M1$ parallel to $E1$ radiation over the narrow range 5-8 MeV approximately. The last result is rather unexpected, since no theory predicts an $M1$ giant resonance coincident with the tail of the $E1$ giant dipole. Much more data are required before $M1$ strengths can be understood in detail.

6. CONCLUSION

Results now available on absolute γ -ray strength functions show roughly their overall energy dependence and some details of substructure. Strength function information promises to be important for the detailed understanding of the giant resonance, in particular, how giant collective effects may be described in terms of the shell model or other microscopic models. For example, it can provide the higher moments of the dipole distribution, hence more stringent tests of the distribution of the small fragments of $E1$ strength among states in the giant dipole tail in ^{208}Pb . It can also test possible theories describing how these distributions are modified as a function of A . The investigation of shell effects in the resonance region, aided by detailed studies of high-energy γ -decay, may also contribute new insight into how the transition (Sol 72) can be made from a statistical description of the compound nucleus to the more physical models appropriate at low excitation energies. Many of the available experimental techniques for strength function measurement have been but little used and much remains to be done in extending their range and accuracy.

ACKNOWLEDGMENTS

The authors acknowledge help and advice on theoretical questions generously given by J. M. Blair, F. C. Khanna, and M. Harvey during preparation of this review and by A. M. Lane throughout the experimental work from this laboratory herein reported. They wish to thank I. Bergqvist and L. M. Bollinger for permission to display some of their results prior to publication. They are grateful to Mrs. A. Cipriani for typing the manuscript, and to W. F. Mills for technical assistance in its preparation.

REFERENCES

- AB 68 B. J. Allen and J. R. Bird, *Phys. Letters* **27B**:494 (1968).
- AF 65 E. Albertson and B. Forkman, *Nucl. Phys.* **70**:209 (1965).
- All+ 64 R. G. Alias, S. S. Hanna, L. Meyer-Schützmeister, and R. E. Segel, *Nucl. Phys.* **58**:122 (1964).
- All 68 B. J. Allen, *Nucl. Phys.* **A111**:1 (1968).
- AM 71 B. J. Allen and R. L. Macklin, in: *Proceedings of the Third Neutron Cross Section and Technological Conference, Knoxville, Tennessee, 1970*, University of Tennessee, Knoxville (1971), p. 764.
- AMS 70 P. Axel, K. Min, and D. C. Sutton, *Phys. Rev.* **C2**:689 (1970).
- Axe 62 P. Axel, *Phys. Rev.* **126**:671 (1962).
- Axe 63 P. Axel, *Phys. Letters* **4**:320 (1963).
- Axe+ 63 P. Axel, K. Min, N. Stein, and D. C. Sutton, *Phys. Rev. Letters* **10**:299 (1963).
- Axe 68 P. Axel, in: *Proceedings of International Symposium on Nuclear Structure, Dubna, 1968*, IAEA Vienna (1968), p. 299.
- BBV 68 R. Bergère, H. Beil, and A. Veyssiére, *Nucl. Phys.* **A121**:463 (1968).
- BK 53 G. A. Bartholomew and B. B. Kinsey, *Can. J. Phys.* **31**:1051 (1953).
- Bar+ 57 G. A. Bartholomew, P. J. Campion, J. W. Knowles, and G. Manning, in: *Proceedings of the International Conference on Neutron Interactions with the Nucleus, New York 1957*, U.S. Atomic Energy Commission Technical Information Service, Oak Ridge, Tenn., Report TID-7547 (1957), p. 252.
- Bar 61 G. A. Bartholomew, *Ann. Rev. Nucl. Sci.* **11**:259 (1961).
- Bar 62 G. A. Bartholomew, in: *Proceedings of Conference on Electromagnetic Lifetimes and Properties of Nuclear States, Gatlinburg 1961*, Nuclear Science Series Report Number 37, National Academy of Sciences—National Research Council, Washington D.C. (1962), p. 209.
- Bar+ 67 G. A. Bartholomew, S. I. H. Naqvi, M. R. Gunye, and E. D. Earle, *Can. J. Phys.* **45**:1517 (1967).
- Bar 69 G. A. Bartholomew, in: *Proceedings of the International Symposium on Neutron Capture Gamma-Ray Spectroscopy, Studsvik, 1969*, IAEA, Vienna (1969), p. 553.
- Bar+ 69 G. A. Bartholomew, E. D. Earle, A. J. Ferguson, and M. A. Lone, *Bull. Am. Phys. Soc.* **14**:590 (1969).
- Bar+ 70 G. A. Bartholomew, I. Bergqvist, E. D. Earle, and A. J. Ferguson, *Can. J. Phys.* **48**:687 (1970).
- BBB 71 R. J. Baglan, C. D. Bowman, and B. L. Berman, *Phys. Rev.* **C3**:2475 (1971).
- Bei+ 69 H. Beil, R. Bergère, P. Carlos, and A. Veyssiére, *Comp. rendus* **269B**:216 (1969).
- Bei+ 71 H. Beil, R. Bergère, P. Carlos, A. Leprêtre, A. Veyssiére, and A. Parlag, *Nucl. Phys.* **A172**:426 (1971).
- Ben+ 66 G. Ben-David, B. Arad, J. Balderman, and Y. Schlesinger, *Phys. Rev.* **146**: 852 (1966).
- Ber+ 66a I. Bergqvist, B. Lundberg, L. Nilsson, and N. Starfelt, *Nucl. Phys.* **80**:198 (1966).
- Ber+ 66b I. Bergqvist, B. Lundberg, L. Nilsson, and N. Starfelt, in: *Proceedings of the International Conference on the Study of Nuclear Structure with Neutrons, Antwerp, 1965* (M. Neve de Meervignies, P. Van Assche, and J. Vervier, eds.), North Holland Publishing Co., Amsterdam (1966), p. 504.

- Ber 70 I. Bergqvist, private communication (1970).
- Ber+ 69a R. Bergère, H. Beil, P. Carlos, and A. Veyssiére, *Nucl. Phys.* **A113**:417 (1969).
- Ber+ 69b B. L. Berman, M. A. Kelly, R. L. Bramblett, J. T. Caldwell, H. S. Davis, and S. C. Fultz, *Phys. Rev.* **185**:1576 (1969).
- Ber+ 72 R. Bergère, H. Beil, P. Carlos, A. Veyssiére, and A. Leprêtre, in: *Proceedings of the International Conference on Nuclear Structure Studies Using Electron Scattering and Photoreaction, Sendai 1972* (K. Shoda and H. Ui, eds.) (supplement to Research Report of Laboratory of Nuclear Science Tohoku University, Vol. 5, 1972, Tomizawa, Sendai, Japan) (1972) p. 273, and private communication.
- Bet 36 H. A. Bethe, *Phys. Rev.* **50**:332 (1936).
- BF 63 C. Block and H. Feshbach, *Ann. Phys.* **53**:47 (1963).
- BGE 67 G. A. Bartholomew, M. R. Gunye, and E. D. Earle, *Can. J. Phys.* **45**:2063 (1967).
- Bha+ 70 M. R. Bhat, R. E. Chrien, D. I. Garber, and O. A. Wasson, *Phys. Rev.* **C2**:1115 (1970).
- Blo 72 C. Bloch, in: *Statistical Properties of Nuclei* (J. B. Garg, ed.), Plenum Press, New York (1972), p. 379.
- BM 69 A. Bohr, and B. R. Mottelson, in: *Nuclear Structure*, Benjamin, New York (1969), Vol. 1.
- Bol 68 L. M. Bollinger, in: *Proceedings of International Symposium on Nuclear Structure, Dubna, 1968*, IAEA Vienna (1968), p. 317.
- Bol 70 L. M. Bollinger, in: *Proceedings of the International Meeting on Perspectives of Neutron Spectroscopy, Dubna, 1970*, AED-CONF.-70-364-002, ZAED Zentralstelle für Atomkernenergie-Dokumentation, Kernforschungszentrum Karlsruhe.
- Bow+ 70 C. D. Bowman, R. J. Baglan, B. L. Berman, and T. W. Phillips, *Phys. Rev. Letters* **25**:1302 (1970).
- Bri 55 D. M. Brink, Doctoral Thesis, Oxford University (1955).
- Bri 63 D. M. Brink, in: *Proceedings of the International Conference on Nuclear Physics with Reactor Neutrons, Argonne 1963* (F. E. Throw, ed.), ANL 6797 (1963), p. 194.
- Brz+ 69 J. S. Brzosko, E. Gierlik, A. Soltan, and Z. Wilhelmi, *Can. J. Phys.* **47**:2849 (1969).
- Brz+ 71 J. S. Brzosko, E. Gierlik, A. Soltan Jr., Z. Szeflinski, and Z. Wilhelmi, *Acta Phys. Polon.* **B2**:489 (1971).
- BS 62 I. Bergqvist and N. Starfelt, *Nucl. Phys.* **39**:353 (1962).
- BS 70a I. Bergqvist and N. Starfelt, *Prog. Nucl. Phys.* **11**:1 (1970).
- BS 70b B. J. Buss and R. K. Smither, *Phys. Rev. C2*:1513 (1970).
- BSB 66 B. L. Berman, G. S. Sidhu, and C. D. Bowman, *Phys. Rev. Letters* **17**:761 (1966).
- BST 63 W. Bertozzi, C. P. Sargent, and W. Turchinetz, *Phys. Letters* **6**:108 (1963).
- BT 67 L. M. Bollinger and G. E. Thomas, *Phys. Rev. Letters* **18**:1143 (1967).
- BT 70 L. M. Bollinger and G. E. Thomas, *Phys. Rev. C2*:1951 (1970).
- BT 72 L. M. Bollinger and G. E. Thomas, *Phys. Rev. C6*:1322 (1972).
- Bus+ 72 F. R. Buskirk, H. D. Graf, R. Pitthan, H. Theissen, O. Titze, and T. Watcher, *Phys. Letters* **42B**:194 (1972).

- BW 52 J. M. Blatt and V. F. Weisskopf, *Theoretical Nuclear Physics*, John Wiley and Sons, New York (1952).
- Cam 59 A. G. W. Cameron, *Can. J. Phys.* **37**:322 (1959).
- Car 62 R. J. Carpenter, Argonne National Laboratory report ANL-6589 (1962).
- Chr 72 R. E. Chrien, in: *Proceedings of the International Conference on Nuclear Structure Study with Neutrons, Budapest, 1972*, to be published.
- Coh 71 B. L. Cohen, *Concepts of Nuclear Physics*, McGraw-Hill Inc., New York (1971) p. 84.
- CWG 73 R. E. Chrien, O. A. Wasson, and R. G. Greenwood, *Bull. Am. Phys. Soc.* **18**:59 (1973).
- DG 65 M. Danos and W. Greiner, *Phys. Rev.* **B138**:876 (1965).
- DS 68 A. M. Demidov and N. Shadiev, *Akad. Nauk SSSR* **32**:111 (1968).
- dST 63 A. de Shalit and I. Talmi, *Nuclear Shell Theory*, Academic Press, New York (1963).
- EB 71 E. D. Earle and G. A. Bartholomew, *Nucl. Phys.* **A176**:363 (1971).
- Ear+ 70 E. D. Earle, A. J. Ferguson, G. van Middelkoop, G. A. Bartholomew, and I. Bergqvist, *Phys. Letters* **32B**:471 (1970).
- Ear+ 71 E. D. Earle, G. A. Bartholomew, M. A. Lone, B. J. Allen, J. A. Harvey, and G. G. Slaughter, *Bull. Am. Phys. Soc.* **16**:496 (1971).
- Ear+ 72a E. D. Earle, M. A. Lone, G. A. Bartholomew, B. J. Allen, G. G. Slaughter, and J. A. Harvey, in: *Statistical Properties of Nuclei* (J. B. Garg, ed.), Plenum Press, New York (1972), p. 263.
- Ear+ 72b E. D. Earle, M. A. Lone, G. A. Bartholomew, W. J. McDonald, K. H. Bray, G. A. Moss, and G. C. Nielson, in: *Contributions to Conference on Nuclear Structure Study with Neutrons, Budapest, 1972*, Central Research Institute of Physics, Budapest (1972), p. 262.
- Ear+ 73 E. D. Earle, J. W. Knowles, M. A. Lone, and G. A. Bartholomew, *Contributions to the XXIII National Conference on Nuclear Spectroscopy and Structure of the Atomic Nucleus, Tbilisi, U.S.S.R. 1973*, and to be published.
- ELB 69 E. D. Earle, M. A. Lone, and G. A. Bartholomew, *Bull. Am. Phys. Soc.* **14**:515 (1969).
- Eri 60 T. Ericsson, *Adv. Phys.* **9**:425 (1960).
- Fag+ 73 L. W. Fagg, W. L. Bendel, E. C. Jones, N. Ensslin, and F. E. Cecil, *Contribution to Proceedings of International Conference on Nuclear Physics Munich, 1973*, to be published.
- FC 72 J. B. French and F. C. Chang, *Statistical Properties of Nuclei* (J. B. Garg, ed.), Plenum Press, New York (1972), p. 405.
- FGC 70 E. G. Fuller, H. M. Gerstenberg and T. M. Collins, *Photonuclear Data Index, January 1965 through January 1970, Special Publication 322* (1970), U.S. Government Printing Office, Washington D.C. 20402.
- FH 56 E. G. Fuller and E. Hayward, *Phys. Rev.* **101**:692 (1956).
- FH 62a E. G. Fuller and E. Hayward, *Nucl. Phys.* **33**:431 (1962).
- FH 62b E. G. Fuller and E. Hayward, *Nuclear Reactions* (P. M. Endt and P. B. Smith, eds.), Vol. II, North Holland, Amsterdam (1962), p. 113.
- Fir 70 F. W. K. Firk, *Ann. Rev. Nucl. Sci.* **20**:39 (1970).
- Ful+ 62 S. C. Fultz, R. L. Bramblett, J. T. Caldwell, and N. A. Kerr, *Phys. Rev.* **127**:1273 (1962).
- FW 58 E. G. Fuller and M. S. Weiss, *Phys. Rev.* **112**:560 (1958).

- Ful+ 69 S. C. Fultz, B. L. Berman, J. T. Caldwell, R. L. Bramblett, and M. A. Kelly, *Phys. Rev.* **186**:1255 (1969).
- GC 65 A. Gilbert and A. G. W. Cameron, *Can. J. Phys.* **43**:1446 (1965).
- GDP 60 L. V. Groshev, A. M. Demidov, and V. I. Pelekhover, *Nucl. Phys.* **16**:645 (1960); V. M. Strutinski, L. V. Groshev, and M. K. Akimova, *Nucl. Phys.* **16**:657 (1960).
- GF 67 H. M. Gerstenberg and E. G. Fuller, *National Bureau of Standards, Technical Note 416*, United States Department of Commerce, Government Printing Office, Washington, D.C. 20402 (1967).
- GGS 66 V. Gillet, A. M. Green, and E. A. Sanderson, *Nucl. Phys.* **88**:321 (1966).
- GL 57 B. I. Gavrilov and L. E. Lazareva, *Soviet Physics JETP* **3**:871 (1957).
- Gol+ 66 M. D. Goldberg, S. F. Mughabghab, S. N. Purohit, B. A. Magurno, and V. M. May, Brookhaven National Laboratory Report, *BNL 325 Supplement 2*, Volumes IIB and IIC (Physics TID-4500) (1966).
- GR 71 R. C. Greenwood and C. N. Reich, *Trans. Am. Nucl. Soc.* **14**:905 (1971).
- Gre+ 69 R. C. Greenwood, R. A. Harlan, R. G. Helmer, and C. W. Reich, in: *Proceedings of the International Symposium on Neutron Capture Gamma-Ray Spectroscopy, Studsvik, 1969*, IAEA, Vienna (1969), p. 607.
- Gro 55 L. V. Groshev, *Dokl. Akad. Nauk SSSR* **100**:651 (1955).
- Gro+ 58 L. V. Groshev, A. M. Demidov, V. N. Lutsenko, and V. I. Pelekhover, in: *Proceedings of the 2nd International Conference on the Peaceful Uses of Atomic Energy, Geneva*, (1958), Vol. 15, p. 138.
- Gro+ 68 L. V. Groshev, A. M. Demidov, V. I. Pelekhover, L. L. Sokolovskii, I. V. Kurchatov, G. A. Bartholomew, A. Doveika, K. M. Eastwood, and S. Monaro, *Nuclear Data Tables A5*, No. 1, 2 (1968).
- Gro+ 69 L. V. Groshev, A. M. Demidov, V. I. Pelekhover, L. L. Sokolovskii, G. A. Bartholomew, A. Doveika, K. M. Eastwood, and S. Monaro, *Nuclear Data Tables A5*, No. 3, 4:243 (1969).
- Han 73 P. G. Hansen, in: *Advances in Nuclear Physics*, Vol. 7 (M. Baranger and E. Vogt, eds.), Plenum Press, New York (1973), p. 159.
- Hay 65 E. Hayward, in: *Nuclear Structure and Electromagnetic Interactions, Scottish Universities, Summer School 1964* (N. MacDonald, ed.), Oliver and Boyd Press (1965), p. 141.
- HG 69 M. Hillman and J. R. Grover, *Phys. Rev.* **185**:1303 (1969).
- HGR 71 R. G. Helmer, R. C. Greenwood, and C. W. Reich, *Nucl. Phys.* **A168**:449 (1971).
- HKW 72 O. Haussler, F. C. Khanna, and D. Ward, *Nucl. Phys.* **A194**:113 (1972).
- HSM 65 J. A. Harvey, G. G. Slaughter, and M. J. Martin, Oak Ridge National Laboratory report ORNL-p-1353 (1965).
- Hui+ 62 J. R. Huizenga, K. M. Clarke, J. E. Gindler, and R. Vandenbosch, *Nucl. Phys.* **34**:439 (1962).
- Hui 72 J. R. Huizenga, in: *Statistical Properties of Nuclei* (J. B. Garg, ed.), Plenum Press, New York (1972), p. 425.
- Jac 67 R. Jackiw, *Phys. Rev.* **157**:1220 (1967).
- Jai 72 A. P. Jain, *Phys. Letters* **42B**:419 (1972).
- JK 51 J. D. Jackson and B. B. Kinsey, *Phys. Rev.* **82**:345 (1951).
- Joh+ 66 L. V. Johnson, L. B. Hughes, T. J. Kennett, and W. V. Prestwich, *Nucl. Phys.* **84**:113 (1966).
- JS 71 H. E. Jackson and E. N. Strait, *Phys. Rev.* **C4**:1314 (1971).

322 G.A. Bartholomew, E.D. Earle, A.J. Ferguson, J.W. Knowles, M.A. Lone

- JS 73 H. E. Jackson and E. N. Strait, *Bull. Am. Phys. Soc.* **18**:592 (1973).
- KA 66 J. W. Knowles and N. M. Ahmed, Atomic Energy of Canada Limited report AECL-2535 (1966).
- KBB 70 T. T. S. Kuo, J. Blomqvist, and G. E. Brown, *Phys. Letters* **31B**:93 (1970).
- KH 73 F. C. Khanna and M. Harvey, *Contribution to Proceedings of International Conference on Photonuclear Reactions and Applications, Asilomar, California, 1973*, CONF 730301, Ernest O. Lawrence Livermore Laboratory, U. of California (1973), p. 2E-12, and private communication (1973).
- Kin 55 B. B. Kinsey, in: *Beta and Gamma Ray Spectroscopy* (K. Siegbahn, ed.), North Holland, Amsterdam (1955), p. 795.
- KK 67 A. M. Khan and J. W. Knowles, *Bull. Am. Phys. Soc.* **12**:538 (1967).
- KK 73 J. W. Knowles and A. M. Khan, to be published (1973).
- KKC 70 J. W. Knowles, A. M. Khan, and W. G. Cross, in: *XX Annual National Conference on Nuclear Spectroscopy and Structure of the Atomic Nucleus, Leningrad, U.S.S.R. 1970; Izv. Akad. Nauk SSSR (ser. fiz.)* **34**:1627 (1970).
- KM 73 J. W. Knowles and O. Y. Mafra, to be published (1973).
- Kno 70 J. W. Knowles, *Bull. Can. Assn. of Physicists* **26**:78 (1970).
- Lan 71 A. M. Lane, *Ann. Phys. (N.Y.)* **63**:171 (1971).
- Lan 72a A. M. Lane, in: *Statistical Properties of Nuclei* (J. B. Garg, ed.), Plenum Press, New York (1972), p. 271.
- Lan 72b A. M. Lane, private communication (1972).
- LB 50 J. S. Levinger and H. A. Bethe, *Phys. Rev.* **78**:115 (1950).
- LBE 72 M. A. Lone, G. A. Bartholomew and E. D. Earle, Atomic Energy of Canada Limited Physics Division Progress Report, AECL 4257 (1972) p. 42.
- LBT 72 G. D. Loper, L. M. Bollinger, and G. E. Thomas, *Bull. Am. Phys. Soc.* **17**:580 (1972); Argonne National Laboratory Progress Report, ANL 7971 (1972), and private communication from L. M. Bollinger (1972).
- LD 70 M. B. Lewis and W. W. Daehnick, *Phys. Rev.* **C1**:1577 (1970).
- LEB 70 M. A. Lone, E. D. Earle, and G. A. Bartholomew, *Nucl. Phys.* **A156**:113 (1970).
- LEB 73 M. A. Lone, E. D. Earle, and G. A. Bartholomew, to be submitted to *Nucl. Phys.* (1973).
- Lep + 71 A. Leprêtre, H. Beil, R. Bergère, P. Carlos, A. Veyssiére, and M. Sugawara, *Nucl. Phys.* **A175**:609 (1971).
- LL 60 A. M. Lane and J. E. Lynn, *Nucl. Phys.* **17**:563 and 586 (1960).
- Lon + 72 M. A. Lone, G. A. Bartholomew, E. D. Earle, and A. J. Ferguson, *Contributions to Conference on Nuclear Structure Study with Neutrons, Budapest, 1972*, Central Research Institute of Physics, Budapest (1972), p. 264.
- Lon 73 M. A. Lone, Atomic Energy of Canada Limited report AECL-4372, to be published.
- Lon + 73 M. A. Lone, G. A. Bartholomew, E. D. Earle, A. J. Ferguson, and J. W. Knowles, *Contribution to Proceedings of International Conference on Photonuclear Reactions and Applications, Asilomar, California, 1973*, CONF 730301, Ernest O. Lawrence Livermore Laboratory, University of California (1973), p. 2E-11.
- LP 71 A. Lottin and D. Paya, *J. de Phys.* **32**:849 (1971).
- LS 65 B. Lundberg and N. Starfelt, *Nucl. Phys.* **67**:321 (1965).
- Luc + 72 R. Lucas, R. Babinet, J. Fagot, and H. Nifenecker, *Contributions to Conference*

- on Nuclear Structure Study with Neutrons, Budapest, 1972*, Central Research Institute of Physics, Budapest (1972), p. 36.
- Lyn 68 J. E. Lynn, *The Theory of Neutron Resonance Reactions*, Clarendon Press, Oxford (1968).
- Mar 69 M. Maruyama, *Nucl. Phys.* **A131**:145 (1969).
- Mas+ 69 W. M. Mason, G. Kernel, J. L. Blackand, and N. W. Tanner, *Nucl. Phys.* **A135**, 193 (1969).
- MKB 67 C. F. Moore, J. G. Kulleck, and P. von Brentano, *Phys. Rev.* **164**:1559 (1967).
- MKG 72 O. Y. Mafra, S. Kuniyoshi, and J. Goldemberg, *Nucl. Phys.* **A186**:110 (1972).
- Mot 60 B. R. Mottelson, *Proceedings of the International Conference on Nuclear Structure, Kingston 1960* (D. A. Bromley and E. W. Vogt, eds.), University of Toronto Press, Toronto (1960), p. 525.
- MSW 70 R. Moreh, S. Shlomo, and A. Wolf, *Phys. Rev.* **C2**:1144 (1970).
- Mug 72 S. F. Mughabghab, in: *Proceedings of the Conference on Nuclear Structure Study with Neutrons, Budapest, 1972*, to be published.
- MW 69 R. Moreh and A. Wolf, *Phys. Rev.* **182**:1236 (1969).
- New 56 T. D. Newton, *Can. J. Phys.* **34**:804 (1956).
- New 72 H. W. Newson, in: *Statistical Properties of Nuclei* (J. B. Garg, ed.), Plenum Press, New York (1972), p. 309.
- NH 54 R. Nathans and J. Halpern, *Phys. Rev.* **93**:437 (1954).
- NMH 70 D. O. Nellis, I. L. Morgan, and E. L. Hudspeth, *Bull. Am. Phys. Soc.* **15**:807 (1970), and private communication from D. O. Nellis (1970).
- ORR 66 E. Obst, F. Rauch, and E. Rossle, *Phys. Letters* **21**:50 (1966).
- ORW 67 E. Obst, F. Rauch, and H. G. Wahsweiler, *Nucl. Phys.* **A103**:17 (1967).
- OTA 62 J. S. O'Connell, P. A. Tipler, and P. Axel, *Phys. Rev.* **126**:228 (1962).
- Per 66 C. F. Perdrisat, *Rev. Modern Phys.* **38**:41 (1966).
- Per 70 S. M. Perez, *Phys. Letters* **33B**:317 (1970).
- PSS 64 M. K. Pal, J. M. Soper, and A. P. Stamp, United Kingdom Atomic Energy Research Establishment report T. P. 148 (1964).
- PT.56 C. E. Porter and R. G. Thomas, *Phys. Rev.* **104**:483 (1956).
- PW 71 R. Pitthan and T. H. Walcher, *Phys. Letters* **36B**:563 (1971).
- Ras+ 69 N. C. Rasmussen, Y. Hukai, T. Inouye, and V. J. Orphan, Massachusetts Institute of Technology report MIT NE-85 (1969).
- Ras+ 70 N. C. Rasmussen, V. J. Orphan, T. L. Harper, J. Cunningham, and S. A. Ali, Gulf General Atomic Inc., report DSA 2570 (1970).
- Rim+ 70 K. Rimawi, J. B. Garge, R. E. Chrien, and R. G. Graves, *Phys. Rev.* **C2**:1973 (1970).
- RM 60 K. Reibel and A. K. Mann, *Phys. Rev.* **118**:701 (1960).
- Ros 68 N. Rosensweig, *Nucl. Phys.* **A118**:650 (1968).
- Sam+ 68 C. Samour, H. E. Jackson, J. Julien, A. Bloch, J. M. Kuchly, C. Lopata, and J. Morgenstern, *Nucl. Phys.* **A121**:65 (1968).
- SE 69 C. S. Shapiro and G. T. Emery, *Phys. Rev. Letters* **23**:244 (1969).
- SG 65 P. H. Stelson and L. Grodzins, *Nuclear Data* **A1**:1 (1965).
- SH 68 E. B. Shera and D. W. Hafemeister, private communication (1968), and see (Gro+ 68).
- She+ 72 E. B. Shera, U. Gruber, B. P. K. Maier, H. R. Koch, O. W. B. Schult, R. G. Lanier, N. Onishi, and R. K. Sheline, *Phys. Rev.* **C6**:537 (1972).
- SHR 66 S. J. Skorka, J. Hertel, and T. W. Retz-Schmidt, *Nuclear Data* **A2**:347 (1966).

- SM 68 O. D. Simpson and L. G. Miller, *Nucl. Instr. and Meth.* **61**:245 (1968).
- Smi+ 72 R. K. Smith, D. J. Bus, D. L. Bushnell, and G. E. Thomas, *Bull. Am. Phys. Soc.* **17**:28 (1972).
- SNG 71 A. Stolovy, A. I. Namenson, and T. F. Godlove, *Phys. Rev.* **C4**:1466 (1971).
- Sol 72 V. G. Soloviev, *Sov. J. Nucl. Phys.* **15**:410 (1972).
- Sta 64 N. Starfelt, *Nucl. Phys.* **53**:397 (1964).
- Ste+ 65 P. H. Stelson, R. L. Robinson, H. J. Kim, J. Rapaport, and G. R. Satchlu, *Nucl. Phys.* **68**:97 (1965).
- Ste+ 72 M. Stefanon, F. Corvi, C. Coceva, and P. Giacobbe, *Contributions to Conference on Nuclear Structure Study with Neutrons, Budapest, 1972*, Central Research Institute of Physics, Budapest (1972), p. 74.
- Swa 73a C. P. Swann, *Contribution to Proceedings of International Conference on Photonuclear Reactions and Applications, Asilomar, California 1973*, CONF 730301, Ernest O. Lawrence Livermore Laboratory, University of California (1973) p. 2E-13, and private communication.
- Swa 73b C. P. Swann, *Nucl. Phys.* **A201**:534 (1973).
- TJ 72 R. E. Toohey and H. E. Jackson, *Phys. Rev.* **C6**:1440 (1972).
- Tro 61 E. S. Troubetzkoy, *Phys. Rev.* **122**:212 (1961).
- UVL 66 J. Urbanec, J. Vrzal, and J. Liptak, in: *Proceedings of the International Conference on the Study of Nuclear Structure with Neutrons, Antwerp, 1965* (M. Nève de Mévergnies, P. Van Assche, and J. Vervier, eds.), North Holland Publishing Co., Amsterdam (1966), p. 535.
- Was+ 68 O. A. Wasson, R. E. Chrien, M. R. Bhat, M. A. Lone, and M. Beer, *Phys. Rev.* **173**:1170 (1968).
- Was+ 69 O. A. Wasson, R. E. Chrien, M. A. Lone, M. R. Bhat, and M. Beer, *Nucl. Phys.* **A132**:161 (1969).
- Was+ 71 O. A. Wasson, R. E. Chrien, G. G. Slaughter, and J. A. Harvey, *Phys. Rev.* **C4**:900 (1971).
- WC 70 O. A. Wasson and R. E. Chrien, *Phys. Rev.* **C2**:675 (1970).
- Wei 70 M. S. Weiss, private communication in (Bow+ 70).
- Wei+ 69 C. Weitkamp, J. A. Harvey, G. G. Slaughter, and E. C. Campbell, in: *Proceedings of International Symposium on Neutron Capture Gamma-Ray Spectroscopy, Studsvik, 1969*, IAEA, Vienna (1969), p. 421.
- Win+ 70 E. J. Winhold, E. M. Bowey, D. B. Gayther, and B. H. Patrick, *Phys. Letters* **32B**:607 (1970).
- Wol+ 72 A. Wolf, R. Moreh, A. Nof, O. Shahal, and J. Tanenbaum, *Phys. Rev.* **C6**:2276 (1972).